NASA TECHNICAL NOTE

NASA TN D-8197

20- AND 30-GHz MILLIMETER WAVE EXPERIMENTS WITH THE ATS-6 SATELLITE

Louis J. Ippolito

Goddard Space Flight Center
Greenbelt, Md. 20771

NATIONAL AERONAUTICS AND SPACE ADMINISTRATION • WASHINGTON, D. C. • APRIL 1976

1. Report No.	2. Government Accession No.	3. Recipient's Catalog No.
NASA TN D-8197		

4. Title and Subtitle
20- and 30-GHz Millimeter Wave Experiments with the ATS-6 Satellite

5. Report Date
April 1976

6. Performing Organization Code
951

7. Author(s)
Louis J. Ippolito

8. Performing Organization Report No.
G-7649

9. Performing Organization Name and Address
Goddard Space Flight Center
Greenbelt, Maryland 20771

10. Work Unit No.

11. Contract or Grant No.

13. Type of Report and Period Covered
Technical Note

12. Sponsoring Agency Name and Address
National Aeronautics and Space Administration
Washington, D.C. 20546

14. Sponsoring Agency Code

15. Supplementary Notes

16. Abstract

The Applications Technology Satellite-6 (ATS-6) millimeter wave experiment, developed and implemented by the NASA Goddard Space Flight Center, provides the first direct measurements of 20- and 30-GHz earth-space links from an orbiting satellite. Studies at 11 locations in the continental United States were directed at an evaluation of rain attenuation effects, scintillations, depolarization, site diversity, coherence bandwidth, and analog and digital communications techniques. In addition to direct measurements on the 20- and 30-GHz links, methods of attenuation prediction with radars, rain gages, and radiometers were developed and compared with the directly measured attenuation.

This report contains the first comprehensive publication of initial data results of the ATS-6 millimeter wave experiment from the major participating organizations.

The first section describes the experiment objectives, flight hardware, and modes of operation. The remaining six sections present papers prepared by the major participating organizations in the experiment. The papers present a comprehensive summary of the significant results of the initial 11 months of ATS-6 experiment measurements and related radiometric, radar, and radio-meteorology studies.

17. Key Words (Selected by Author(s))	18. Distribution Statement
Millimeter wave, Space communications, Rain attenuation, Scintillation, Propagation, Depolarization, Site diversity, Radio meteorology	Unclassified—Unlimited Cat. 32

19. Security Classif. (of this report)	20. Security Classif. (of this page)	21. No. of Pages	22. Price*
Unclassified	Unclassified	140	$5.75

For sale by the National Technical Information Service, Springfield, Virginia 22161

This document makes use of international metric units according to the Systeme International d'Unites (SI). In certain cases, utility requires the retention of other systems of units in addition to the SI units. The conventional units stated in parentheses following the computed SI equivalents are the basis of the measurements and calculations reported.

ACKNOWLEDGMENT

The contributions of Erwin Hirschmann, NASA Goddard Space Flight Center, in the coordination and technical monitoring of the many participating organizations of the ATS-6 Millimeter Wave Experiment are gratefully acknowledged.

CONTENTS

THE ATS-6 MILLIMETER WAVE EXPERIMENT

L. J. Ippolito
Goddard Space Flight Center
Greenbelt, Maryland

INTRODUCTION

The Applications Technology Satellite-6 (ATS-6) millimeter wave experiment, developed and implemented by the NASA Goddard Space Flight Center (GSFC), has provided the first direct measurements of 20- and 30-GHz earth-space links from an orbiting satellite. Studies at 11 locations in the continental United States were directed at an evaluation of rain attenuation effects, scintillations, depolarization, site diversity, coherence bandwidth, and analog and digital communications techniques. In addition to direct measurements on the 20- and 30-GHz links, methods of attenuation prediction with radars, rain gages, and radiometers were developed and compared with the directly measured attenuation.

This section presents a summary of the satellite hardware, experiment configuration, and operations. The following sections present data measurements and analysis results from a number of the participating organizations in the experiment.

The ATS-6 millimeter wave experiment (MWE) is designed to measure and evaluate the propagation characteristics of space-to-earth links centered at 20 GHz and 30 GHz.* The ATS-6 MWE is the second NASA flight experiment to evaluate propagation effects above 10 GHz. The first experiment, launched on board the ATS-5 in July 1969, provided measurements at 15.3 GHz and 31.65 GHz (Ippolito, 1971).

The ATS-6 was successfully launched into synchronous orbit at 13:00 GMT on Thursday, May 30, 1974, aboard the Titan IIIC launch vehicle, number C-27 (figure 1). Spacecraft weight at the time of lift-off was 1396 kg (3078.3 lb) including the 48-kg adapter, which remained attached at spacecraft separation. Injection occurred at 19:30:49 GMT into a near perfect orbit. The automatic separation and deployment sequence was successfully completed, and the spacecraft was commanded through the sun and earth acquisition, and yaw reference sequences, with all operations being completed by 02:19 GMT the day after launch. During the next two weeks of flight, the spacecraft was commanded into its normal in-orbit configuration, and all systems were evaluated. Following this spacecraft checkout phase, a series of

*Ippolito, L. J., "The ATS-F Millimeter Wave Propagation Experiment," NASA Goddard Space Flight Center, Greenbelt, Maryland, TM X-65752, October 1971.

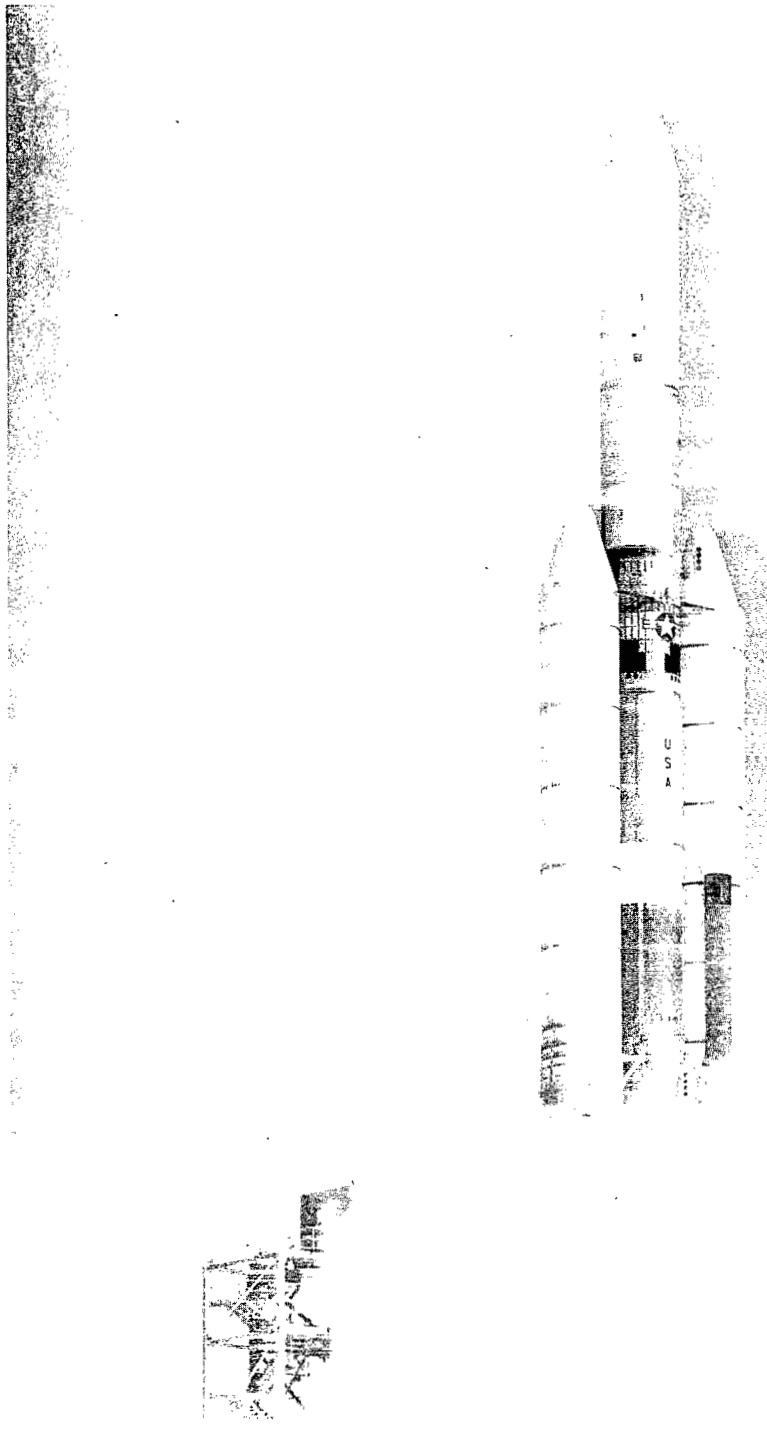

Figure 1. ATS-6 launch, May 30, 1974.

tests were conducted to evaluate the performance of the onboard experiment systems and their respective ground system interfaces. At the end of the first month of flight, all systems had been successfully evaluated with very few anomalies encountered, and the spacecraft was declared operational.

SATELLITE HARDWARE

The major elements of the MWE satellite system are shown in figure 2. The experiment has three modes of operation: continuous wave (CW), multitone, and communications, selectable at 20 and/or 30 GHz. In the CW mode, a 10-GHz signal is developed by multiplication from the 5-MHz master oscillator, then doubled for the 20-GHz carrier, and tripled for the 30-GHz carrier. The carriers are used to drive 2-W traveling wave tube amplifiers (TWTA) and then transmit through either of two antenna systems to the earth. The parabolic antenna is used when a narrow spot beam is required, and the horn antennas are used for wide coverage of the continental United States area.

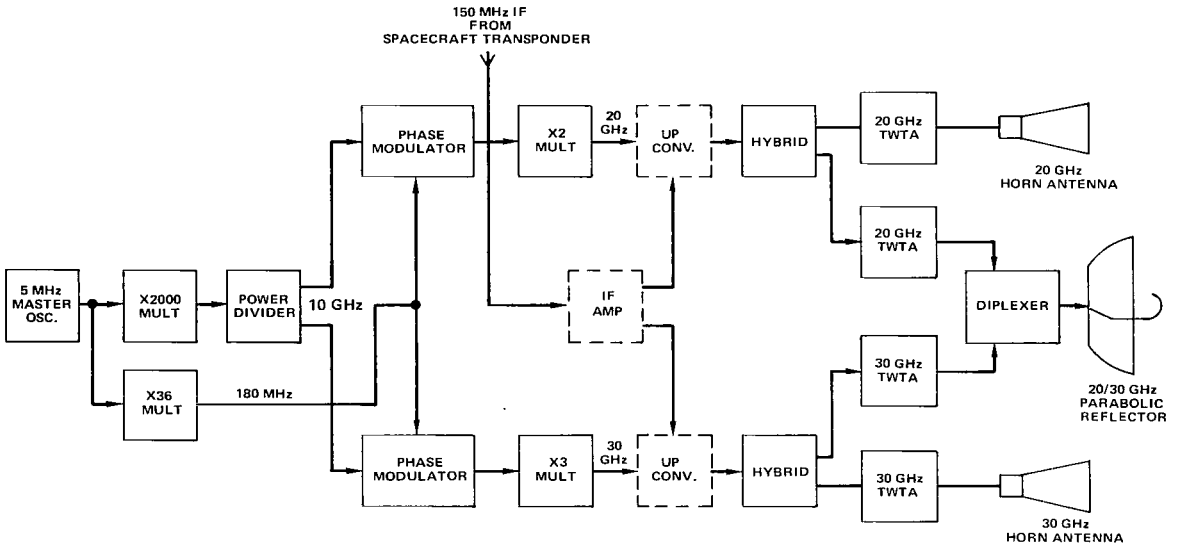

Figure 2. ATS-6 millimeter wave experiment flight hardware elements.

In the multitone mode, a 180-MHz signal is developed from the 5-MHz master oscillator and is used to phase modulate the 10-GHz carriers in the 20- and 30-GHz chains. A comb of nine tones is generated, four on either side of the carrier spaced 180 MHz apart, resulting in a total spectrum of 1440 MHz. This signal is used to evaluate the coherence bandwidth characteristics of the space-to-earth path. In the communications mode, the 150-MHz IF from the spacecraft is used to drive an upconverter which produces a 30.15-GHz or 20.15-GHz transmitted signal for communications tests. Bandwidths of 25 MHz or 12 MHz are available, on command, for the 150-MHz IF signal. The uplink frequency of the spacecraft transponder is one of three in the 6-GHz band, and the downlink is one of three in the 4-GHz band.

The experiment hardware, located in the ATS-6 earth viewing module (EVM), is physically divided into four units shown in figure 3: (a) the RF multiplier; (b) the 20/30-GHz modulator/power amplifier; (c) the 20/30-GHz horn antenna assembly; and (d) the 0.45 meter 20/30-GHz parabolic antenna. The package weighs a total of 40.3 kg (91.4 lb) and consumes about 39 W with one TWTA on, and 70 W with both frequencies operating. The frequency deviation of the oscillator was measured at about 1 part in 10^{10} over a temperature range of 263 to 323 K (-10° to 50° C).

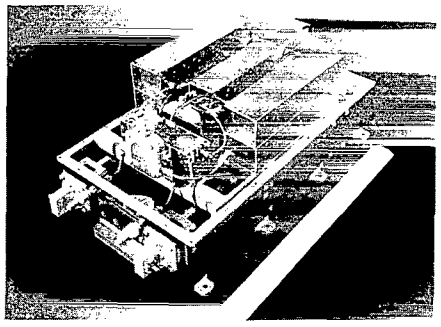

(a) RF Multiplier

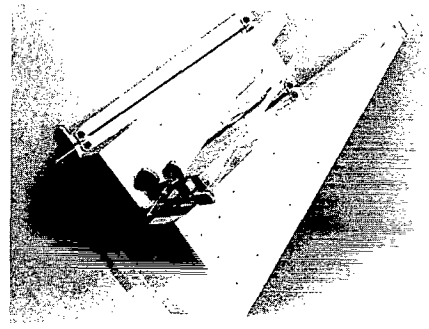

(c) 20/30-GHz Horn Antenna Assembly

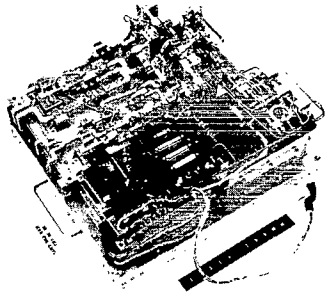

(b) 20/30-GHz Modulator/Power Amplifier

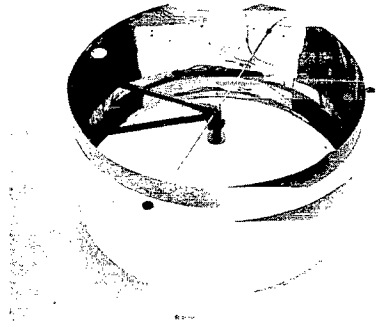

(d) 20/30-GHz Parabolic Antenna

Figure 3. Millimeter wave experiment flight hardware.

MODES OF OPERATION

The experiment is commandable into three modes of operation: a continuous wave mode in which the 20- and 30-GHz carriers only are transmitted; a multitone mode in which nine spectral lines spaced 180 MHz apart, centered at 20 and at 30 GHz, are transmitted; and a communications mode in which the FM communications signals received on the spacecraft transponder are retransmitted at 20.15 and 30.15 GHz.

Simplified block diagrams of the experiment configuration for the CW mode are shown in figure 4 for the cases of radiation from the horn antennas and the parabolic antenna, respectively. In each case a 10-GHz signal is generated in the RF multiplier which uses a very stable 5-MHz crystal oscillator as a reference. The 10-GHz signal is applied to X2 and X3 frequency multipliers, and the resulting 20- and 30-GHz signals are amplified by TWTAs for radiation by the antennas.

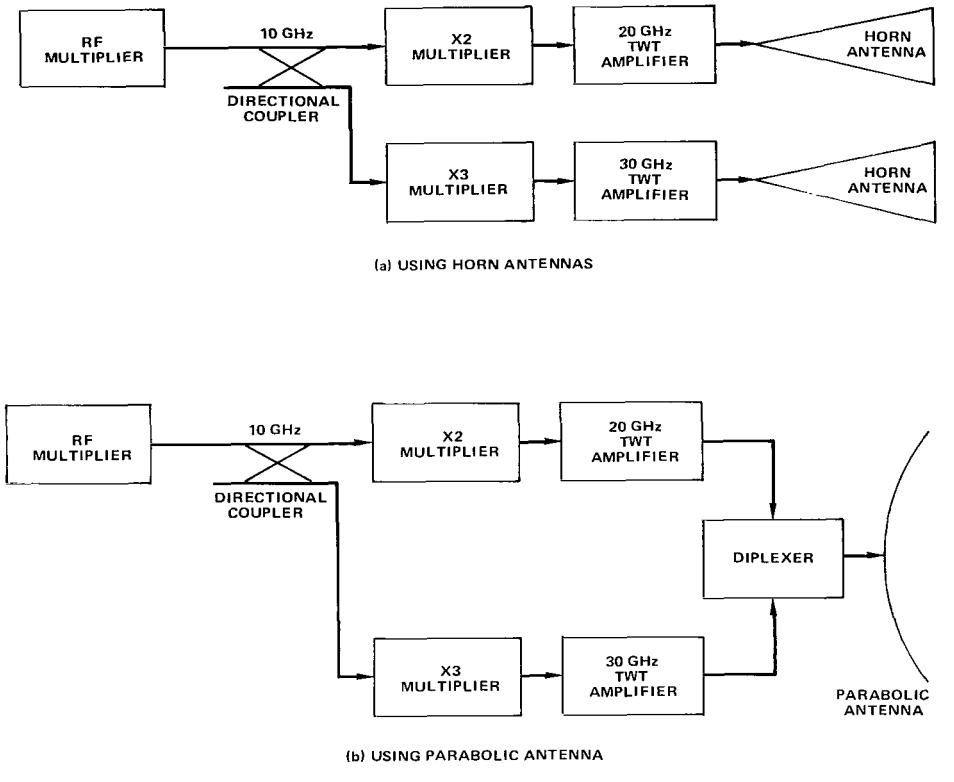

Figure 4. CW mode simplified block diagram.

Simplified block diagrams of the experiment configuration for the multitone mode are shown in figure 5 for the cases of horn antennas and the parabolic antenna. In this mode, a 180-MHz modulating signal is derived from the same 5-MHz master oscillator as the 10-GHz signal. The 180-MHz signal drives the phase modulators at 10 GHz, and the modulated signal is frequency multiplied X2 and X3 to achieve multitone spectrums at 20 and 30 GHz. The 20- and 30-GHz multitone signals are amplified by traveling wave tube amplifiers for radiation by the antennas.

The configuration of the experiment for the communications mode is shown in simplified form in figure 6. In this mode, the 10-GHz signal is again frequency multiplied to 20 and 30 GHz as in the CW mode, and these two frequencies are used to pump two upconverters.

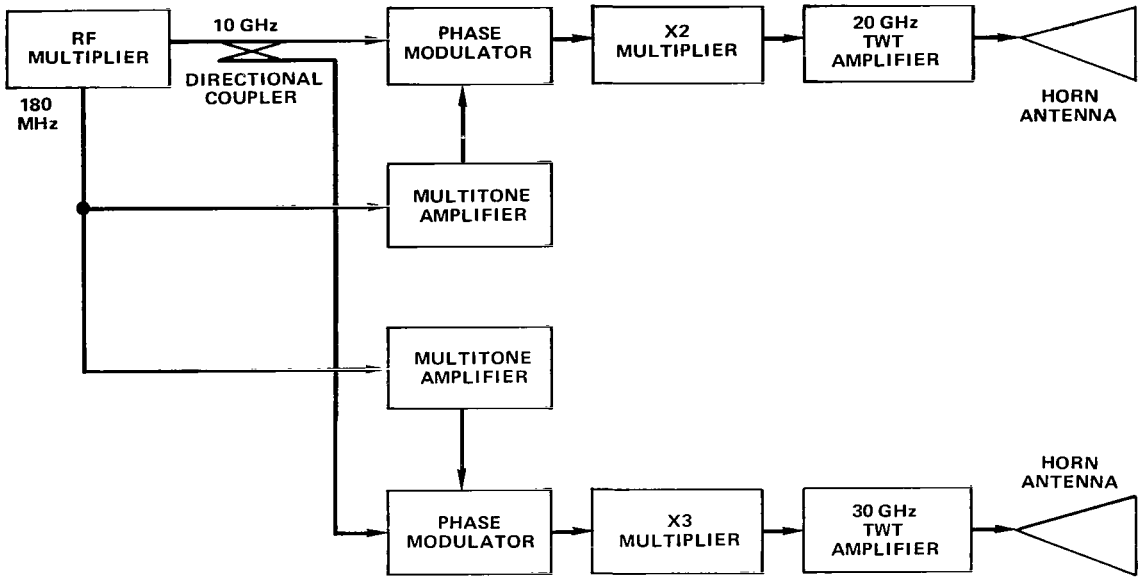

(a) USING HORN ANTENNAS

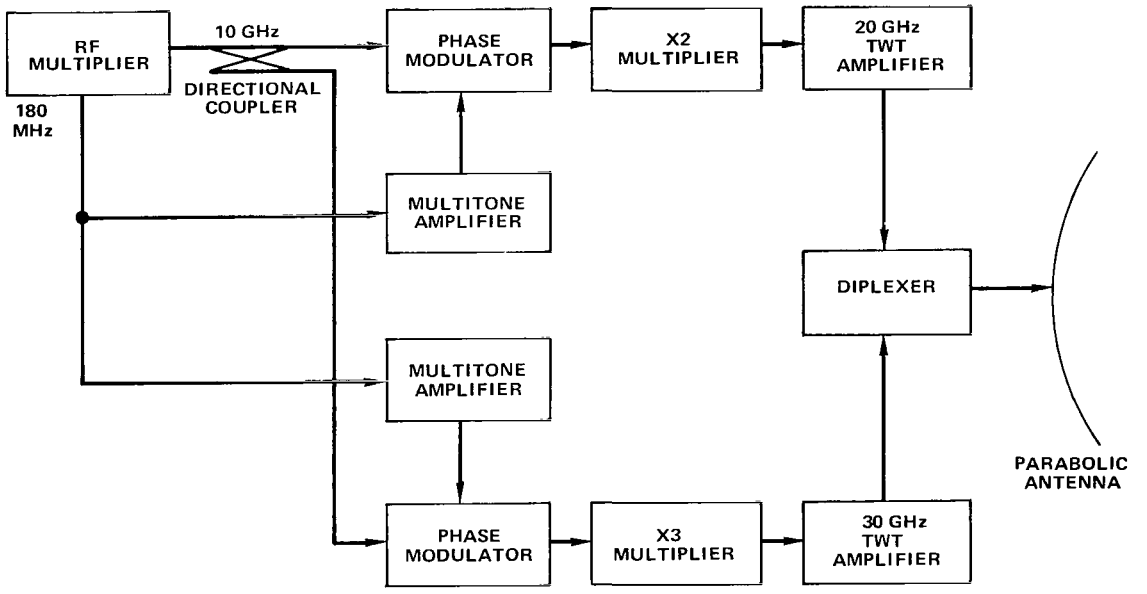

(b) USING PARABOLIC ANTENNA

Figure 5. Multitone mode simplified block diagram.

Signal drive for the upconverters consists of the frequency modulated 150-MHz IF signal from the spacecraft transponder suitably amplified by an IF amplifier. The resulting 20.15- and 30.15-GHz FM signals are then amplified by TWTAs for radiation by the parabolic antenna.

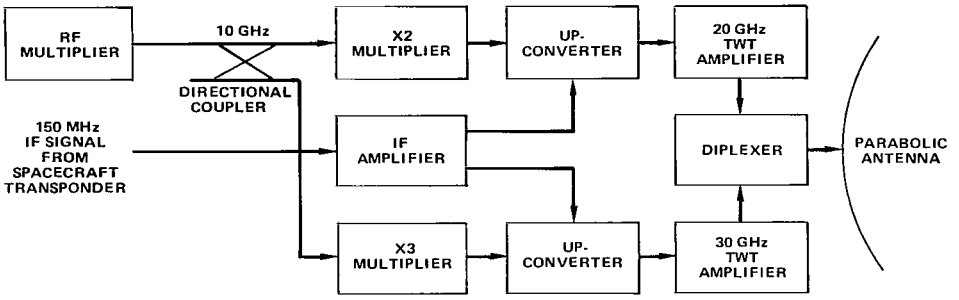

Figure 6. Communications mode simplified block diagram.

Three antennas are provided in the experiment: a 20-GHz horn antenna, a 30-GHz horn antenna, and a 20/30-GHz parabolic antenna. In each case, the radiated RF is linearly polarized with the plane of the E-vector aligned to the north-south axis of the spacecraft. For both horn antennas, the 3-dB bandwidths are approximately 6° in the north-south direction and approximately 8° in the east-west direction. The parabolic antenna provides a 3-dB beamwidth of approximately 2.3° at 20 GHz and approximately 1.6° at 30 GHz. The effective isotropic radiated power (EIRP) of the antennas at the peak of the beam, based on measured performance, is listed in table 1.

Table 1
EIRP at Antenna Beam Maximum

Antenna	EIRP, dBm	
	20 GHz	30 GHz
Horn		
CW mode	61.0	59.8
Multitone mode	60.1	59.9
Communications mode	60.3	60.1
Parabolic		
CW mode	70.3	73.6
Multitone mode	70.2	73.8
Communications mode	71.3	73.3

GROUND TERMINAL LOCATIONS

The ATS-6 MWE consists of ground terminals at 11 locations throughout the United States. The prime facility is the NASA station at Rosman, North Carolina, which is equipped to

measure 20- and 30-GHz attenuation, coherence bandwidth, communications link characterization, and prediction techniques with radars and rain gages. A second NASA terminal, located at Goddard Space Flight Center, Greenbelt, Maryland, performs 20- and 30-GHz attenuation measurements and performs scintillation studies.

A major element of the ATS-6 MWE involved the participation of a number of organizations with unique specialties in the millimeter wave propagation area. Nine organizations with 13 ground terminals participated in the ATS-6; their locations and major areas of measurement are summarized in table 2.

Table 2
ATS-6 MWE Participating Terminals

Location Organization	Elevation Angle (Antenna Dia.)	Major Areas of Investigation
Rosman, N. Carolina NASA GSFC	47° 4.6 m (15 ft)	Prime facility 20 and 30 GHz - Attenuation, coherence bandwidth, differential phase effects, scintillation, communications links, radars, radiometers, rain-gage network
Greenbelt, Maryland NASA GSFC	41° 3.0 m (10 ft)	20 and 30 GHz—Attenuation, site diversity**, radiometers
Austin, Texas Univ. of Texas (2)*	54° 1.5, 3.0 m (5, 10 ft)	30 GHz—Attenuation, 2-terminal site diversity, radiometer
Blacksburg, Virginia VPI & SU*	45° 1.2 m (4 ft)	20 GHz—Attenuation, depolarization
Clarksburg, Maryland COMSAT (2)*	41° 3.0, 4.6 m (10, 15 ft)	20 and 30 GHz—Attenuation, site diversity**, radiometers
Columbus, Ohio Ohio State Univ. (3)*	42° 3.0, 4.6 m (10, 15 ft)	20 and 30 GHz—Attenuation, 3-terminal site diversity, scintillation, radars, radiometers
Holmdel, New Jersey Bell Laboratories	39° 3.6 m (12 ft)	20 GHz—Depolarization
Baltimore, Maryland Westinghouse*	41° 3.6 m (12 ft)	20 GHz—Attenuation; site diversity**
Waldorf, Maryland NRL*	42° 18.2 m (60 ft)	20 and 30 GHz—Attenuation, site diversity**, radiometers
Richland, Washington Battelle Northwest Laboratories*	31° 9.1 m (30 ft)	20 GHz—Attenuation, radiometer
Ft. Monmouth, New Jersey USASCA	39° 4.6 m (15 ft)	30 GHz—Attenuation

*GSFC supported participation.
**Washington, D.C., area diversity experiment.

All terminals were equipped to measure attenuation at 20 or 30 GHz, or both, and all, except for Bell Laboratories, had rain gage measurements as well. The Washington, D.C., area diversity experiment consisted of four terminals in the Washington metropolitan area which jointly observed 20-GHz attenuation events from which site diversity statistics were developed.

Most of the participating stations used receiver systems that were designed for the ATS-5 program and converted to 20 and 30 GHz for use on the ATS-6 MWE.* Antenna sizes varied

*Calhoon, C.D., Jr., "ATS-F Millimeter Wave Experiment Ground Receiver Systems for NASA Sponsored Participating Stations," NASA Goddard Space Flight Center, Greenbelt, Maryland, private communication, January 1973.

from 1.2 to 18.3 m (see table 2) and the front-end characteristics varied with the particular sites. Descriptions of the ground systems will be included in the papers from the participating organizations.

EXPERIMENT OPERATIONS

The millimeter wave experiment flight hardware was first energized on June 13, 1974, and all modes were operational except for the 20-GHz horn antenna TWTA. Repeated attempts to energize the 20-GHz horn antenna were unsuccessful. All other modes have performed within the expected parameters.

The MWE operated with both scheduled tests and unscheduled periods when a callup was requested by a participant. Other ATS-6 experiments, primarily the health education telecommunications (HET) and position location aircraft communication experiment (PLACE), had priority for operations over the MWE, hence all request periods could not be honored. Figure 7 summarizes the hours of on-time, both scheduled and unscheduled, for the 13 months of MWE operations. The number of requests granted for each month is also shown. For many of the request periods, more than one ground terminal was monitoring the satellite signal; the numbers on the figure only indicate the initial request.

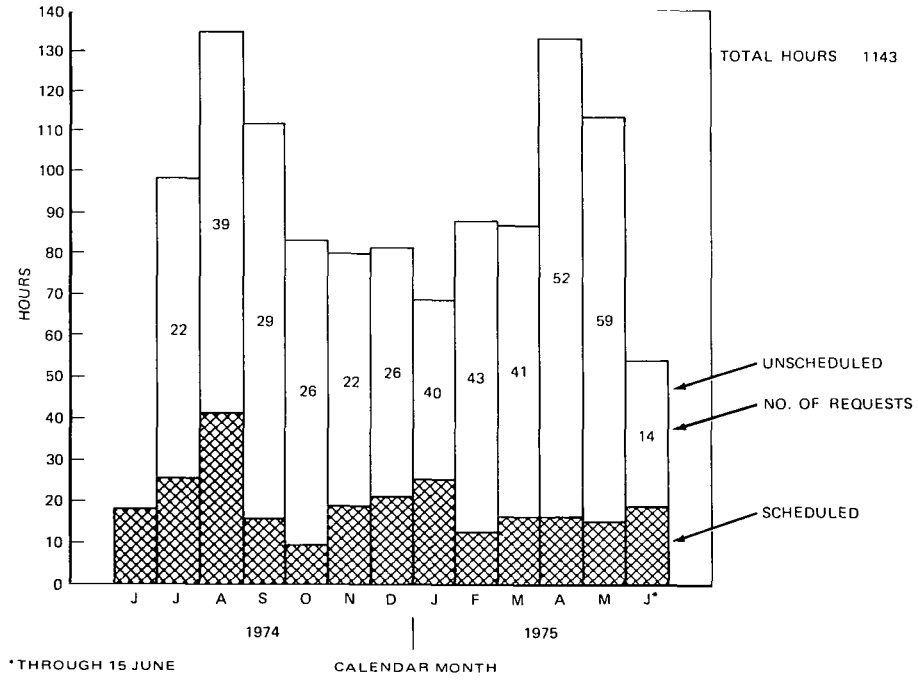

Figure 7. ATS-6 millimeter wave experiment—hours of spacecraft on-time.

The ATS-6 MWE has logged over 1143 hours of operations since launch in all modes; over 900 of these hours were for unscheduled callup measurements during rain periods or for special tests.

MWE operations at the new spacecraft location at 35° E. longitude are continuing at both 20 and 30 GHz, and further tests are planned when the ATS-6 returns to 105° W. longitude in the fall of 1976.

REFERENCE

Ippolito, L. J., "Effects of Precipitation on 15.3 and 31.65 GHz Earth Space Transmissions with the ATS-5 Satellite," *Proc. IEEE*, **59**, (2), pp. 189-205, 1971.

ATS-6 ATTENUATION AND DIVERSITY MEASUREMENTS AT 20 AND 30 GHz

W. J. Vogel, A. W. Straiton, B. M. Fannin, and N. K. Wagner
Electrical Engineering Research Laboratory
The University of Texas at Austin
Austin, Texas

INTRODUCTION

General

Satellite-terrestrial communication systems depend upon the propagation of electromagnetic waves through the atmosphere. A successful design of such a system is one that meets realistic specifications. These must be based on the knowledge of any limitations introduced by the atmosphere. At millimeter wave frequencies for elevation angles above about 15° two mechanisms exist that introduce limitations: (1) the absorption and reradiation of radio waves by oxygen and water vapor and (2) the absorption and scattering of radio waves by precipitation. While the first mechanism can be essentially determined (Straiton, 1975), the second one requires that propagation measurements be made. This is because, while the interaction can be theoretically analyzed if the physical parameters of the precipitation are known (Vogel et al., 1973), the frequency of occurrence and the severity of precipitation events are not well enough defined to allow a purely theoretical prediction.

For this purpose, and in anticipation of the future need of satellite systems operating at 20 and 30 GHz, the ATS-6 satellite included a millimeter wave experiment. The signals from the 20- and 30-GHz transmitters could be used by participating experimenters for pertinent measurements. This report describes the efforts by the Electrical Engineering Research Laboratory of The University of Texas at Austin.

EXPERIMENT OBJECTIVES AND DATA CORRELATION

Statistical data were collected on the attenuation due to the atmosphere for the transmission from the satellite at both 20 and 30 GHz. The 30-GHz data were obtained by using the satellite signal, and the 20-GHz data were obtained by radiometric means. From the 20-GHz data, the 30-GHz attenuation could be estimated for the times during which the satellite signal was not received because of the unavailability of the transmitter or rare failures of the receiver.

Space diversity studies were accomplished with a radiometer and a receiver located at Balcones Research Center and a second radiometer and a second receiver located on the main campus of The University of Texas (UTC) at a distance of 11 km to the south. This distance was selected based on the results of the ATS-5 satellite experiments which indicated that thunderstorms that produced attenuation of a severe nature are commonly less than 12 km in diameter. The thunderstorms with widths less than the separation of the terminals would not be covering both stations at the same time.

Data obtained from the Weather Bureau both by radar and by other techniques were compared to the measured attenuations to try to extrapolate the measurements made in Austin to other sites which might later be used for ground terminals and for which similar meteorological data are available. For this extrapolation, an understanding of the nature of the thunderstorm is important background information. The results of studies made on the ATS-5 satellite indicated that severe attenuations were experienced only during the periods of very severe thunderstorms. The area around Austin, Texas, has a relatively high number of thunderstorms per year and, therefore, provides a location where this effect can be studied effectively.

Ground station instrumentation and the operational procedures and statistics are described in the following section. The meteorological characterization of Austin includes a general climatologic description and various relevant statistics published by the U.S. Weather Bureau. Where and how the weather data were obtained is also explained. The results of the measurements are given both from single site and diversity points of view, and conclusions are presented in the final sections.

GROUND STATIONS

Instrumentation

Antennas

The two ground stations had different antenna systems. The northern site, Balcones Research Center (BRC), utilized two 3-m parabolic dishes attached side by side to one azimuth-elevation, steerable, converted ballistic radar mount (see figure 1a). The pointing of these antennas was controlled by the observer with setting accuracy within 0.03°. Both antennas had prime focus feeds. For this purpose each had a 30-cm-long aluminum cylinder with 23.5-cm-diameter mounted at the focus which served as a universal receiver box. The side that pointed toward the dish was covered by a half sphere, 7.5-cm-radius plexiglass radome with the focal point at its center. The thickness was selected to achieve a quarter wave match at either 20 or 30 GHz, and reflections off the radome were minimized. The outside was coated with water repellant (Silanox 101) causing immediate beading and runoff of any water. The antenna for the second site (on the main campus of The University of Texas) was a 1.5-m converted searchlight (see figure 1b). It was outfitted with a stepping motor

and digital shaft encoders to allow automatic pointing in azimuth and elevation to within 0.02°. This antenna had a prime focus feed support structure. For the simultaneous operation at 20 and 30 GHz, the feeds were placed into the focus side by side. This caused the two beams to be slightly divergent. The front of the antenna was covered with a plexiglass plate (matched to 20 GHz and coated with water repellant) that enclosed both the antenna and the receiver box.

To prevent condensation, refrigerated air was blown into this cavity. Minimum elevation angles at BRC were 15° to the east and west because of the structure of the mount; elevation angles were about 35° on campus because of adjacent buildings.

Satellite Receivers

The 30-GHz satellite receivers had superheterodyne front ends in which 28.95-GHz crystal multiplier local oscillators were mixed with the signal from the feed into a 1.05-GHz IF. This allowed the utilization of back ends built for the ATS-5 experiment by Martin-Marietta Corporation. These receivers have been documented elsewhere (Martin-Marietta, 1969). They are phase-locked loop receivers in which the downconverted carrier is locked to a 10-MHz crystal oscillator. The noise bandwidth of these receivers is 50 to 100 Hz. With the typical 12-dB single sideband (SSB) noise figure of the mixers the noise power P_N of the receivers $P_N = kTB$ is -142 dBm. To improve the reliability of the local oscillators in continuous operation even during the hottest summer weather, all active front end components were mounted on a water-cooled plate. This plate could be inserted into the focal cylinder of the 3-m antenna or into the support structure of the 1.5-m antenna. Figure 2a is a block diagram of the satellite receivers. The fade margins when the satellite was pointed at Rosman, North Carolina, and when transmitting through the 30-GHz horn antenna were better than about 33 dB for both receivers. The only difference between the 3-m and 1.5-m antenna systems can be explained by the fact that the 3-m dish is degraded at 30 GHz, and the mixer with the better noise figure was used for the smaller antenna.

Radiometers

The 20-GHz sky-noise radiometers were Dicke switched receivers. Their local oscillator frequency was chosen to coincide with the first lower sideband frequency of the 20-GHz satellite transmitter at 19.82 GHz. Thus it was ensured that the 30-MHz IF (total bandwidth = 20 MHz) would not allow any satellite signals to introduce errors into the measurements. For additional isolation, the radiometers were approximately cross-polarized to the satellite signals. Even during clear air propagation conditions, no satellite signals were ever noted in the radiometer outputs. A plot of the spectrum is given in figure 2b.

The sensitivity of the radiometers was approximately 1 K with a 1-s integration time. Their block diagram is given in figure 3. The components were mounted on a water-cooled plate. For the searchlight system they shared the plate with the satellite receiver.

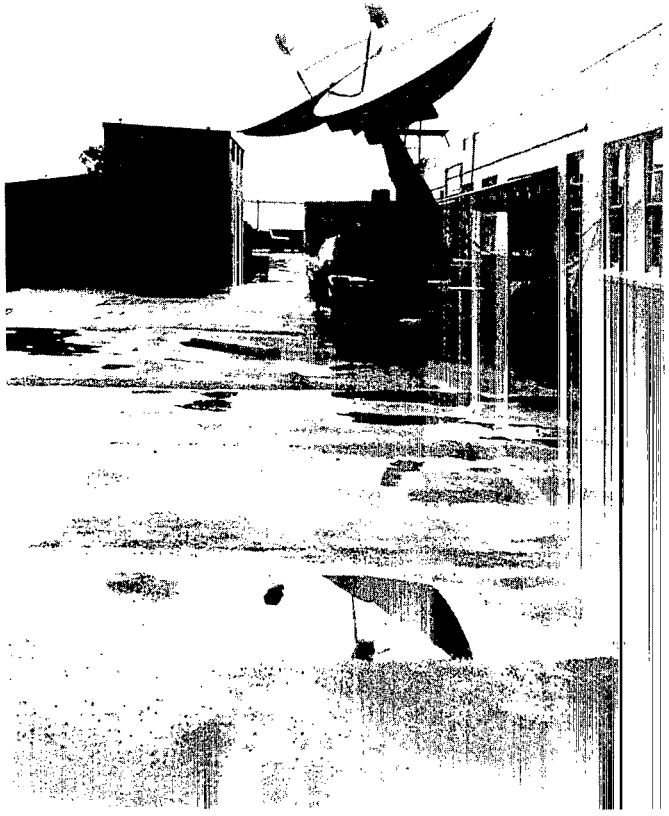

Figure 1a. Balcones Research Center antenna system.

Figure 1b. University of Texas campus site antenna.

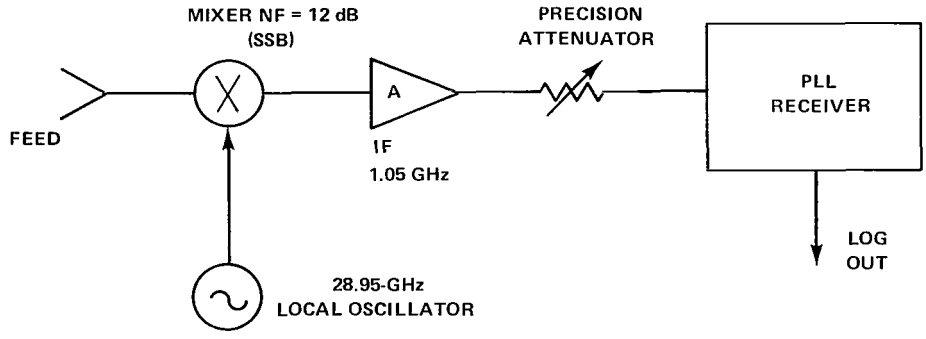

Figure 2a. Satellite receiver block diagram.

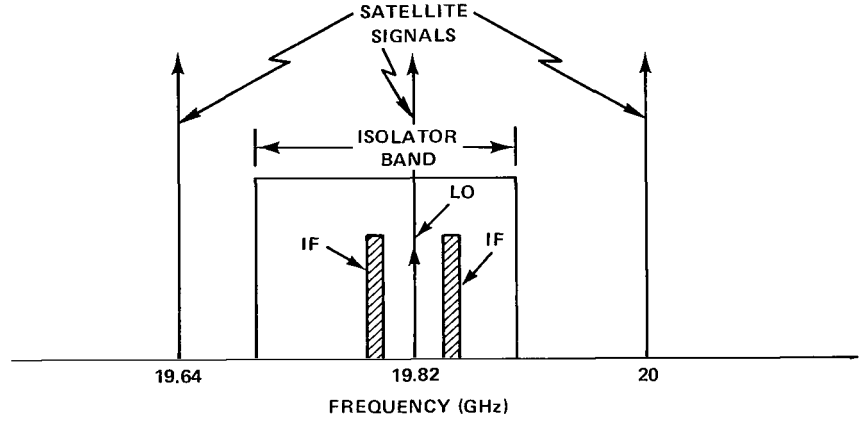

Figure 2b. Spectrum for 20-GHz radiometer.

Station Location

Site 1, at BRC, was located at the northern edge of Austin, Texas. Its coordinates are shown in figure 4. Site 2 on the campus of The University of Texas was 11 km south of site 1. Figure 5 gives the relevant data and shows that the two sites were almost aligned along the direction of the satellite.

Calibration

Satellite Receivers

Because of weight and space limitations for the front end, all calibrations were performed by attenuating the satellite signal with a calibrated attenuator during periods when no rain was in the propagation path. Because the attenuation was introduced in the IF (1.05 GHz–

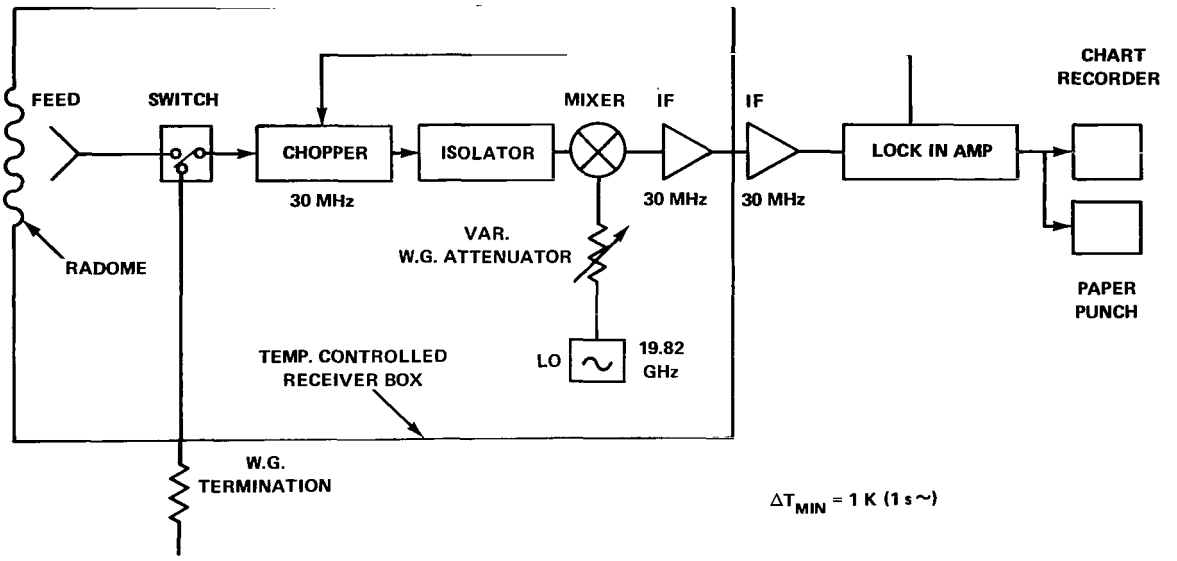

Figure 3. Radiometer system simplified block diagram—20 GHz.

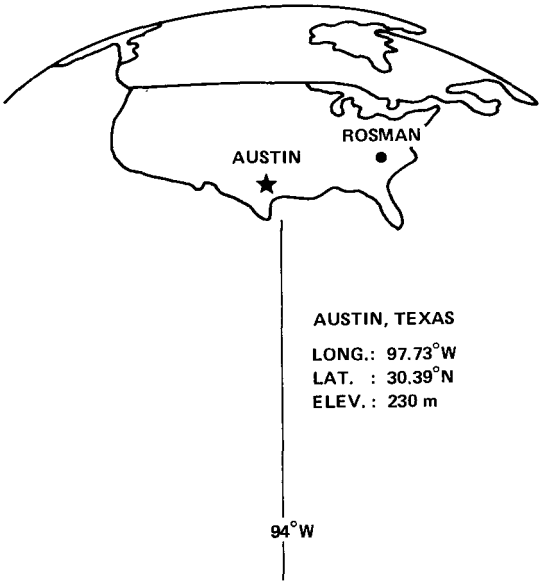

Figure 4. Geography seen from the satellite.

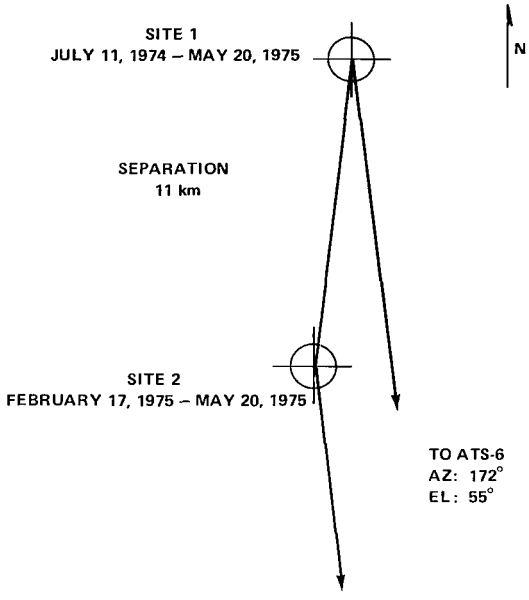

Figure 5. Station layout in Austin, Texas.

BRC site; 60 MHz—campus site), noise generated in the front end was attenuated also. Therefore the attenuation at 30 GHz has to be related to the attenuation at the IF level by

$$L_{RF} = L_{IF} + \left\{(SNR - 10 \log (10^{SNR/10} - 10^{L_{IF}/10} + 1)\right\} \quad (1)$$

where SNR is the signal-to-noise ratio in dB under clear weather transmission condtions. L_{RF} and L_{IF} are the RF and IF attenuation in dB. Because of the difficulty in exactly measuring the SNR of the phase-locked receiver for all the possible clear-air levels which existed for the many combinations of pointing and mode of the spacecraft, the data analysis was restricted to a maximum fade depth of 25 dB. For these levels the above relation simplifies to

$$L_{RF} \approx L_{IF} \quad (2)$$

Calibrations were performed as frequently as the weather and the operation of the satellite allowed. At the BRC station, this was typically at least once for each turn-on period and each spacecraft pointing. At the automated receiver site on campus, calibrations were usually made once during days with attenuation events. The accuracy of the calibrations is estimated to be ± 0.5 dB.

Radiometers

The radiometers were calibrated about once a week during cloudless periods. Because they operated in a temperature controlled environment of about 313 K, the "hot" point was found by disconnecting the IF preamplifiers from the IF amplifier. The output then corresponds

to a zero signal level at the chopper frequency and equals the temperature of the chopper, typically 313 K. The second point to define—the linear relationship between sky temperature and radiometer output voltage—was found by calculating the clear-air, sky-noise temperature from a measurement of the absolute ground humidity, resulting in typical sky temperatures of between 15 and 25 K. This method of calibration has the advantage that the losses from the input of the antenna to the output of the feed need not be measured. It is estimated that the absolute accuracy of the calibrations is ± 5 K at low sky temperatures and ± 2 K at high sky temperatures.

Clocks

Because the data from each of the two stations had to be compared, another calibration was required, consisting of synchronizing a 60-Hz clock at each site. This was done with a WWV receiver and through telephone communications. The clocks were checked regularly and discrepancies were kept to less than 1 s.

Operation

Regular observations of the 30-GHz satellite signal started at the BRC site on July 11, 1974, and lasted until May 20, 1975, for a total of 314 days. The 20-GHz radiometer at this site was put into operation on October 30, 1974, and continued until May 20, 1975, for a total of 203 days. During the period from July 11, 1974, to October 30, 1974, the time required to make the station operational was the same as required for satellite transmitter turn-on. This fact, combined with a relative high priority, ensured that few attenuation events were missed.

The geographical location of Austin (see figure 4) proved to be of significant advantage. Regardless of the pointing of the spacecraft, the Austin station was nearly always within the 3-dB beamwidth of the 30-GHz horn. Therefore, the transmitter could be utilized while other experiments were conducted (as long as no other restrictions on the satellite prevented this). All systems, except the antenna drive, were in continuous operation or standby. This allowed monitoring of the system, eliminated warm-up problems, and ensured instantaneous response to the weather. The antenna was pointed manually for satellite observations with the pointing coordinates supplied to us by the ATS Operations Control Center (OCC) and peaked regularly.

The second station, on the University of Texas campus, was in operation from February 17, 1975, to May 20, 1975, for a total of 93 days. This station's operations were fully automated. The antenna was pointed at all times by the antenna controller which also used the ATSOCC-supplied pointing data as input. The phase-lock loop (PLL) receiver continuously searched over a range of ± 12 kHz around the 30-GHz carrier and locked on to the signal when present. The outputs from the radiometer and the receiver were sampled every 10 min in clear weather and every 20 s when the sky temperature exceeded 80 K. The data, with the time and rain-gage information, were then punched on paper tape.

METEOROLOGY OF AUSTIN

Thunderstorm Climatology for Central Texas

High attenuation events were always associated with thunderstorms in the Austin area. The storm climatology is given to help in the interpretation of the attenuation data.

Information on thunderstorms in central Texas is given in table 1. The frequency of occurrence refers to the mean over a 30-year observational period and was obtained from National Weather Service data for Austin, Texas. The other information was obtained from William Hare, Meteorologist in Charge at the National Weather Service Meteorological Observatory, Radar Center, Hondo, Texas. Data obtained from the radar at Hondo (which includes Austin in the scope area) for the two years this site has been in operation were used. These data should be fairly representative of the Austin area. Cloud (thunderstorm) tops are given in 1000's of meters (feet) above mean sea level, the translational speed of the individual rain cells is given in m/s (knots), and the direction of movement of the rain cells is given as the direction from true north from which the cell is moving. It should be noted that when the showers are arranged in a line (a squall line), as they frequently are in the spring (March through May), the line usually moves from 300° to 310° (i.e., from the northwest). The individual shower cells within the line, however, move in the direction as indicated in table 1. Thunderstorm frequency is bimodal, as shown.

Table 1
Thunderstorm Statistics for Central Texas

Month	Frequency of Occurrence	Height of Cloud Tops meters (ft)	Cell Speed m/s (knots)	Direction of Movement degrees
January	1	8.51 (28)	12.8 (25)	240
February	2	9.12 (30)	15.4 (30)	250
March	3	11.55 (38)	17.9 (35)	270
April	5	12.16 (40)	15.4 (30)	250
May	7	12.76 (42)	12.8 (25)	240
June	4	10.64 (35)	10.3 (20)	180
July	4	9.72 (32)	7.7 (15)	170
August	5	9.72 (32)	7.7 (15)	150
September	4	12.16 (40)	12.8 (25)	230
October	3	11.55 (38)	12.8 (25)	230
November	2	9.12 (30)	12.8 (25)	240
December	1	8.51 (28)	12.8 (25)	240

Thunderstorm frequency is bimodal, as shown in table 1. The highest observed mean frequencies occurred in May and August (though the standard deviation is very large throughout the year). Maximum cloud tops occur almost concurrently with maximum frequency. Translational speed of individual cells is at a maximum in early spring (March) when mean wind speeds within the troposphere at this location are at a maximum. Minimum speeds are observed in late summer. The direction of movement of individual cells has a strong southwesterly-to-westerly component most of the year, except in the summertime when cells move from the south (June) to southeast (August).

Meteorology for July 11, 1974, to May 20, 1975

The 40-year mean rainfall for July 11, 1974, to May 20, 1975, is 78.8 cm (31.04 in.) with a standard deviation of 22.25 cm (8.76 in.). The amount measured for this time period was 87.63 cm (34.5 in.). During this 314-day period, there were 54 days with more than 0.25 mm (0.1 in.) total precipitation. Significant attenuation events, defined by the 30-GHz attenuation exceeding 3 dB and/or the 20-GHz sky temperature exceeding 80 K, were measured on 50 days.

A total of 37 thunderstorms occurred. The direction from which the rain cells were moving and their speed are given in figure 6. The mean direction was 233° and the mean speed was 37.7 km/hr (20.4 knots). The tops of the clouds extended from 3 km to 15.2 km. Their relation to the measured attenuations will be given later.

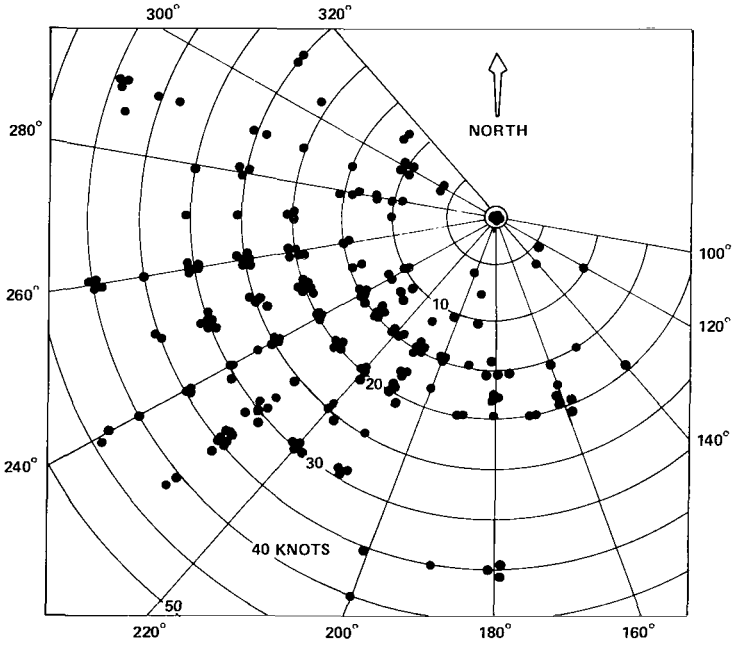

Figure 6. Direction from which storm cells moved and their speed (1 knot = 0:514 m/s) (July 11, 1974, to May 20, 1975).

Another quantity obtainable from the Weather Bureau is the grid value. It is a numerical indication, manually derived from a weather radar, of the rain intensity and percent coverage of the grid. The grid including Austin is a square with 80.47-km sides. The grid values are the integers 0 through 9. Their interpretation is given in table 2. The last column in the table gives the percentage of time (based on hourly reporting intervals by the Weather Bureau) assigned to each value for the Austin area.

Table 2
Interpretation of Weather Bureau Grid Values*

Grid Value Code No.	Maximum Observed VIP Level	Coverage in Box	Rainfall Rate mm/hr	Intensity Category	Austin Grid % Time
0	No echoes				85
1	1	Any VIP1	< 2.5	Weak	5.4
2	2	$\leqslant 1/2$ of VIP2	2.5 - 12.7	Moderate	3.7
3	2	$> 1/2$ of VIP2			
4	3	$\leqslant 1/2$ of VIP3	12.7 - 25.4	Strong	1.1
5	3	$> 1/2$ of VIP3			
6	4	$\leqslant 1/2$ of VIP3 and 4	25.4 - 50.8	Very Strong	0.73
7	4	$> 1/2$ of VIP3 and 4			
8	5 or 6	$\leqslant 1/2$ of VIP3 4, 5 and 6	> 50.8	Intense or Extreme	0.35
9	5 or 6	$> 1/2$ of VIP3 4, 5 and 6	> 50.8	Intense or Extreme	

*Ignore additional coverage by weak echoes for all DR code numbers above 1. Intensity categories and rainfall rates correspond to maximum observed VIP levels.
Priority for additive data group giving row-column position of blocks with present or past severe weather or lines is: 1 +, 2, 3/.
No box shown more than once, group in left-to-right, top-to-bottom order.

RESULTS

Single Site

The 20-GHz sky noise temperature and the 30-GHz attenuation of the satellite signals are shown in figure 7 as they were recorded on paper charts during one typical rain storm. One notes that a general agreement between crests and valleys exists. The sky temperature curve seems to be relatively smoother, however. This can be explained with the following argument. The 20-GHz beam is wider for the same size antenna (compared to 30 GHz), and the noise power is received from the whole volume of the beam; whereas, the 30-GHz

attenuation is caused by precipitation close to the line-of-sight. Other variations can be expected because of changes in the drop size distribution or by frozen particles in the path.

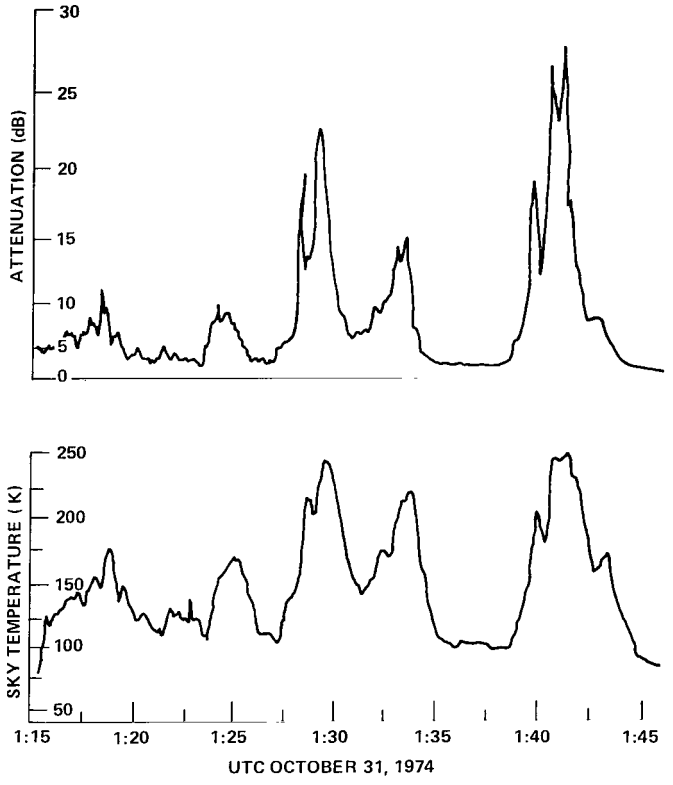

Figure 7. 30-GHz attenuation and 20-GHz sky temperature.

Assuming the rain to be an absorbing, nonscattering medium with a physical temperature of 284 K, the measured noise temperature T_{sky} can be converted to attenuation A with

$$A = 10 \log \left[\frac{284}{284 - T_{sky}} \right] \quad \text{dB.} \tag{3}$$

This formula can be derived from the theory of radiative transfer (Kraus, 1966). It can be used with reasonable accuracy for attenuations of up to about 10 dB. Figure 8 shows the measured 30-GHz attenuation plotted versus the calculated 20-GHz attenuation for the BRC site. Each point represents a sample taken at 1-min intervals for most of the periods for which such simultaneous data were available. The average ratio between the two attenuations is 2.65. The straight line drawn through the points does not intercept at (0, 0) because the 30-GHz values do not include the attenuation caused by oxygen and water vapor. The 20-GHz attenuations include these losses because they contribute to the sky noise temperature. Therefore, to find the attenuation ratio due to precipitation, the abscissa zero

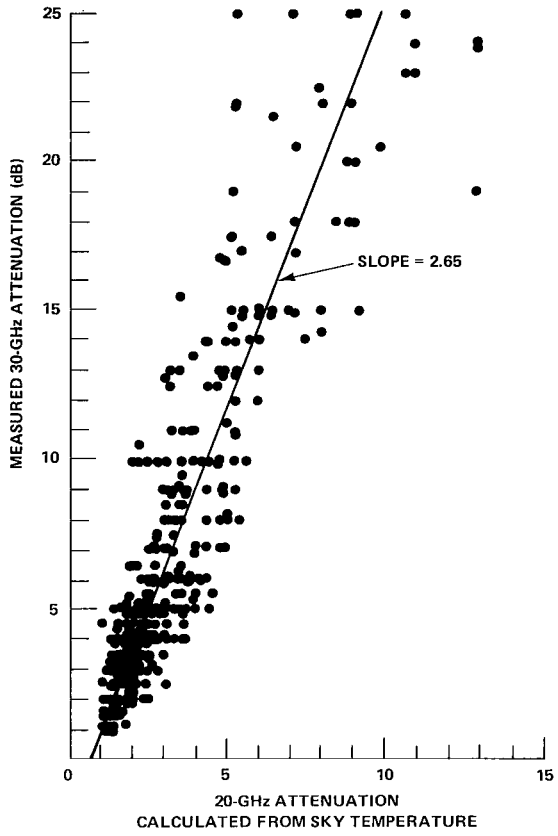

Figure 8. 20-GHz versus 30-GHz attenuation from July 11, 1974, to May 20, 1975, at the BRC site.

should be shifted to the intercept. Figure 9 shows the same kind of plot for data collected on April 28, 1975, at the campus site with essentially the same slope. The spread of the points in figure 8 is larger than in figure 9 because the values were taken from strip chart recordings at the BRC site as compared to digital recordings at the campus site. The relationship between the 20-GHz and the 30-GHz values is well enough defined to allow an estimation of the 30-GHz attenuation from 20-GHz sky temperature data.

The fade histogram for the 30-GHz attenuation at the BRC site from July 11, 1974, to May 20, 1975, is given in figure 10. The dark areas derive from direct measurements, and the light ones are based on the 20-GHz sky temperature for times when the satellite was not available. The 5-dB level, for instance, was exceeded for a total of 18.17 hours while the satellite was on and for 11.45 hours while it was off. Table 3 summarizes these results. The satellite was available for an average of 61.4 percent of the measured attenuation events. As stated earlier, the availability was much higher before November 1974 than afterward.

Table 3
Summary of the Fade Histogram (figure 10) Results

Attenuation exceeded at 30 GHz	Time (hrs) Satellite		Total (hrs)
	On	Off	
5 dB	18.17	11.45	29.62
10	8.45	4.33	12.76
15	5.73	3.33	9.07
20	3.37	2.35	5.72
25	2.55	1.82	4.37

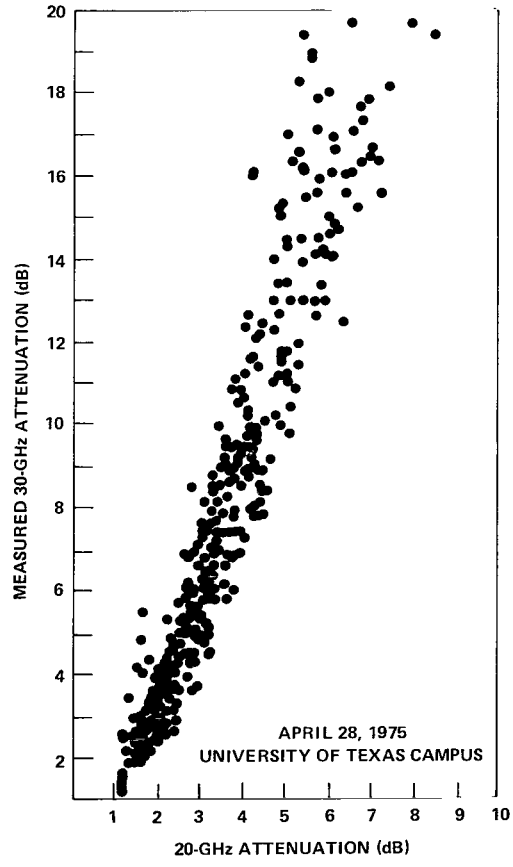

Figure 9. 20-GHz versus 30-GHz attenuation.

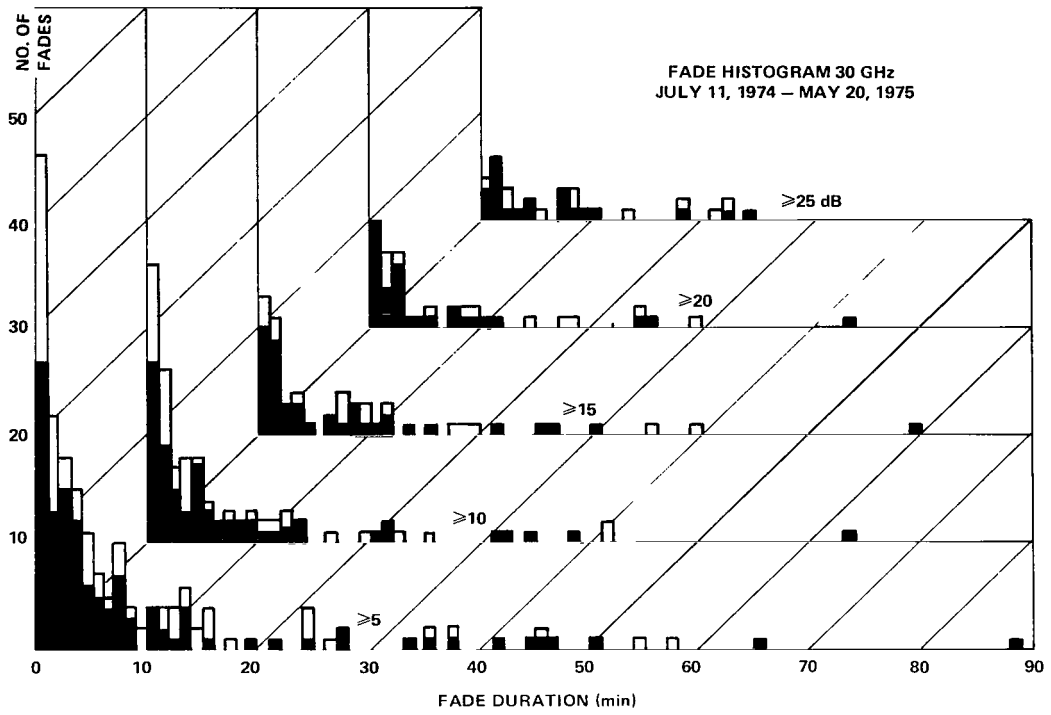

Figure 10. Fade histogram.

The cumulative probability in percent of time the 30-GHz attenuation exceeds a certain fade depth is given in figure 11 for fades between 5 and 25 dB. It can be seen that in Austin, Texas, 10-dB attenuation is exceeded at 30 GHz for 0.17 percent and 25 dB for 0.058 percent of the time. This corresponds to about 15 and 5 hours, respectively, on an annual basis.

A comparison of rain rates (measured with one tipping bucket at the antenna) with the attenuation at 30 GHz as given in figure 12 shows that it is not possible to predict the fade depth from point rain data. The effective path lengths L that have been added to the plot are based on the theoretical relationship between rain rate and attenuation for homogeneous rain. They vary over an order of magnitude for a given rate. A statistical comparison of these data also has been made. For this purpose, the attenuations A and rain rates R for equal cumulative probabilities were compared. The effective cloud heights were then derived with

$$H_{eff} = \frac{A}{A_{theoretical}\,(R)} \times \sin(\text{angle of elevation}) \qquad (4)$$

The results are given in table 4. From these data one would conclude that the highest attenuation occurs when the clouds are lowest. This is probably due to the higher probability of rain occurring at the gage when clouds are low. The data, in table 4, are in contradiction

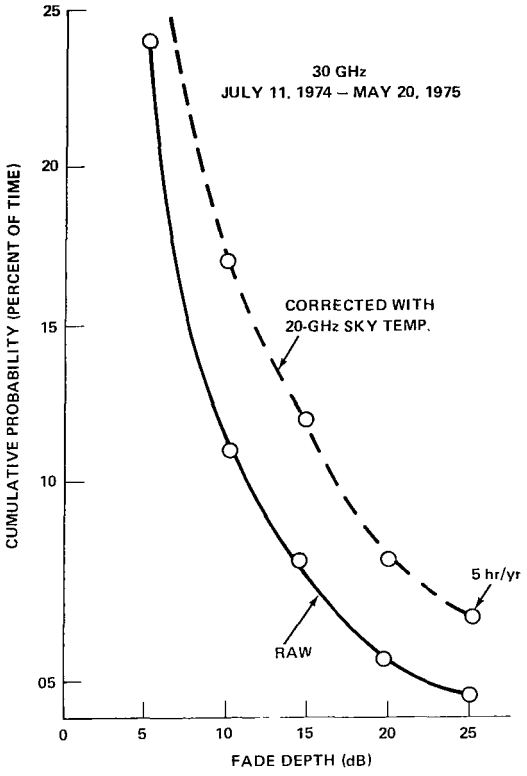

Figure 11. Cumulative fade probabilities at 30 GHz.

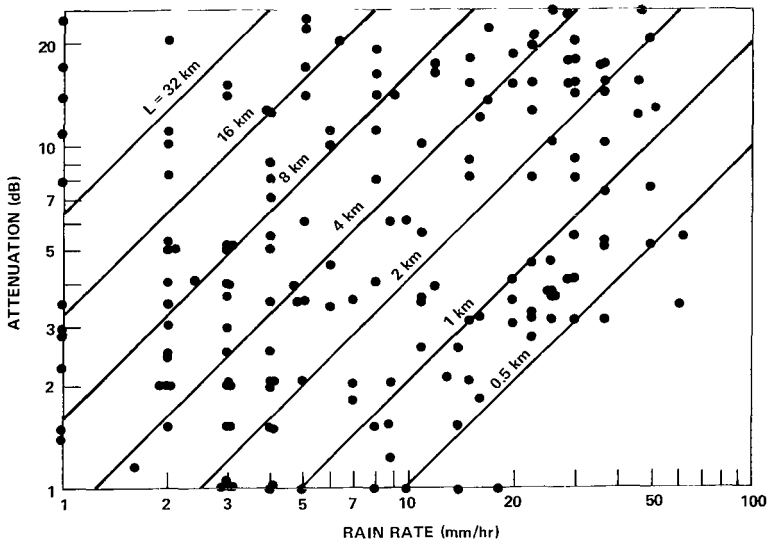

Figure 12. Attenuation versus point rain rate.

to the results from the ATS-5 experiment, where a direct correlation of attenuation with cloud heights was found (Straiton, 1971). It also does not agree with the cloud height data obtained from the Weather Bureau for this experiment. Figure 13 is derived from the hourly location reports. It gives the maximum cloud height within the radar range of the weather station (40,250 km^2 (250 X 250 mi)) including the Austin area versus the maximum attenuation at 30 GHz that was measured. This figure establishes a minimum cloud top height increasing roughly linearly with increasing attenuation. The scatter of points above this line relates to the fact that higher clouds were present at other locations and did not cause attenuation at the receiver site. The relation between attenuation and cloud height suggested by figure 13 is roughly

$$A = 1.62 \cdot H \cdot \text{cosec}\,(\epsilon)\ \text{dB} \tag{5}$$

where H is the cloud height in km and ϵ is the angle of elevation.

Figure 14 is a plot of the attenuation versus the associated values assigned by the Weather Bureau radar at Hondo for the Austin grid. Because of the areal extent of the grid, a correlation of attenuation versus grid value is not apparent.

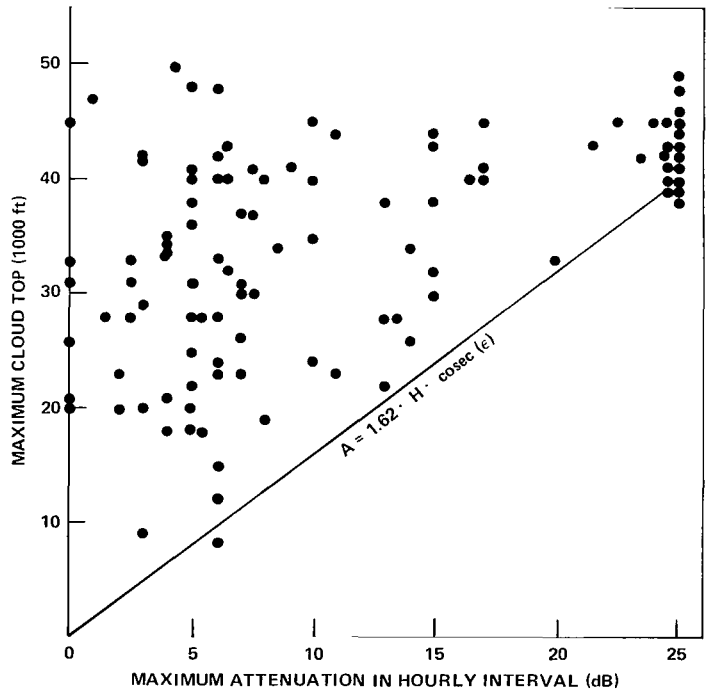

Figure 13. Cloud top height versus attenuation at 30 GHz (1 ft = 0.304 m).

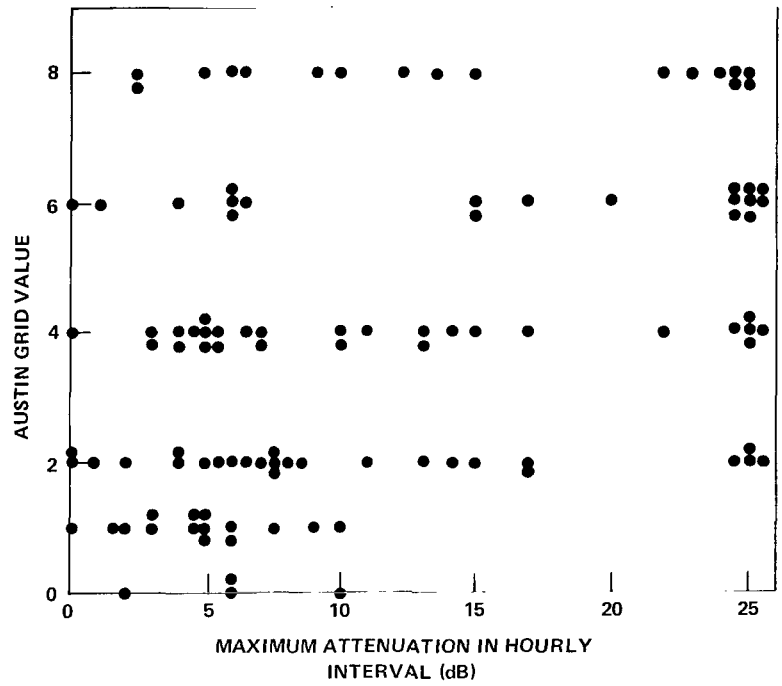

Figure 14. Grid value versus attenuation at 30 GHz.

Space Diversity Results

The measured cumulative probabilities of the fade depth for the single sites and the joint probability for the pair of satellite receivers operating at 30 GHz have been plotted in figure 15. In these plots, use has been made of the 20-GHz sky temperatures to augment the fade data for times of satellite unavailability. For the single sites, the 93-day campus statistics and the 314-day BRC statistics agree very closely. The 93-day BRC probabilities deviate for the higher fades. This type of behavior can be expected, considering the relatively short period of sampling. In this plot, 100 percent of the time represents the total 93 days of common operation. If one were to multiply the single site probabilities to get the joint probability of fades with zero correlation, the measured joint probability is far above the calculated value, indicating that some correlation of attenuation at the two sites existed. Naturally, during the extended periods of clear weather, both stations are correlated. Therefore, the curves have been redrawn in figure 16 as conditional probabilities. The 100 percent time base is now the time during which the attenuation exceeded 2 dB at either station, thereby eliminating the correlated clear weather data. It can be seen that the joint probability approaches the squared, single site probability much closer. The result would differ if one conditioned the probabilities on another fade level. The diversity

Table 4
Probabilistic Effective Cloud Heights

Attenuation dB	Rain Rate mm/hr	A Theoretical dB/km	Effective Cloud Top Height meters (ft)
Exceeded for Equal Percentage			
5	3.4	0.6	6718.4 (22,100)
10	7	1.3	6201.6 (20,400)
15	9.6	1.75	6900.8 (22,700)
20	17.5	3.2	5046.4 (16,600)
25	24	4.4	4590.4 (15,100)

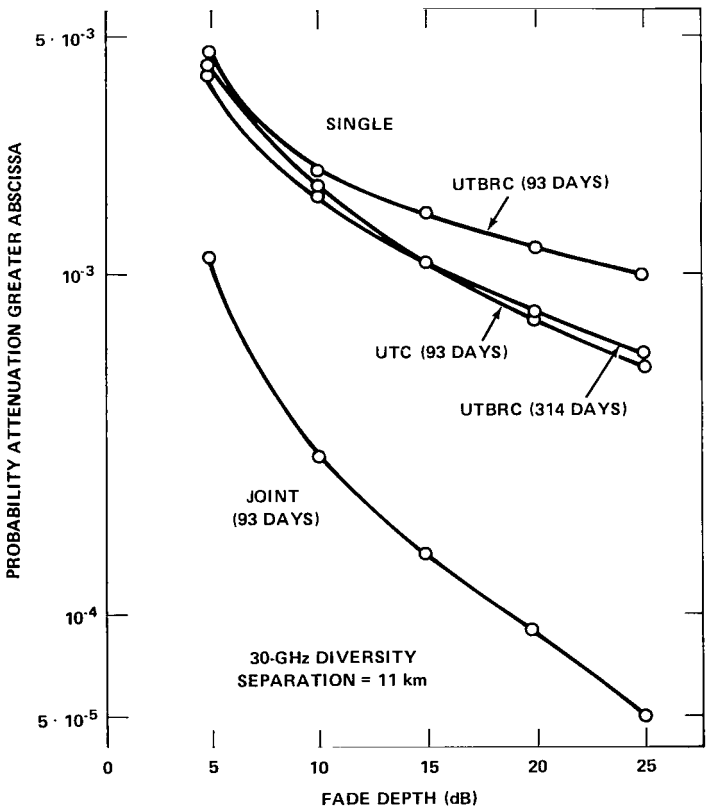

Figure 15. Diversity results.

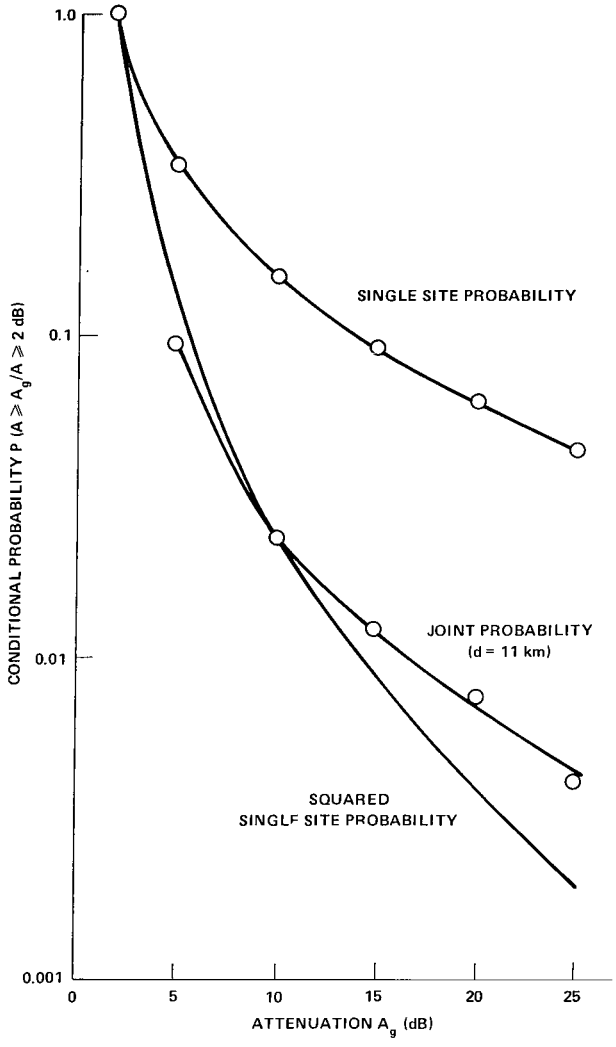

Figure 16. Conditional space diversity for A ≥ 2dB.

gain has been defined by Hodge (1973) as the reduction in fade depth for equal probabilities. This gain has been plotted in figure 17 versus the single station attenuation. The points lie on a straight line defined by

$$\text{diversity gain} = (0.7)\ \text{attenuation}. \tag{6}$$

Another approach is to determine the diversity advantage which is the factor by which the probability that simultaneous fades exceed a certain level is decreased. In our case, this value varies between 3 and 11 for attenuations between 5 and 25 dB. The curve is given in figure 18.

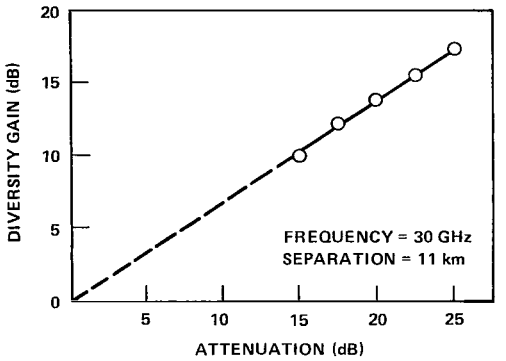

Figure 17. Diversity gain as a function of single site attenuation.

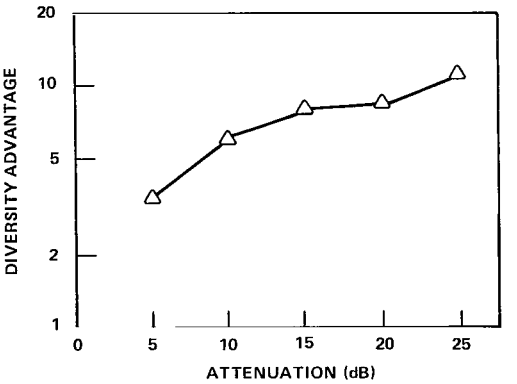

Figure 18. The diversity advantage of two receiver sites at 30 GHz.

CONCLUSIONS

Satellite propagation experiments that require unscheduled transmission in response to the weather while all other experiments sharing the spacecraft can be scheduled ahead are at an obvious disadvantage when it comes to full coverage of all fade events. Despite this, nearly complete coverage was achieved because (1) the geographical location of the stations and the type of measurements made allowed reception largely independent of the spacecraft pointing, and (2) the simultaneous operation of 20-GHz radiometers served both as an effective way of judging if the conditions required a request of the satellite transmitter and, if the request was denied, the sky temperature data could be used to derive the 30-GHz attenuation.

If commercially operating satellite communication links are restricted to a 10-dB fade margin (e.g., for economic reasons), then our measurements show that one station in Austin would achieve 99.83 percent reliability, and a diversity pair with 11-km separation would achieve 99.99 percent reliability, as far as weather influences are concerned. To achieve the same reliability with only one station, the fade margin would have to be increased by over 20 dB, which may be infeasible.

Of all the weather data obtained from the U.S. Weather Bureau, the maximum cloud tops show the best correlation to the attenuation data. It should be worthwhile to make such measurements directly at the site of a propagation experiment to exclude the points in figure 13 not relating directly to the experiment site. A linear relation between attenuation and cloud height is suggested by the data. Other weather parameters, such as rain rate or grid value, show very little promise of allowing an estimate of attenuations. Many of the Weather Bureau data are qualitative rather than quantitative and are not well suited for analysis.

REFERENCES

Hodge, D. B., "Space Diversity for Reception of Satellite Signals," Ohio State University, Columbus, Ohio, Tech. Rept. 2374-16, October 1973.

Kraus, J. D., *Radio Astronomy*, McGraw-Hill Book, Co., N.Y., 1966.

Martin-Marietta Corporation, "15.3 GHz Ground Receiver Systems for the ATS Millimeter Wave Propagation Experiment," Final Technical Report, Report No. OR 10265, September 1969.

Straiton, A. W., W. J. Vogel, and B. M. Fannin, "ATS-5 Signal Characteristics at 15.3 GHz and Related Experiments at 15 and 35 GHz," Part I, Final Technical Report ATS-5 Millimeter Wave Experiments, Electrical Engineering Research Laboratory, The University of Texas, Austin, Texas, 1971.

Straiton, A. W., "The Absorption and Reradiation of Radio Waves by Oxygen and Water in the Atmosphere," *IEEE Trans. Antennas Propagation*, **AP-23**, July 1975.

Vogel, W. J., B. M. Fannin, and A. W. Straiton, "Polarization Effects for Millimeter Wave Propagation in Rain," Electrical Engineering Research Laboratory, The University of Texas, Austin, Texas, Tech. Rept. No. 73-1, December 1973.

INITIAL RESULTS OF THE OHIO STATE UNIVERSITY 20- AND 30-GHz ATS-6 PROPAGATION MEASUREMENTS

D. B. Hodge, D. M. Theobold, and R. C. Taylor
The Ohio State University
Columbus, Ohio

INTRODUCTION

This program is motivated by the increasing demand for utilization of the frequency spectrum above 10 GHz. The kinds of usage under current development range from remote sensing to communications. Nevertheless, the reliable usage of these frequencies, whatever the application, is extremely dependent upon a thorough knowledge of the interactions between propagating millimeter waves and precipitation. In particular, the severest atmospheric attenuation rates are encountered during periods of intense rainfall; this attenuation is also accompanied by increased radiometric noise emission and scattering. In the case of satellite applications, these effects can occur on slant paths from the earth's surface upward to heights on the order of 10 to 20 km and, thus, cannot be measured on terrestrial propagation paths.

The objective of this experiment is to determine the reliability improvement resulting from the use of path diversity on millimeter wavelength, earth-satellite communication links. This will be accomplished by measuring the path attenuation observed on 20- and 30-GHz ATS-6 downlinks at two spatially separated ground terminals. Radiometric noise emission at 20 and 30 GHz along these same propagation paths will also be recorded for correlation with the attenuation date. A third remote terminal will record 20-GHz radiometric noise emission along a propagation path directed toward the position of the ATS-6 satellite to provide an additional estimate of path attenuation and diversity performance. Measurements of radar backscatter and radiometric noise emission at 3, 9, and 15 GHz over the regions through which the propagation paths to the remote terminals pass will also be made using the Ohio State University (OSU) high resolution radar/radiometer system and the OSU low resolution radar system. Finally, a cooperative experiment with the COMSAT Corporation will provide uplink attenuation on four spatially separated propagation paths at 17.8 GHz and on one path at 13.2 GHz

LOCATION OF GROUND TERMINALS

The ground terminals are located approximately as shown in figure 1. The three OSU terminals (fixed, transportable, and unmanned) located approximately at the vertices of an

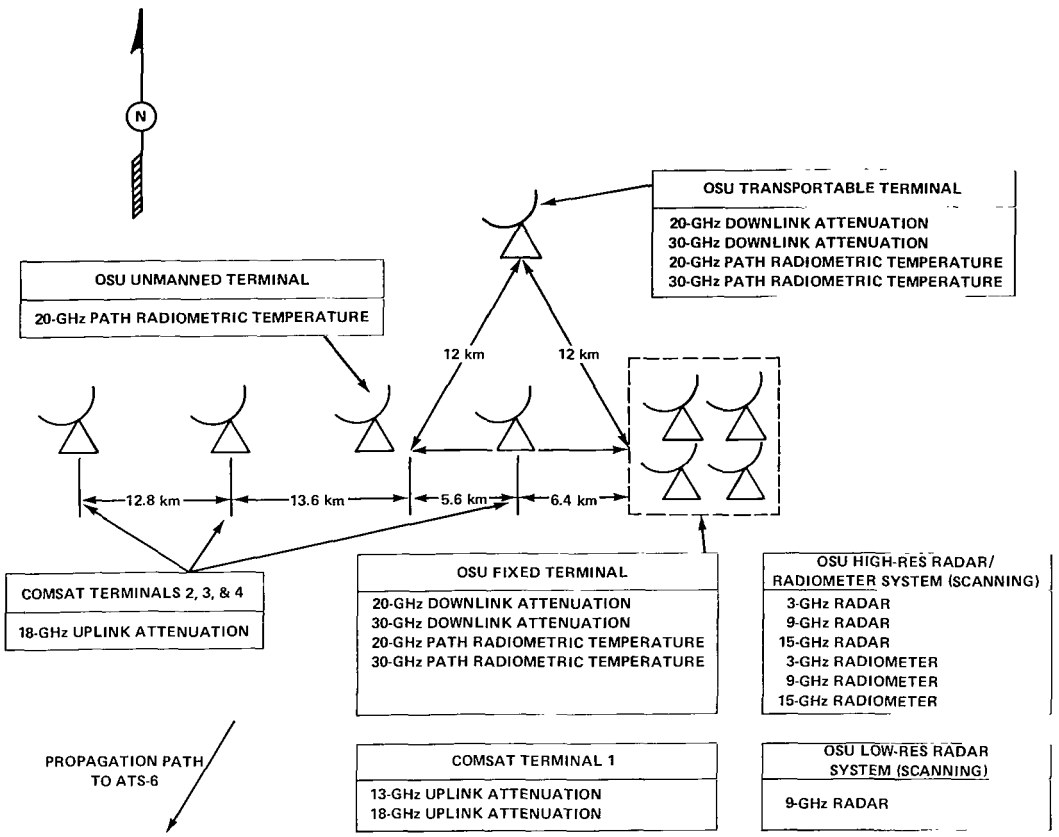

Figure 1. ATS-6 diversity experiment, ElectroScience Laboratory, Ohio State University, Columbus, Ohio.

equilateral triangle having 12-km sides are shown in figures 2, 3, and 4. This arrangement permits one baseline to be oriented along the east-west baseline chosen by the COMSAT Corporation and, consequently, provides correlation with their data. The second baseline is oriented in nearly a northwest-southeast direction, the direction for which optimum diversity improvement is expected (Strickland, 1973). This orientation also permits correlation with data resulting from the ATS-5, 15.3-GHz millimeter wave experiment (Hodge, 1972). The third baseline is almost perpendicular to the optimum orientation for the purpose of comparison. The spacing of 12 km was chosen because nearly optimum performance is expected for terminal spacings greater than 8 to 10 km (Hodge, 1973). Also, because all three baselines are nearly equal, direct comparisons of the resulting data are possible.

A summary of the types of observations and frequencies at the various terminals is presented in table 1.

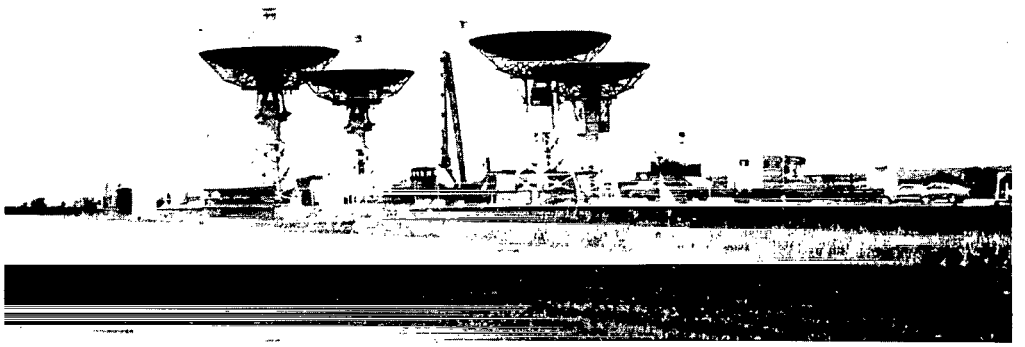

Figure 2. OSU fixed terminal.

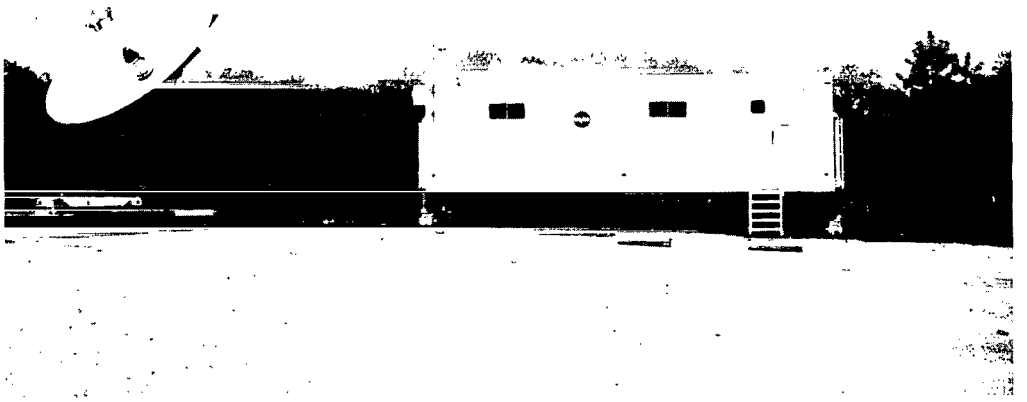

Figure 3. OSU transportable terminal.

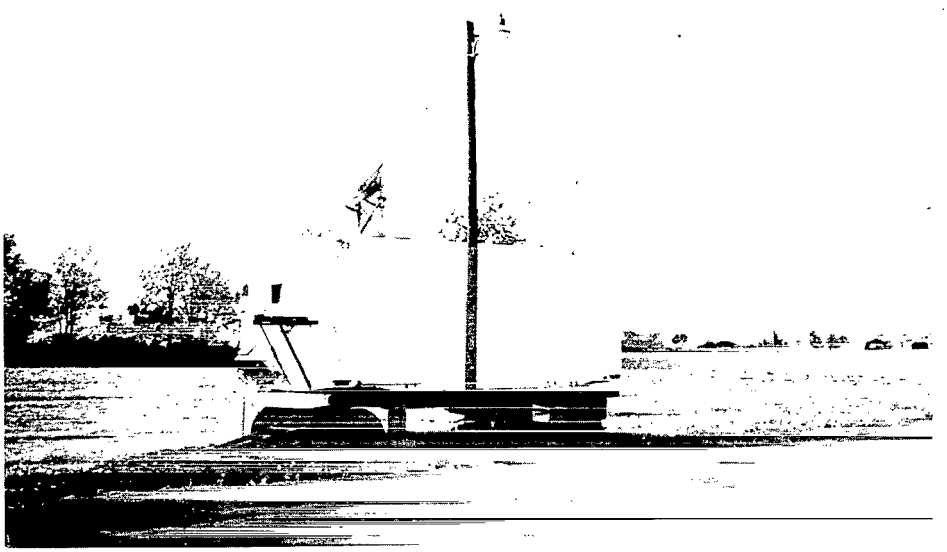

Figure 4. OSU unmanned terminal.

Table 1
Frequencies and Types of Measurements at the Various Terminals

Freq. GHz	Fixed Terminal	Transportal Terminal	Unmanned Terminal	Outlying COMSAT Terminals
3.1	S T			
9.3	S T			
13.2	A			
15.6	S T			
17.8	A			A
20	A T	A T	T	
30	A T	A T		

A = Attenuation T = Radiometric Temperature S = Radar Backscatter

TRANSPORTABLE TERMINAL

The OSU transportable 20/30-GHz ground terminal is housed in a 2.3- by 9-m semitrailer. The heating and cooling unit for the semitrailer is contained in a small 2-wheel trailer, and the 4.6-m parabolic antenna is mounted on a 2.4- by 5.5-m trailer.

The primary transportable terminal instrumentation consists of the 20- and 30-GHz receiver/radiometers. These NASA-supplied receiver/radiometers were built by the Martin-Marietta Corporation and are described in detail.* The output of these receivers and radiometers is sampled, digitized, and merged with terminal status bits. The resulting digital data blocks are transmitted via a duplex telephone line to the fixed terminal for recording. A simplified block diagram of the transportable terminal is shown in figure 5.

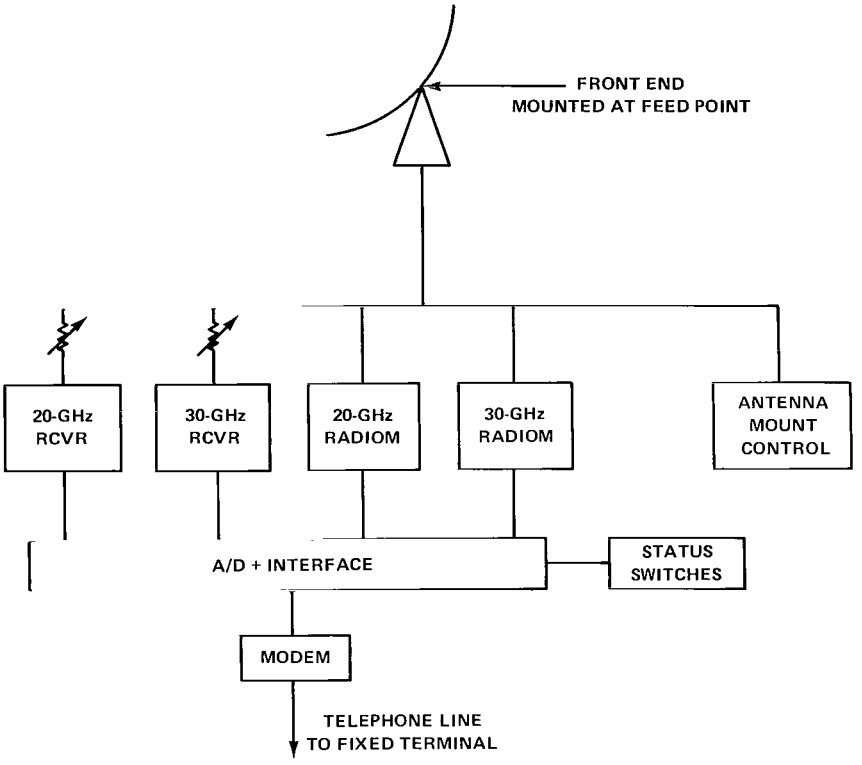

Figure 5. Simplified block diagram of OSU transportable 20/30-GHz ground terminal.

The transportable antenna is a 4.6-m, Cassegrainian fed, parabolic antenna. The antenna pedestal consists of an azimuth-over-elevation-over-azimuth mount so that the polarization is fully controllable. All front-end hardware is mounted in a cylindrical silo located immediately behind the feed horn. The RMS surface tolerance of the fiberglass parabolic surface is 1.14 mm or 0.076λ at 20 GHz and 0.114λ at 30 GHz.

*Calhoon, C. D., Jr., "ATS-F Millimeter Wave Experiment Ground Receiver Systems for NASA Sponsored Participating Stations," NASA Goddard Space Flight Center, Greenbelt, Maryland, X-751-73-3, January 1973.

The feed horn is a square corrugated horn tapered to reduce illumination of the hyperbolic subreflector edge and, thus, to reduce side lobe levels. The feed horn design was provided by Professor L. Peters and Dr. C. Mentzer of the OSU ElectroScience Laboratory. The horn aperture is covered by a 0.2-mm Teflon window. The measured standing wave ratio (SWR) of the radome, horn, transition, diplexer combination was 1.04 at 30 GHz and 1.38 at 20 GHz. The 20- and 30-GHz measured patterns of the feed horn are shown in figure 6.

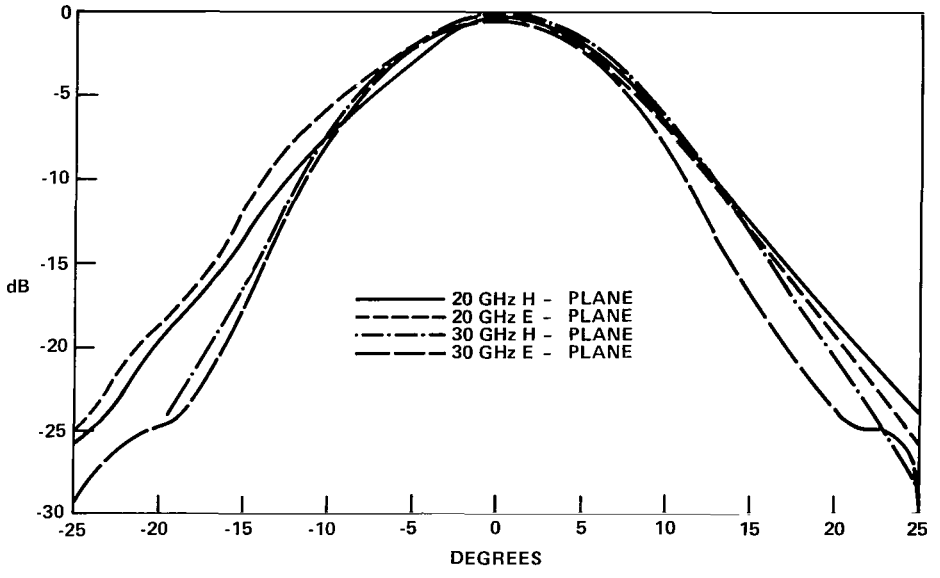

Figure 6. Transportable feed horn patterns.

The patterns of the transportable antenna were measured using the 20- and 30-GHz ATS-6 downlink signals; these patterns are shown in figures 7 and 8. These patterns are in the azimuth and elevation planes rather than the E- and H-planes. The broadening of the pattern in the azimuth plane is not fully understood at the present time. The feed horn has been realigned; however, this did not eliminate the problem. The polarization of the satellite signal at Columbus, Ohio, was calculated to be +12.8° clockwise from vertical when looking toward the satellite along the propagation path; this value agrees well with the observation. The gain of the transportable antenna is estimated to be 53.9 dB at 20 GHz and 57.5 dB at 30 GHz.

The RF front ends for the 20/30-GHz receivers and radiometers are located in the silo of the transportable antenna. The block diagram of the front ends is shown in figure 9. These front ends are almost identical in electrical design to those described by Calhoon and will not be discussed in detail here. The most significant difference is the addition of directional couplers following the waveguide calibrate switches which permit direct injection of RF signals into the receivers and radiometers.

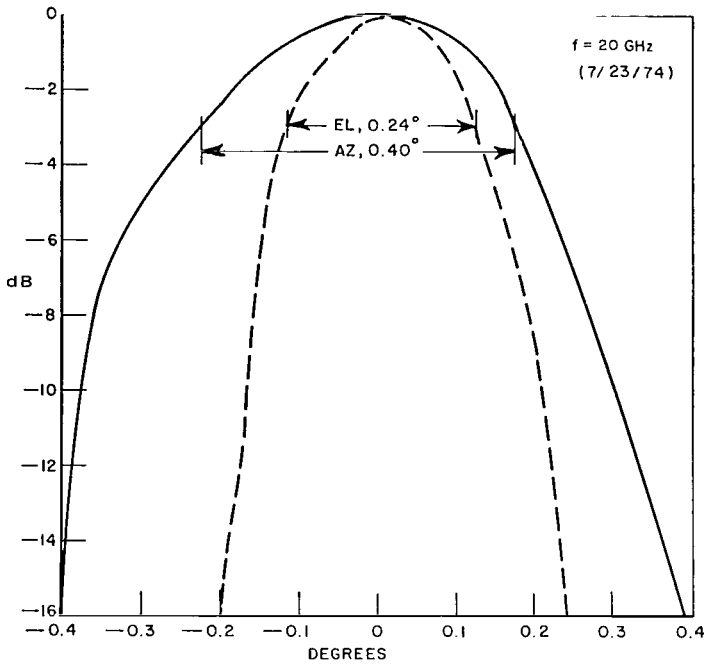

Figure 7. Transportable antenna pattern—20 GHz.

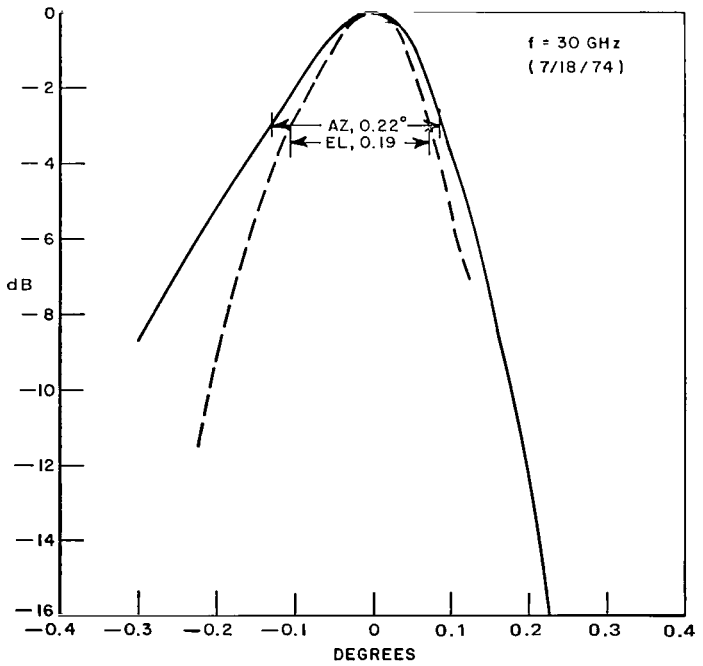

Figure 8. Transportable antenna pattern—30 GHz.

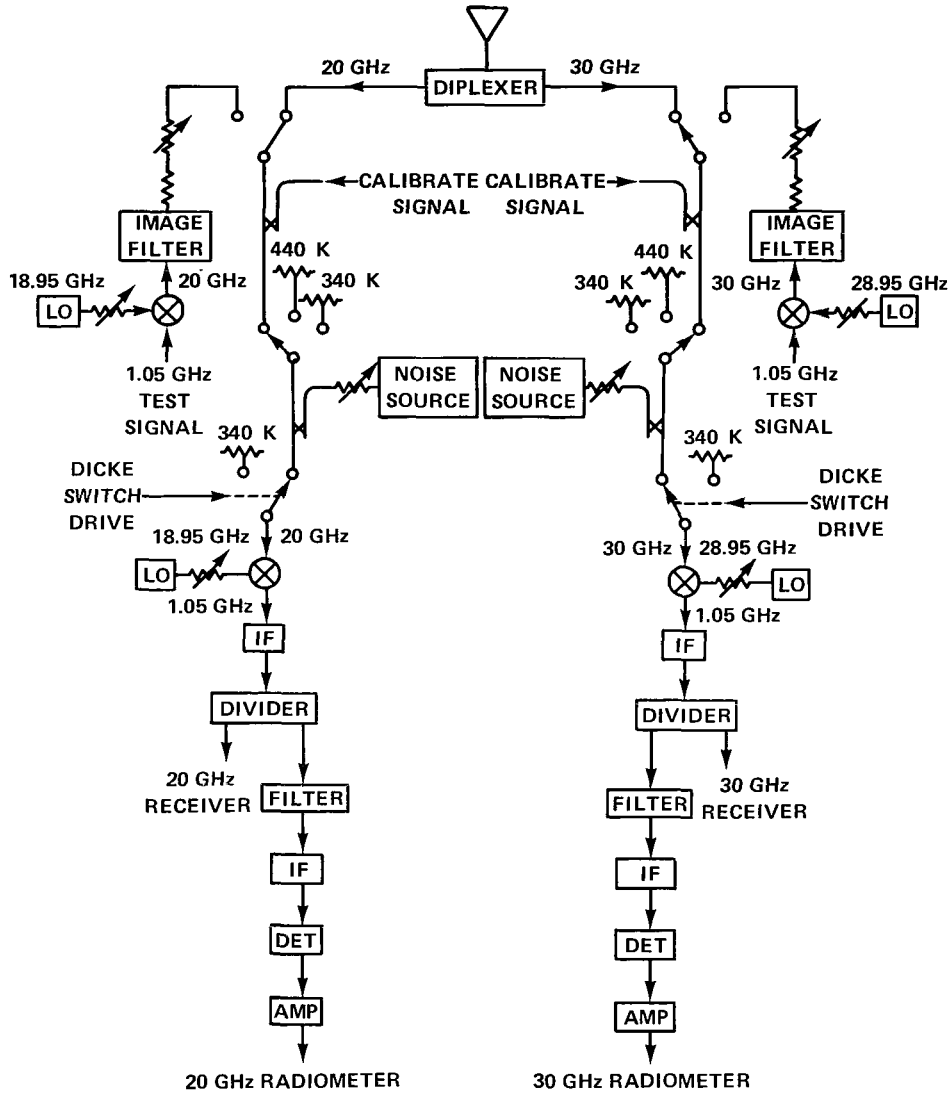

Figure 9. 20/30-GHz front end.

The front end components are mounted on a flat, rectangular plate with all 20-GHz components on one side and all 30-GHz components on the opposite side. The 1.05-GHz IF signal is brought into the transponder equipment now by means of a 39-m (128-ft) RG-9 coaxial cable having an attenuation of 11.8 dB.

The 20/30-GHz receivers used in this experiment are quadruple superheterodyne phase-lock loop receivers built by the Martin-Marietta Corporation and supplied by NASA.* The IF frequencies are 1.05 GHz, 60 MHz, 10 MHz, and 2.5 kHz.

*Calhoon, C. D., Jr., "ATS-F Millimeter Wave Experiment Ground Receiver Systems for NASA Sponsored Participating Stations," NASA Goddard Space Flight Center, Greenbelt, Maryland, X-751-73-3, January 1973.

The various link parameters are tabulated in table 2 and are used to calculate the signal level expected at the input port of the 1.05-GHz phase-lock loop (PLL) receiver under clear sky conditions. Also tabulated in table 2 are the measured dynamic ranges of the two links; these were determined by adding attenuation at the input port of the 1.05-GHz PLL receiver until the receiver could no longer maintain phase lock. The calibration curves produced by this procedure are shown in figure 10. The reduced dynamic range at 30 GHz is not fully understood at the present time.

Table 2
Link Parameters

	20-GHz CW/Dish	30-GHz CW/Horn
XMTR power	+33 dBm	+33 dBm
S/C wave-guide loss	-1 dB	-1 dB
S/C antenna gain	+37 dB	+27.6 dB
Free space loss	-209.5 dB	-213.1 dB
S/C antenna pointing	-1.5 dB	-1 dB
Clear air loss (O_2, H_2O)	-1.4 dB	-1.1 dB
Ground antenna gain	+53.9 dB	+57.5 dB
Ground wave-guide loss	-1.5 dB	-1.5 dB
IF gain	+30 dB	+30 dB
Power splitter	-3 dB	-3 dB
Coaxial line loss	-11.8 dB	-11.8 dB
Signal level at input of 1.05-GHz PLL receiver	-76 dBm	-84 dBm
Measured dynamic range (7/23/74)	55 dB	35 dB

Independent calibrations of the 1.05-GHz PLL receivers were also performed by injecting 1.05-GHz signals of known levels at the receiver inputs. These curves are shown in figure 11.

The difference in received signal level between continuous wave (CW) and multitone modes was checked on July 2, 1974, and the multitone level was found to be approximately 6.5 dB lower at both 20 and 30 GHz.

The difference in received signal level both with and without the Dicke switch operating has also been checked, and the level was found to be approximately 6 dB lower when this switch is operating.

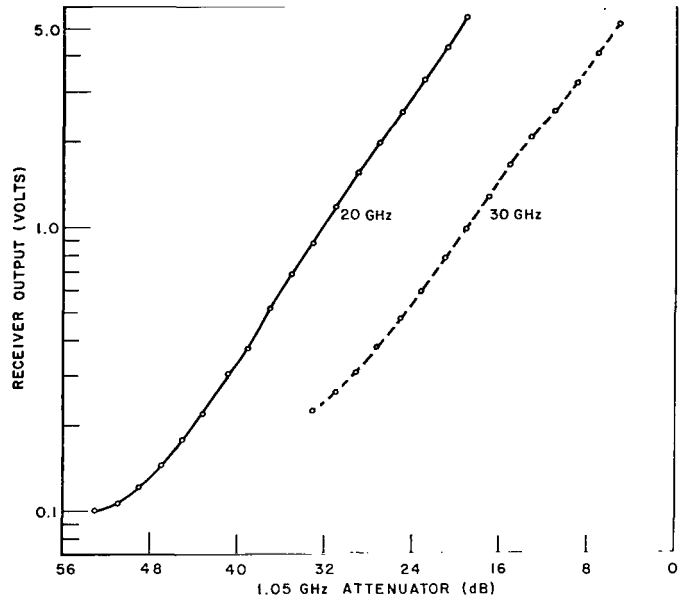

Figure 10. Link calibration using ATS-6 signal (7/22/74).

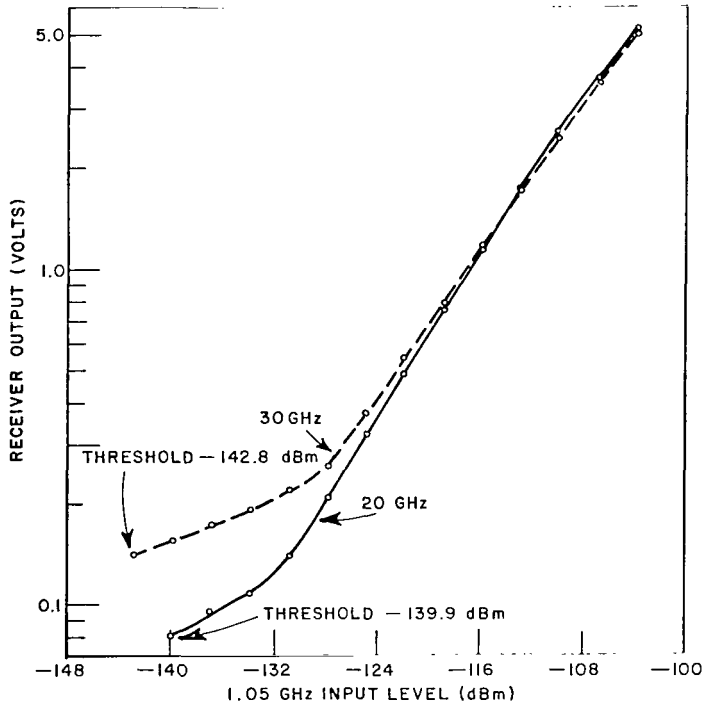

Figure 11. Receiver calibration (9/9/74).

FIXED TERMINAL

The fixed 20/30-GHz ground terminal is located at the Ohio State University ElectroScience Laboratory Satellite Communication Facility. The geographical location of this site is 40°00′10″ N. latitude and 83°02′30″ W. longitude; the site elevation is 252 m above sea level. Both the OSU high resolution radar/radiometer and low resolution radar systems are located at this site (Hodge and Taylor, 1973). In addition, a 13/18-GHz COMSAT ATS-6 uplink terminal is located at this site.

The instrumentation at the fixed terminal consists of 20- and 30-GHz Martin-Marietta phase-lock loop receivers. OSU constructed the 20- and 30-GHz radiometers following the design presented by Calhoon and were added to these receivers.

The digital data handling for the entire experiment is performed at the fixed terminal. This function consists of digitizing and formatting data obtained at the fixed terminal; these data are then merged with the data obtained from the two remote terminals as well as the high resolution radar/radiometer system. All data are then recorded in real time on a single digital magnetic tape.

The 20/30-GHz fixed terminal antenna is a 4.6-m, Cassegrainian fed, parabolic antenna. (See figure 2.) The RMS surface tolerance of this antenna is 0.64 mm or 0.043λ at 20 GHz and 0.064λ at 30 GHz. The antenna is mounted on an azimuth-over-elevation-over-azimuth pedestal so that the polarization can be remotely controlled. A square, corrugated horn is used to feed the antenna. The feed horn and the packaging of front end hardware are identical to those used for the OSU transportable terminal and were described earlier in this report.

The fixed terminal feed horn patterns are shown in figure 12. The measured SWR of this feedhorn was 1.20 at 20 GHz and 1.19 at 30 GHz.

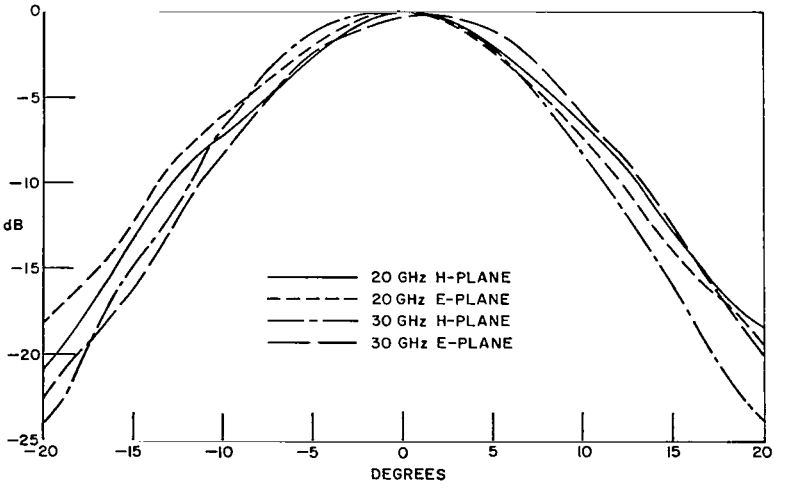

Figure 12. Fixed feed horn patterns.

The patterns of the fixed terminal antenna were measured using the 20- and 30-GHz ATS-6 downlinks. These patterns are shown in figures 13 and 14. The gain of the fixed antenna is estimated to be 53.9 dB at 20 GHz and 57.5 dB at 30 GHz.

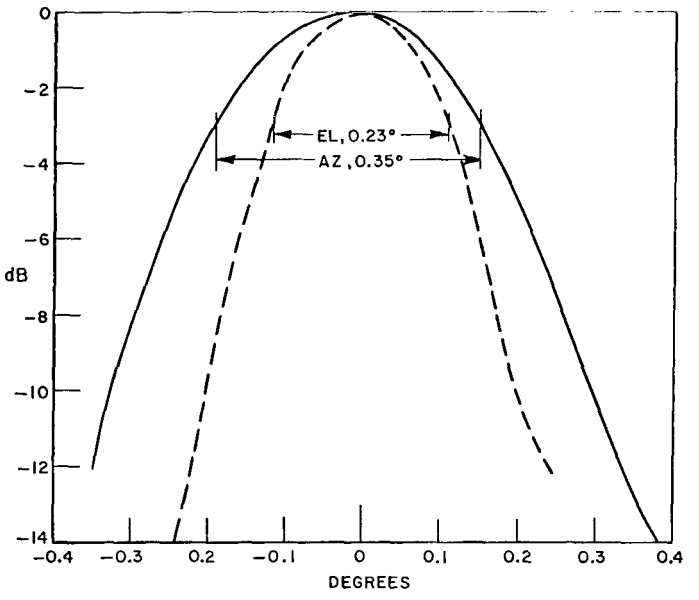

Figure 13. Fixed antenna pattern—20 GHz.

The RF front ends for the 20/30-GHz receivers and radiometers are essentially identical to those used for the transportable terminal. The electrical design has been described by Calhoon and the physical arrangement of components was presented above. The RG-9 coaxial cable carrying the 1.05-GHz IF signal from the RF front end to the fixed receivers is 41 m (135 ft) long and has an attenuation of 12.4 dB.

The link parameters are the same as those listed in table 2, with the exception of 0.6-dB additional coaxial line loss in the case of the fixed terminal. The calculated signal levels at the input of the fixed terminal 1.05-GHz PLL receivers are -76 dBm at 20 GHz and -85 dBm at 30 GHz. These levels are for the 20-GHz CW/dish and 30-GHz CW/horn modes. Measured dynamic ranges at the fixed terminal are 55 dB at 20 GHz (August 27, 1974) and 51 dB at 30 GHz (January 24, 1975).

Calibration curves obtained using the ATS-6 signals and introducing attenuation at the inputs to the 1.05-GHz PLL receivers are shown in figure 15; calibration curves for the PLL receivers using locally injected 1.05-GHz signals are presented in figure 16.

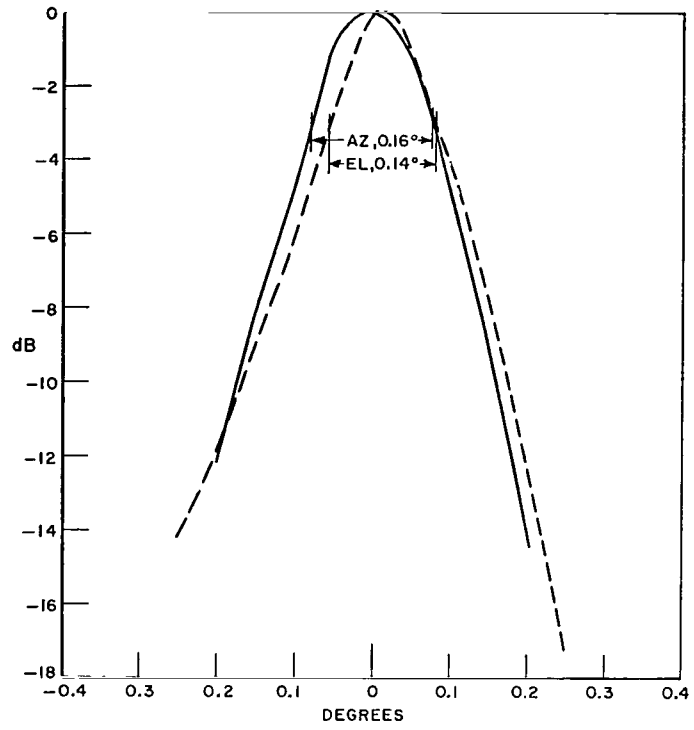

Figure 14. Fixed antenna pattern—30 GHz.

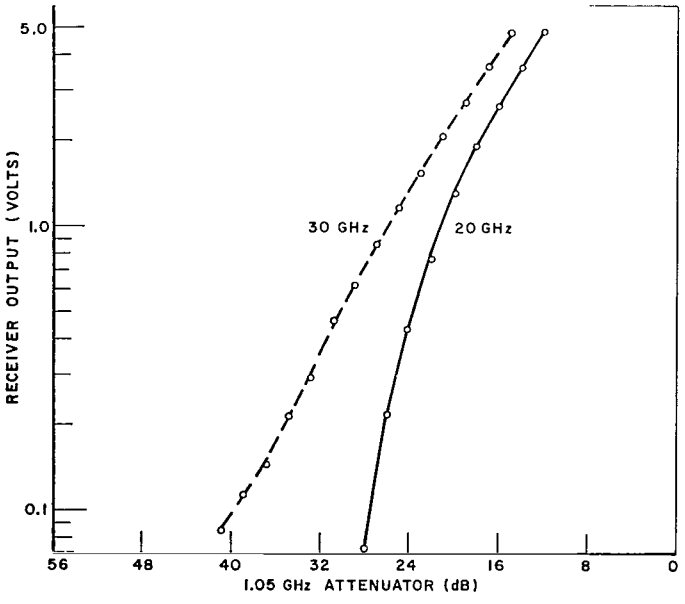

Figure 15. Link calibration using ATS-6 signal (January 24, 1975).

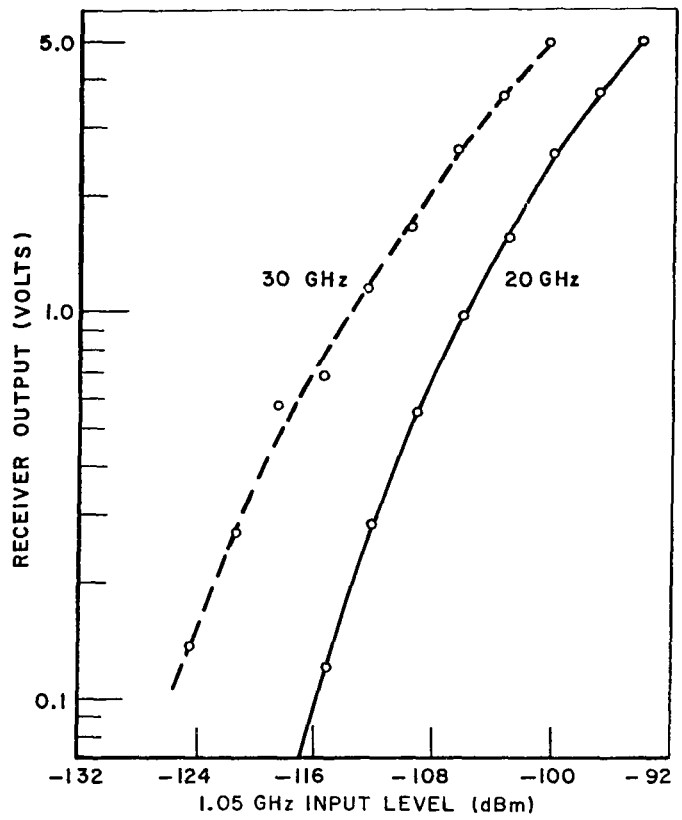

Figure 16. Receiver calibration (September 4, 1974).

Margin measurements were performed on June 6, 1975, with the satellite antennas directed toward Virginia Polytechnic Institute (VPI). The margins were

	20 GHz	30 GHz
Transportable	46 dB	34 dB
Fixed	47 dB	37 dB

for the 20-GHz CW/dish and 30-GHz CW/horn modes.

DIGITAL DATA SYSTEM

All data acquired in this experiment are digitized and recorded on a common digital tape in real time. The data acquired at the remote terminals are digitized at the point of acquisition and transmitted to the fixed terminal by telephone lines. These data together with data from the high resolution radar/radiometer system are merged and recorded on a single digital magnetic tape. In addition to these data, various status switches indicating operating modes and conditions are also monitored and recorded. The operator at the fixed terminal maintains control of the entire data system at all times.

The data acquisition system consists of an HP-2115-A minicomputer and control hardware, a digital magnetic tape deck, and two remote process controllers which are directed by the HP-2115-A through use of commercial telephone lines. One remote controller located at the transportable terminal acquires, buffers, and transfers data blocks at the request of the central computer. The data, which are sampled once a second, consist of status checks and the receiver and radiometer outputs from the transportable terminal. The remote controller, located at the unmanned terminal, samples one radiometer, interrogates a status register, samples test voltages, or performs a control function at the request of the central computer and returns the desired word of information once a second. The central computer must request each word of data or status separately, and the remote controller returns the desired word after a 400-ms delay. The central computer, in addition to controlling the remote processors, examines the status and samples the receivers and radiometers of the fixed terminal at rates of 10 or 200 samples per second, and records all data on magnetic tape.

Analog-to-digital (A/D) conversion, status acquisition, and data transmission and reception are performed by three control units. The analog signals are multiplexed and then converted. All A/D conversions provide seven significant bits plus sign. Provisions were made for 16 sampled analog channels at the fixed terminal and 8 at the transportable terminal. An A/D controller operates the A/D converter and multiplexer and provides an interrupt signal to the I/O bus.

Data are transferred from the remote controllers to the fixed terminal data system via commercial voice-grade telephone lines. A pair of Vadic VA-1600 modems are used for data communication with the transportable terminal and two Bell System type 103 modems are used with the unmanned terminal. Modem controllers at each terminal provide the correct parallel-to-serial conversions, control, and interrupt logic.

EMPIRICAL DIVERSITY GAIN RELATION

Only a limited amount of diversity gain data exists for millimeter wavelength earth-space propagation paths. These data, consisting of measurements performed by the Ohio State University and Bell Telephone Laboratories (BTL), were collected and presented by Hodge (1974). The OSU data were obtained using the ATS-5 15.3-GHz downlink for attenuation measurements; the BTL data were generated from 16-GHz radiometric temperature measurements along a nominal ATS-5 propagation path. In both cases the ground terminals were separated along a baseline oriented in approximately the NW-SE direction; the nominal look angles were 220° azimuth and 35° elevation. Even though these data were collected in different locations, the OSU data in Ohio and the BTL data in New Jersey, and for different time periods, the resulting diversity gain data were remarkably consistent.

Diversity gain is defined here as the difference between the path attenuations associated with the single terminal and diversity modes of operation for a given percentage time. Thus, diversity gain, G, is a function of the single terminal fade depth, A, as well as the terminal separation distance, D.

These data were used to generate an empirical relationship for diversity gain as a function of both separation distance and single terminal fade depth. First, it was recognized that the diversity gain data, figure 17, behaved as

$$G = a(1 - e^{-bD}) \tag{1}$$

for each value of single terminal fade depth. Consequently, a minimum RMS error fit was performed for each fade depth; this procedure yielded a family of coefficients, a and b, which depended only upon the fade depth. These coefficients, figures 18 and 19, were also fit to closed form analytic expressions

$$a = A - 3.6(1 - e^{-0.24A}) \tag{2}$$

$$b = 0.46(1 - e^{-0.26A}) \tag{3}$$

where G and A are expressed in dB, and D is expressed in kilometers. Using equations (1), (2), and (3), diversity gain was calculated as a function of terminal separation distance and single terminal fade depth. The results of these calculations are shown in figure 17; it may be seen that the agreement between the empirical calculation and the data points is at worst approximately 0.75 dB. This agreement is well within the experimental accuracy of the experiment and emphasizes the consistency of these experimental data.

It is of interest to note that the linear portion of the curve relating the coefficient a to the single terminal fade depth intercepts the ordinate at about -3.6 dB. This coefficient may be interpreted as the difference between the diversity gain reached for large separation distances and the ideal diversity gain. Therefore, this result indicates that the diversity gain approaches a level approximately 3.6 dB below the ideal diversity gain as the terminal separation distance becomes large. This behavior is in accord with the concept of optimum diversity gain presented earlier (Hodge, 1974).

It is also of interest to note that the coefficient b approaches a value of approximately 0.4 for large fade depths. This coefficient may be interpreted as the decay rate for diversity gain as a function of terminal separation distance. Thus, one may conclude that diversity performance is largely determined by storm cell cores having diameters on the order of 2.5 km.

Finally, the empirically calculated diversity gain is presented as a function of single terminal fade depth in figure 20. These curves show that the diversity gain has approached its optimum value (i.e., that value associated with an infinitely large separation distance, within 1 dB for terminal separation distances over 8 km).

PRELIMINARY ATS-6 30-GHz DIVERSITY DATA

The initial operation of the ATS-6 millimeter wave downlink occurred on June 13, 1974. Both the 20- and 30-GHz signals were acquired at the OSU transportable terminal during this initial turn-on period. Data acquisition on the ATS-6 20- and 30-GHz downlinks

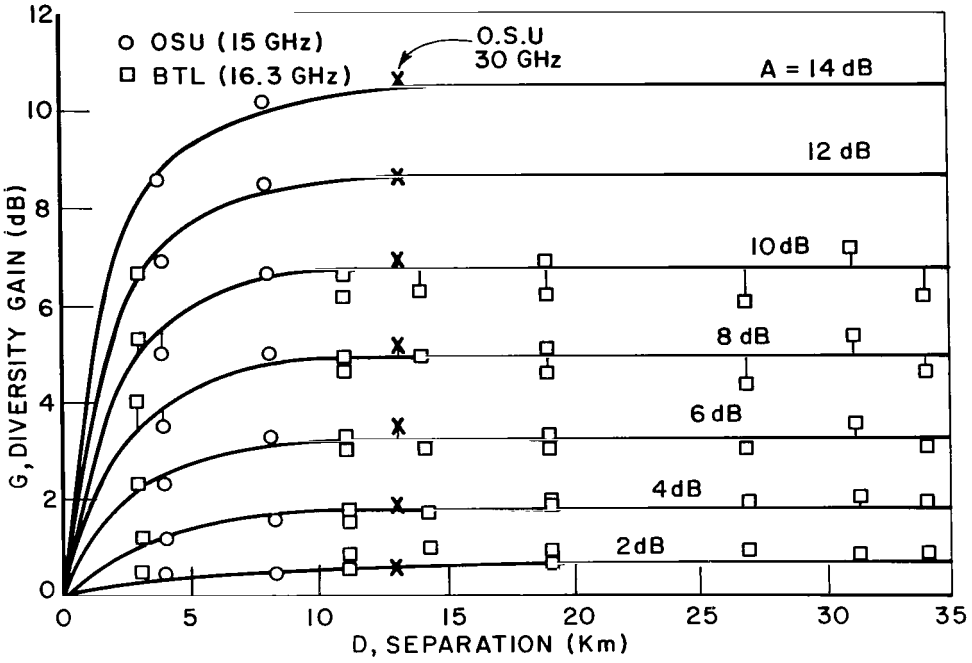

Figure 17. Diversity gain versus terminal separation distance.

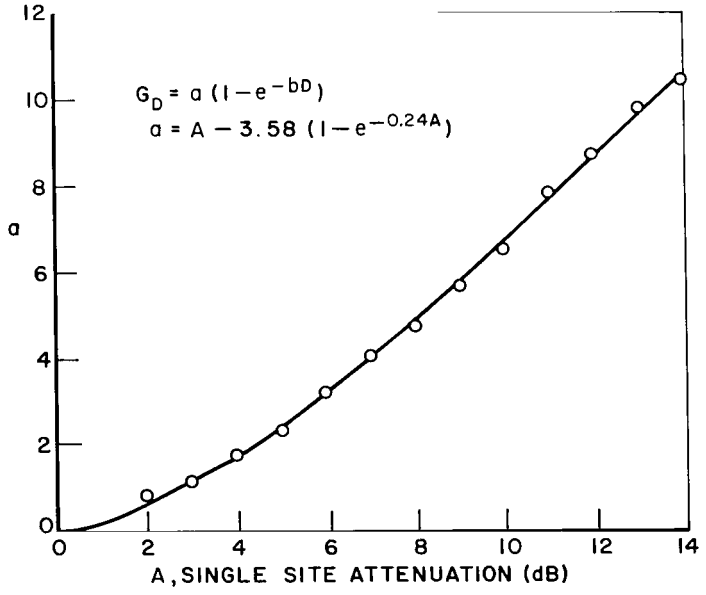

Figure 18. Coefficient a versus single site attenuation, A.

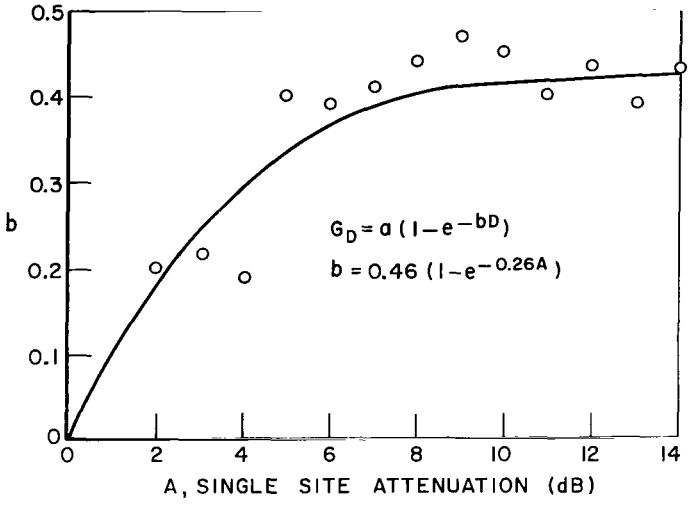

Figure 19. Coefficient b versus single site attenuation, A.

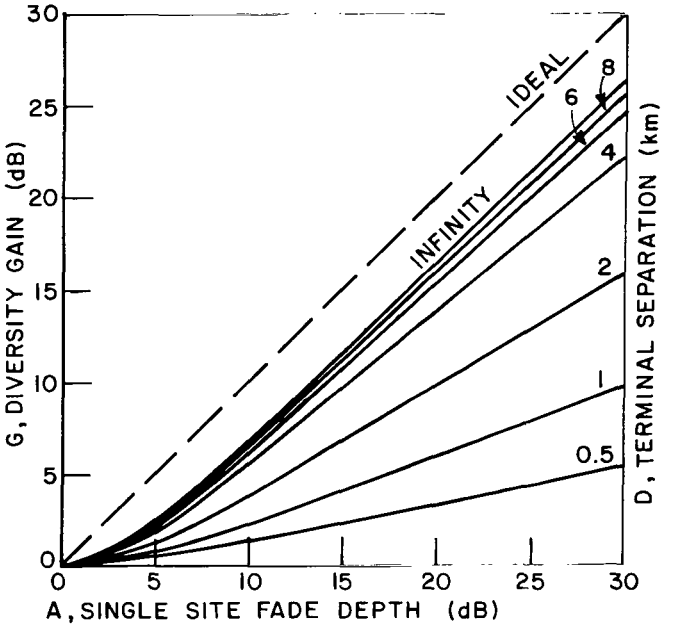

Figure 20. Diversity gain, G, versus single site fade depth, A.

terminated on June 13, 1975. All terminals remained operational until loss of signal as the satellite moved below the horizon. The total data acquisition periods were as follows:

Transportable	20 GHz	7,409 min
	30 GHz	9,281 min

Fixed	20 GHz	6,970 min
	30 GHz	8,317 min
Unmanned	20 GHz	5,438 min
Total		37,415 min

Although a considerable amount of data has been collected at the present time, only initial results for 30-GHz diversity behavior have been analyzed to date. Hence, the following discussion covers only 30-GHz downlink attenuation data from the fixed and transportable terminals.

The relative locations of the ground terminals are shown in figure 21. The nominal look angles to the ATS-6 synchronous satellite were 40° elevation and 200° azimuth.

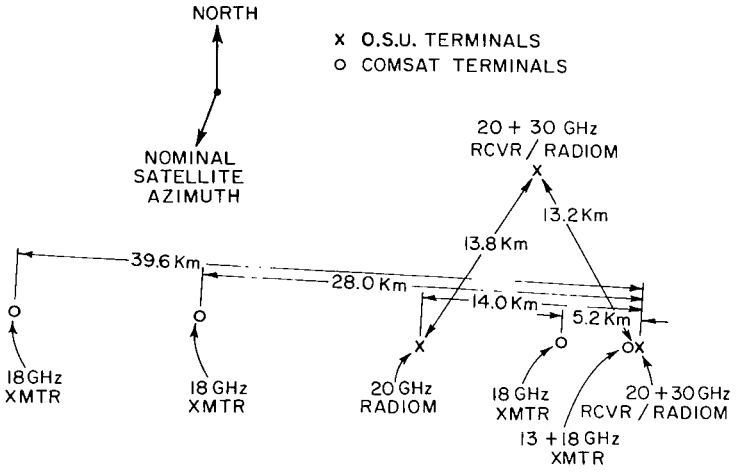

Figure 21. Ohio State University ATS-6 millimeter wave experiment site plan.

Samples of the raw data from these terminals are presented in figure 22. These curves represent the sampled outputs of the 30-GHz receivers before processing. The receiver outputs were sampled at a rate of 10 Hz, although the plots were generated using 10 samples (i.e., 1-s averages). It should be noted that at approximately 22 minutes into this data period, a 10-dB pad was switched out of the receiver input at the transportable terminal. The received signal at that terminal subsequently dropped below threshold for approximately 1 minute, and the 10-dB pad was reinserted at about 32 minutes into the data period. This same segment of data is shown in figure 23 after conversion to a decibel scale and compensation for the pad changes. Finally, fade distributions were generated for this same data segment; these curves are shown in figure 24.

A set of cumulative fade distributions for seven fade events which occurred during early spring 1975 are presented in figure 25. It is interesting to note that the character of the diversity fade distribution has changed little from that shown in figure 24 even though six additional fade events are included. Both terminals experienced fades to depths of 30 dB or more during one or more of these events.

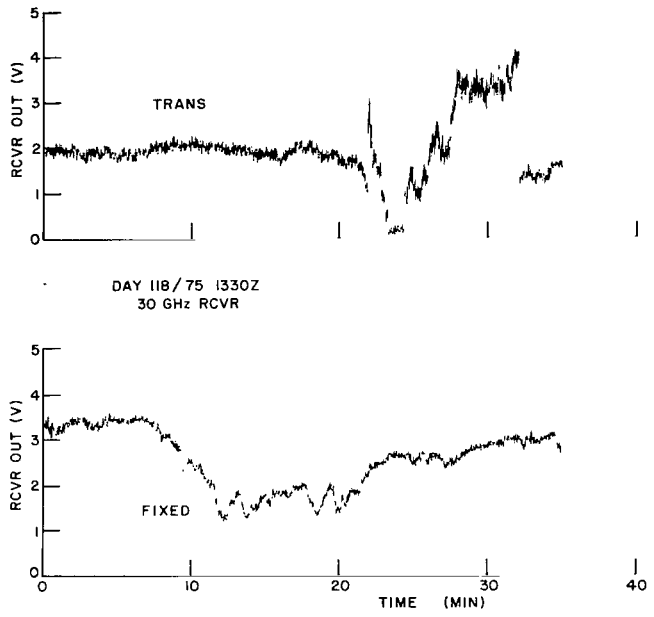

Figure 22. Raw 30-GHz receiver data (April 28, 1975, 1330 UT).

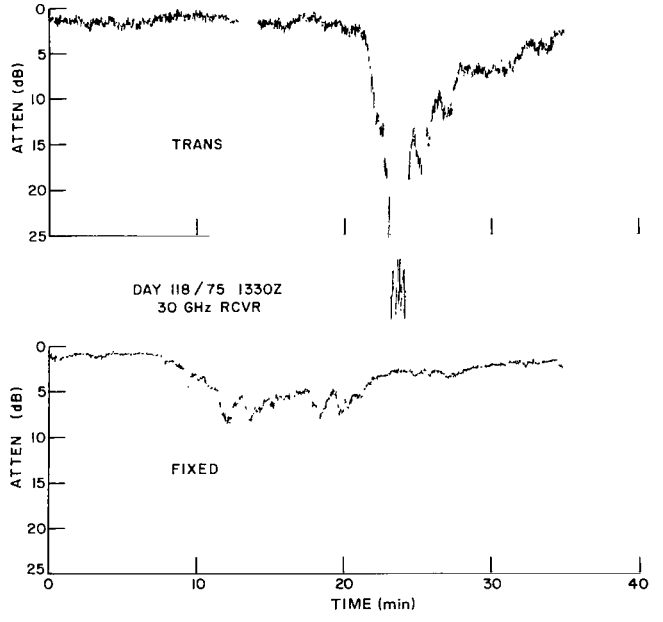

Figure 23. Preprocessed 30-GHz receiver data (April 28, 1975, 1330 UT).

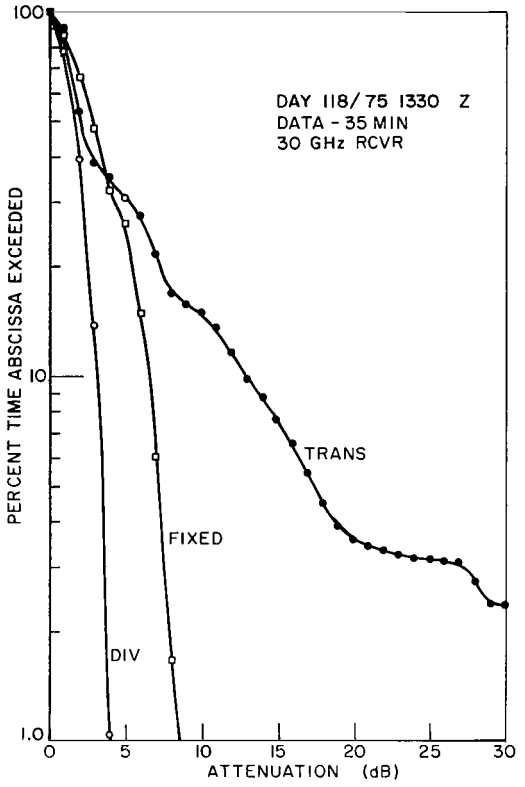

Figure 24. Fade distribution 30-GHz data (April 28, 1975, 1330 UT).

Diversity gain data were extracted from the curves shown in figure 25. These 30-GHz diversity gain data points are shown in figure 17 along with the empirically derived diversity gain curves. The agreement is exceptional; in fact, although not shown in this figure, the 30-GHz data points and the 15-GHz empirical results agree within 0.25 dB for all fade depths up to 30 dB. The calculations were not carried beyond this fade depth due to lack of data.

This preliminary result indicates that diversity gain is not a sensitive function of frequency. Alternatively, this result indicates that terminal separation distances of 8 to 10 km, which provide nearly optimum diversity gain at 15 GHz, will provide the same diversity improvement at 30 GHz. Clearly, this preliminary conclusion rests on a limited data base at the present time; nevertheless, the close agreement with earlier results tends to strengthen the credibility of this conclusion.

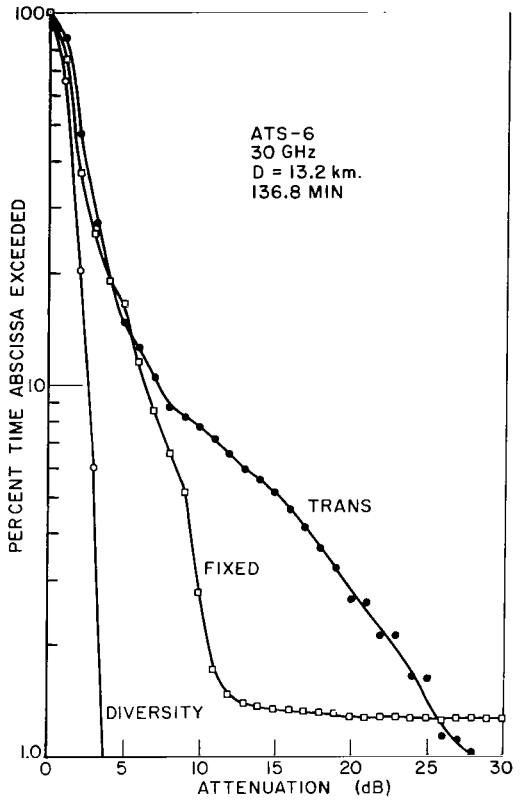

Figure 25. Cumulative 30-GHz fade distributions (7 events).

REFERENCES

Hodge, D. B., "A 15.3 GHz Satellite-to-Ground Diversity Experiment Utilizing the ATS-5 Satellite," The Ohio State University ElectroScience Laboratory, Department of Electrical Engineering; prepared under Grant NGR-008-080 for NASA, Report 2374-11, October 1972.

Hodge, D. B., and R. C. Taylor, "The Ohio State University ElectroScience Laboratory Radar/Radiometer Facilities for Precipitation Measurements," The Ohio State University ElectroScience Laboratory, Department of Electrical Engineering; prepared under Grant No. NGR-008-080 for NASA, Report 2374-13, March 1973.

Hodge, D. B., "Space Diversity for Reception of Satellite Signals," The Ohio State University ElectroScience Laboratory, Department of Electrical Engineering; prepared under Grant NGR-008-080 for NASA, Report 2374-16, October 1973.

Hodge, D. B., "Path Diversity for Reception of Satellite Signals," *Journal de Recherches Atmospheriques*, 8, 1974, p. 443.

Strickland, J. I., "Radar Measurements of Site-Diversity Improvement During Precipitation," *Proceedings of IUCRM Colloquim on the Fine Scale Structure of Precipitation and EM Propagation*, Nice, France, October 1973, p. IV-8.

SOURCES

Hodge, D. B., "ATS-F Millimeter Wavelength Propagation Experiment," The Ohio State University ElectroScience Laboratory, Department of Electrical Engineering; prepared under Contract NAS5-21983 for NASA/GSFC, Report 3863-1, July 1974.

Hodge, D.B., and R. C. Taylor, "ATS-6 Millimeter Wavelength Propagation Experiment," The Ohio State University ElectroScience Laboratory, Department of Electrical Engineering; prepared under Contract NAS5-21983 for NASA/GSFC, Report 3863-2, September 1974.

Hodge, D. B., and R. C. Taylor, "ATS-6 Millimeter Wavelength Propagation Experiment," The Ohio State University ElectroScience Laboratory, Department of Electrical Engineering, prepared under Contract NAS5-21983 for NASA/GSFC, Report 3863-3, March 1975.

ATMOSPHERIC ATTENUATION MEASUREMENTS AND PREDICTION TECHNIQUES AT 20 AND 30 GHz WITH THE ATS-6 SATELLITE

Louis J. Ippolito
Goddard Space Flight Center
Greenbelt, Maryland

ABSTRACT

The ATS-6 millimeter wave experiment (MWE) provided direct rain attenuation measurements at 20 and 30 GHz at a number of locations in the continental United States. Studies at the NASA stations at Rosman, North Carolina, and at Greenbelt, Maryland, were directed at an evaluation of rain attenuation statistics, attenuation ratio variations, scintillation effects, coherence bandwidth in a 1400-MHz band, and attenuation prediction techniques utilizing rain-gage, radar, and radiometer measurements coincident with the earth-space attenuation measurements.

Results of the first 10 months of measurements at Rosman and Greenbelt are presented with major emphasis on the impact of the results on earth-space system design.

INTRODUCTION

The radio frequency bands below 10 GHz presently support virtually all terrestrial and space communications links. Recent needs for additional capacity and expanding coverage have required the systems designer to look to higher frequency bands to provide the needed capabilities without sharing problems or inadequate bandwidth. The frequency bands above 10 GHz are presently allocated for all major space services, including fixed satellite, broadcast satellite, meteorological satellite, and terrestrial services such as fixed line-of-site, mobile, and radiolocation. Some of the bands are shared, many are exclusive or limited to two or three services.

In the design of space communications systems at millimeter wavelengths, consideration must be given to the effects of precipitation on the earth-space propagation path. At frequencies above about 10 GHz, absorption and scattering caused by rain, hail, or wet snow can cause a reduction in signal level (attenuation) which will reduce the reliability of the communications link. Other effects can be generated by precipitation events. They include: depolarization, amplitude and phase scintillations, and bandwidth decoherence. All of these factors can have a degrading effect on space communications at millimeter wavelengths.

The ATS-6 MWE is designed to measure and evaluate propagation characteristics of space-to-earth links at 20 and 30 GHz.*

The measurements at Rosman and Greenbelt were accomplished in three areas.

- The MWE provided the propagation characteristics of earth-to-space links at 20 and 30 GHz under defined meteorological conditions. Included were measurements of attenuation, phase, scintillations, and coherence bandwidth.
- The experiment provided engineering data on communications links: 6 GHz up and 4, 20, and 30 GHz down. Measurements on both analog video and digital biphase signals were made, and the effects of the millimeter space links evaluated.
- The experiment also provided measurements and analyses for the development of methods of attenuation prediction from radar systems, rain gage networks, and radiometers.

GROUND STATION EQUIPMENT

The prime NASA MWE ground terminal was at the NASA tracking station in Rosman, North Carolina, located in the western part of the state (see figure 1). The MWE used a 4.6-m parabolic reflector antenna (figure 2) with a dual frequency feed and RF front end mounted at the antenna. Telemetry and command for the ATS-6 is accomplished with a 26-m antenna located about 60 m from the MWE antenna, as seen in figure 3.

The principal elements of the Rosman MWE ground equipment are shown in figure 4.

The ground receiving system consists of the dual frequency feed and RF front end mounted at the feed point of the antenna, a phase-lock loop/signal processor, a control and monitor unit, and a radiometer chassis. Additionally, automatic calibration and test equipment is provided to facilitate performing the required amplitude and phase calibration.

Figure 5 shows the receiver system mounted in the three racks at the right side of the figure. Strip chart recorders, antenna pointing controls, and other support equipment are seen in the other racks.

A corrugated feed horn provides the required broadband frequency performance (greater than 2 to 1), equal E and H phase beamwidths at 20 and 30 GHz, coincident phase centers, and high illumination efficiencies. A polarization rotation assembly provides the capability of remotely aligning the ground antenna polarization with that of the satellite antennas and operates at 20 GHz and 30 GHz with a ±1000-MHz bandwidth. A diplexer effectively separates the 20- and 30-GHz signals, directs them to their respective front ends, and provides the isolation necessary to prevent the LO signal of one mixer from getting through to the receiver of the opposite band.

*Ippolito, L. J. "The ATS-F Millimeter Wave Propagation Experiment," NASA/GSFC TMX-65752, October 1971.

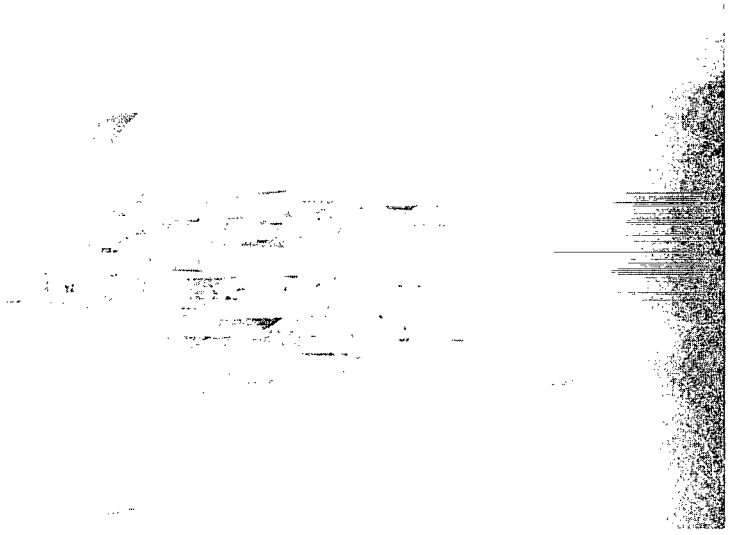

Figure 1. NASA Rosman, North Carolina, tracking station.

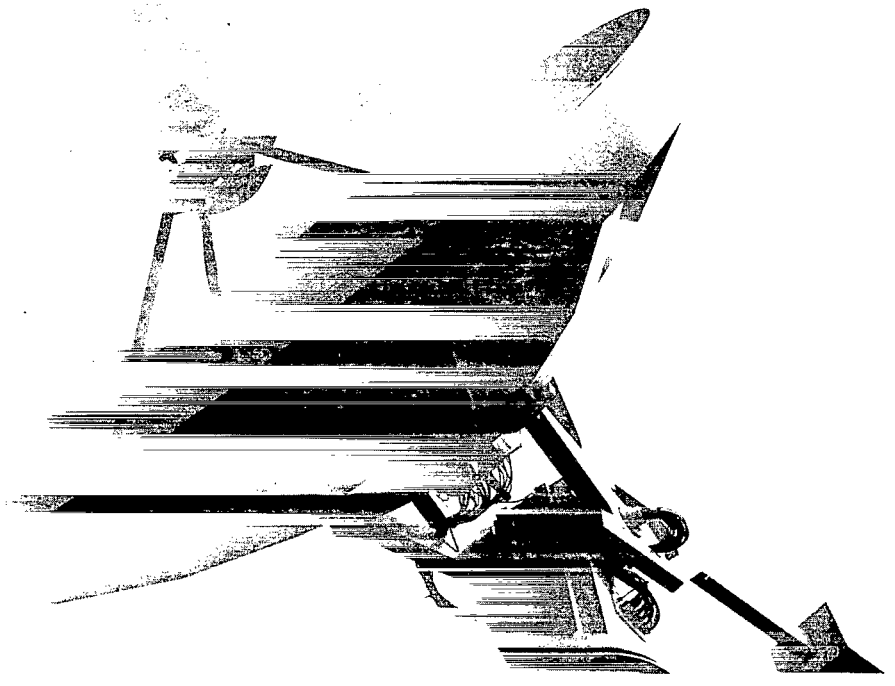

Figure 2. The millimeter wave experiment, 4.6-m antenna, Rosman, North Carolina.

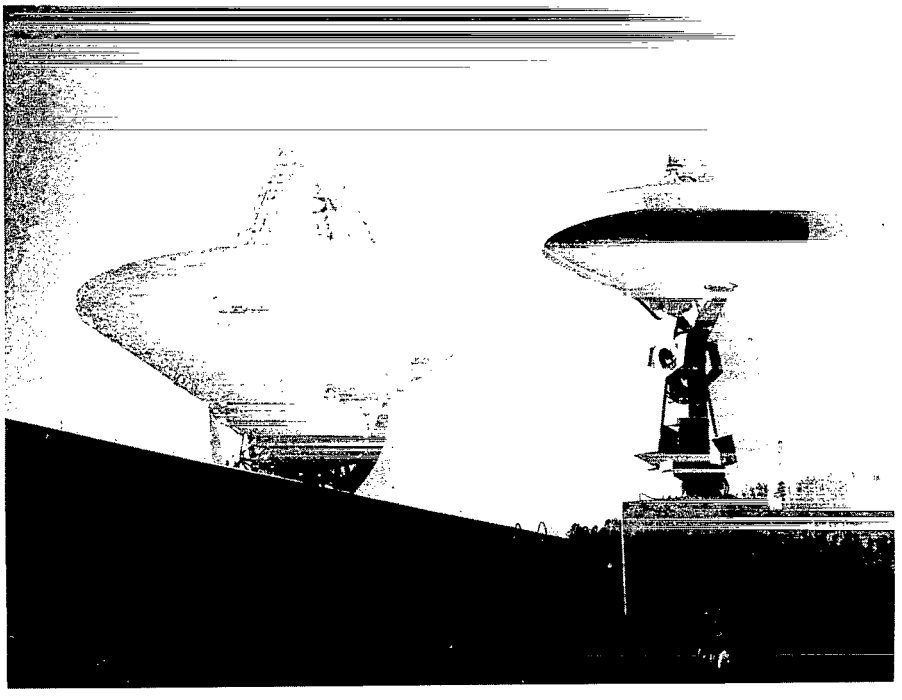

Figure 3. ATS-6 tracking antenna and MWE antenna, Rosman, North Carolina.

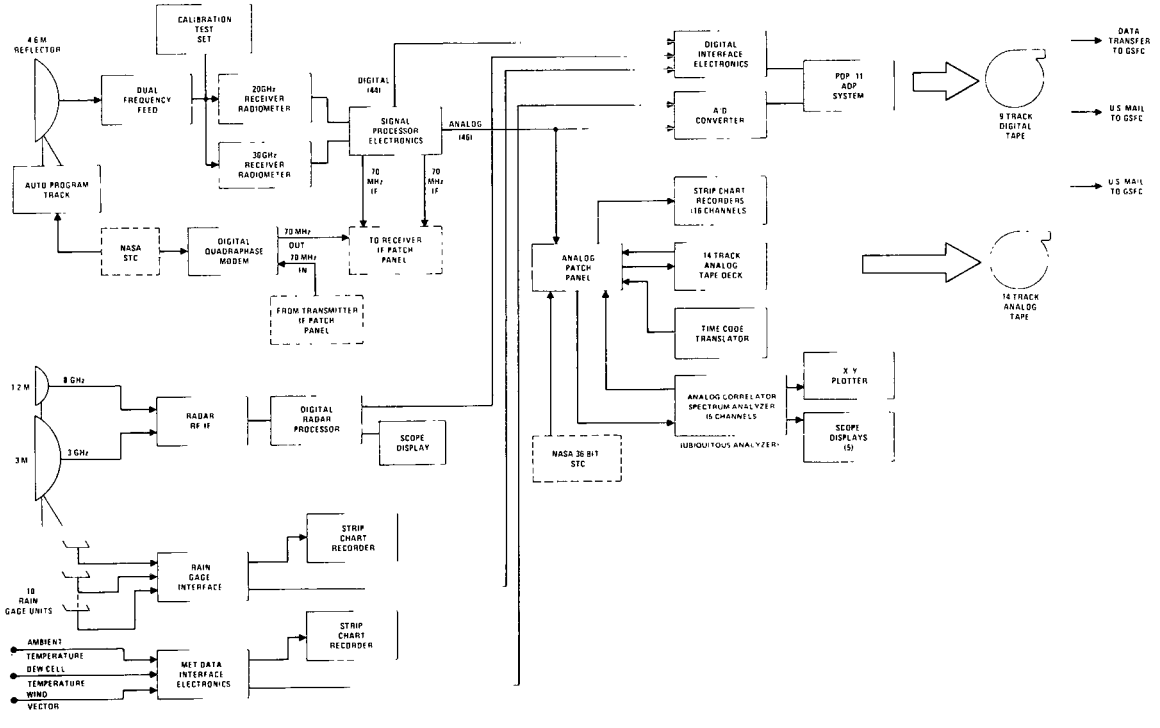

Figure 4. The NASA Rosman, North Carolina, MWE ground terminal block diagram.

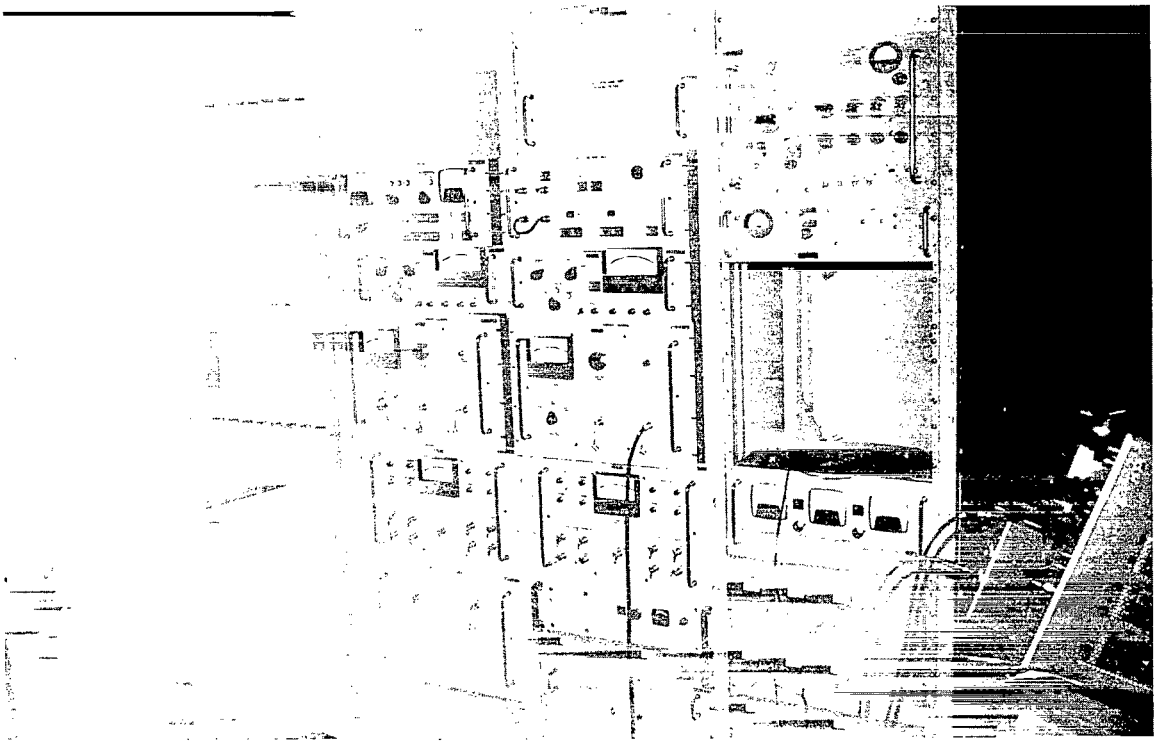

Figure 5. MWE 20- and 30-GHz receiver, Rosman, North Carolina.

The 4.6-m parabolic antenna has 56-dB gain and a 0.23° halfpower beamwidth at 20 GHz, and has 58-dB gain and 0.15° halfpower beamwidth at 30 GHz. Side lobes for both frequencies are below 15 db. A remote feed polarization positioning technique is used, and the autotrack is accomplished by scanning the subreflector in a conical scan mode (see subreflector on figure 2). The program track capability utilizes a small digital processor to compare time and orbit data to track the satellite. The antenna system is capable of providing selectable conical scan autotracking and simultaneous reception at 20 GHz and 30 GHz.

The 20- and 30-GHz front ends are similar in design, and the block diagram of the 30-GHz system is shown in figure 6.

The inputs are derived from the diplexer on two separate waveguide ports and the outputs are applied separately to the phase-lock loop/signal processor (PLL/SP) and radiometer IFs. The front ends are completely independent of each other. The receiver system front ends incorporate uncooled parametric amplifiers to provide moderately low system noise temperatures. Both front ends contain all of the circuits necessary to convert propagation/

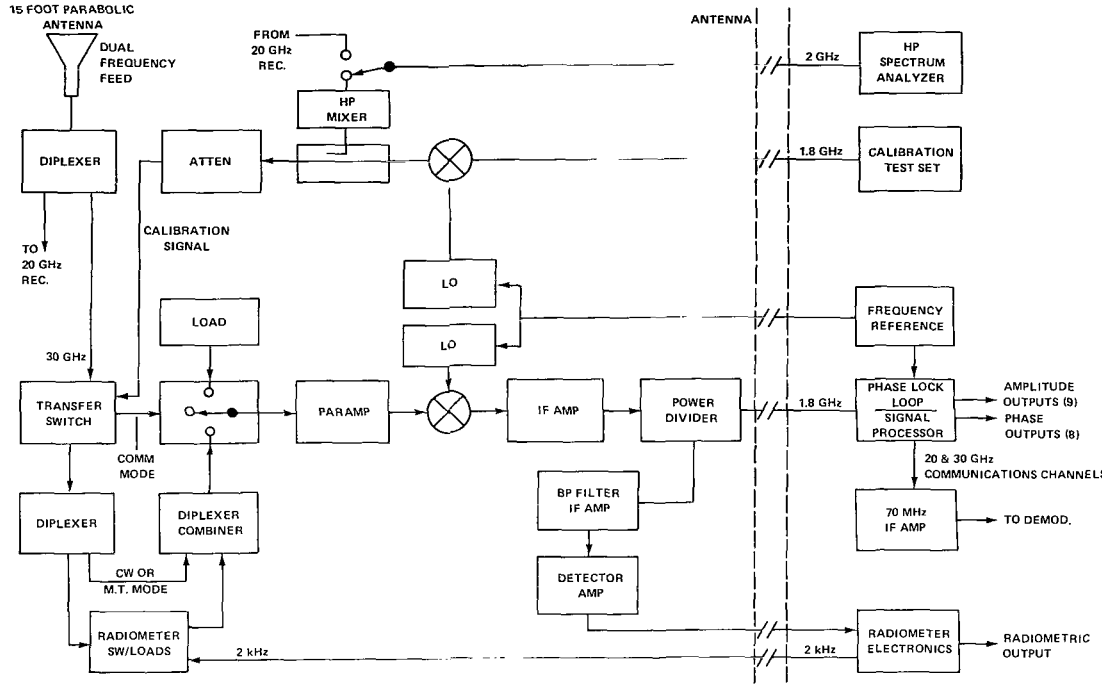

Figure 6. Front ends for Rosman, North Carolina, terminal.

communications signals to an IF and process the radiometer signal through the video detector back to the original Dicke switching rate.

Two diplexers are used, one to separate the radiometric and propagation channels and the other to sum the propagation and radiometric inputs to the paramp. This prevents loss of 6 dB of propagation signal power when the radiometer is operating.

In order to minimize communications signal losses preceding the parametric amplifier for both frequencies, transfer switches are used to bypass the radiometer and propagation channels, including the two diplexers. The receiver noise figures are 4.6 dB at 20 GHz and 5.6 dB at 30 GHz, without the radiometer in the system.

The radiometer is designed to aid in the correlation of the received propagation signal characteristics with sky temperature. Simultaneous measurement of received signal characteristics and sky temperature using the same antenna permits a direct correlation to be done under various meterological conditions. The radiometer is an absolute reading, self-calibrating unit capable of measuring sky temperature over a range from 0 to 350 K. Additionally, a high isolation Dicke switch is included to allow sun temperature measurements.

The RF front end components used in the radiometer include one of the two transfer switches used to bypass the radiometer in the communications mode, two diplexers, a switching circulator for modulating the RF signal to operate the synchronous detector, calibration equipment consisting of a three position waveguide switch, two waveguide termination ovens

with their control circuits, and a solid-state noise source with a waveguide attenuator and cross-guide directional coupler. Other components include an IF amplifier, a power drive for splitting the IF signal between the CW receiver and the radiometer channel, and an envelope detector/video amplifier module. Additional radiometer circuits include a lock-in amplifier and the control circuits to perform the calibration of the radiometer. The lock-in amplifier is basically a reference generator used to synchronize the RF switching with the reference signal to provide low level signal detection.

The radiometer utilizes a 100-MHz bandwidth centered at 20.270 or 30.270 GHz. The radiometer has a T_{min} sensitivity of 0.24 K and 0.87 K for a 10-s integration time at 20 GHz and 30 GHz, respectively. These sensitivities can be achieved at the Rosman site with the parametric amplifier on.

The PLL/SP processes the IF signals from the 20-GHz and 30-GHz front ends and provides the frequencies necessary to translate the IF signals to the required processing frequencies. The signal processor operates in two modes. In the multitone (MT) mode, there are 13 outputs provided which are proportional to the amplitude and phase of the nine MT signals. In the communications mode, the 20- and 30-GHz signals are translated to 70 MHz.

Each receiver system is calibrated using equipment whose signal level and frequency stability simulate those of the received propagation signal. The calibration and test equipment provides carriers at 20 and 30 GHz with four pairs of sidebands spaced 180 MHz apart and of equal amplitude. The signal levels are variable over a 45-dB range in 3-dB steps. An additional variation of 25 dB is provided to simulate the spacecraft high gain antenna and CW capability. The phase of the carrier is varied over a 180° range, simulating a relative differential sideband phase of 360°. The calibration system is completely automatic with preprogrammed circuits to control the amplitude and phase calibration.

The modulation signals from the PLL/SP are the four sidebands at 180, 360, 540, and 720 MHz. These signals are applied to a balanced modulator along with the 1.8-GHz carrier suppressed. Additional carrier suppression is realized in the carrier reject filter and sideband amplitude adjust circuit which reduces the carrier to at least 40 dB below the sidebands. The sideband amplitude adjust circuit is a 9-channel band reject filter used to equalize the nine signals to within ±0.5 dB or less. This sideband signal and the phase shifted carrier are combined and the resultant signal is a 9-line equal amplitude spectrum with a carrier at 1.8 GHz and four sidebands on either side of the carrier spaced 180 MHz apart. This signal is applied to an automatically controlled attenuator and sideband amplitude adjust circuit and is then transmitted to the RF front end with a low loss RG 218/U coaxial cable. Here the signal is split and applied to the 20- and 30-GHz upconverters. The output of the upconverters is attenuated by fixed attenuators to the levels required for receiver calibration.

In addition to the signal processor outputs, a number of other functions are measured and recorded for later analysis, including 3- and 8-GHz radar, 10 rain gages, meterological data, and housekeeping data. All parameters are recorded on a single 8-track digital tape with the aid of a PDP-11 minicomputer system, which sorts, formats, and samples the data as

required (see figure 4). Table 1 lists the parameters of the ATS-6 MWE recorded at Rosman, and indicates their major characteristics.

All experiment functions are controlled by the experiment status panel (ESP), shown in figure 7, which provides equipment status, fault status, antenna pointing inputs, spacecraft telemetry conditions, and other control functions.

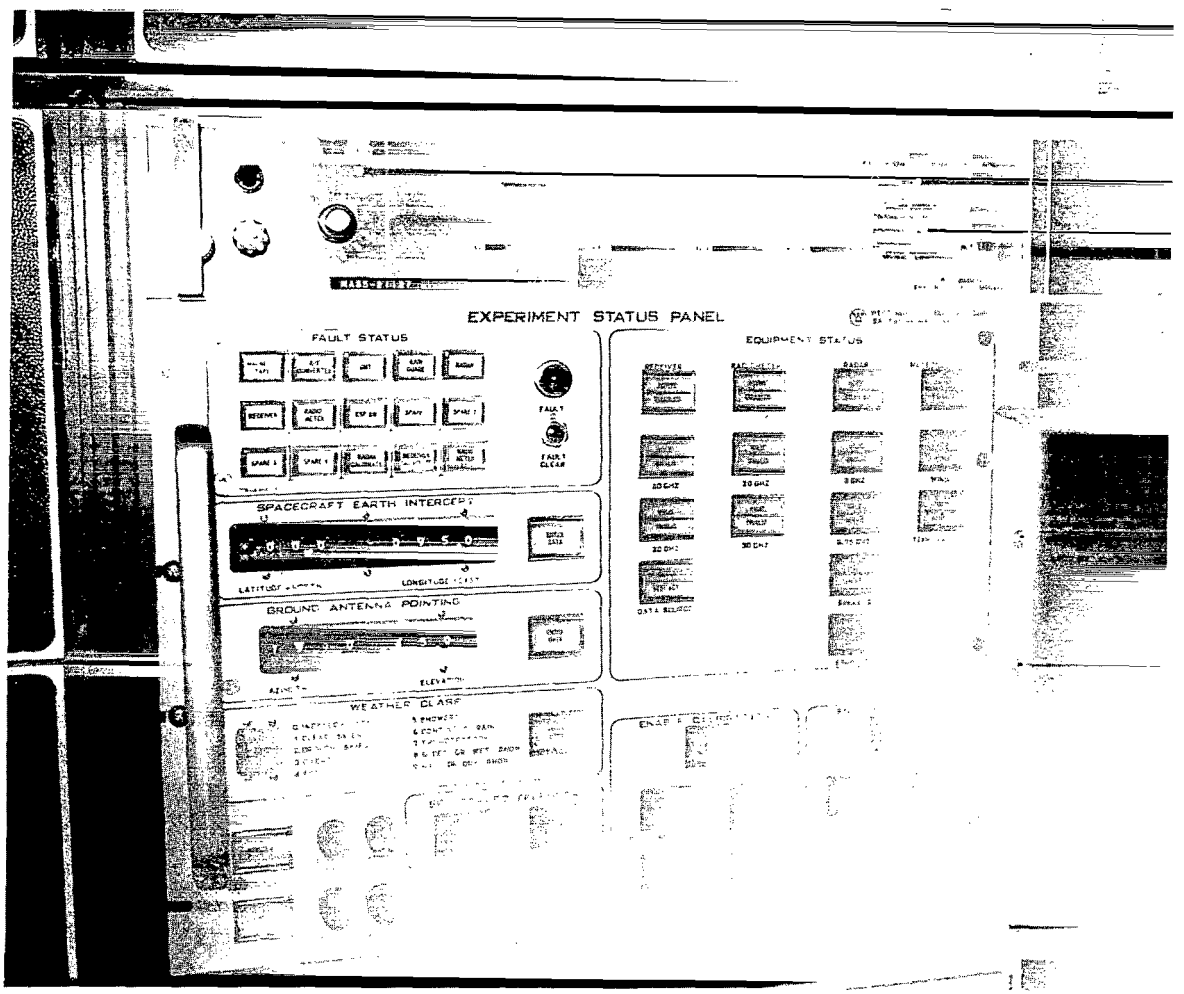

Figure 7. Experiment status panel (ESP).

Experiment data acquisition, formatting, calibration, and recording is accomplished with the PDP-11 computer system, shown with the ESP on figure 8.

An analog recording system (see figure 4) is also included for scintillation and bandwidth coherence measurements and analysis. A special purpose correlator/spectrum analyzer developed for the ATS-5 millimeter wave experiment is used for detailed evaluation of the channel time-frequency characteristics.

Table 1
Data Parameters for the ATS-6 MWE

Test Period Mode		Item	Signal Source	Digital Sample Rate (per second)	Digital Dynamic Range (Digital Counts)	Parameter Dynamic Range (Engineering Units)	Number of Separate Parameters Recorded
CW	Multitone						
		Propagation Parameters					
X	X	20-GHz carrier amplitude	Receiver	20	8 bits	45 dB	1
	X	20-GHz sideband amplitude (8)	Receiver	20	8 bits	45 dB	8
	X	20-GHz sideband phase (4)	Receiver	20	8 bits	0-360°	4
X	X	30-GHz carrier amplitude	Receiver	20	8 bits	45 dB	1
	X	30-GHz sideband amplitude (8)	Receiver	20	8 bits	45 dB	8
	X	30-GHz sideband phase (4)	Receiver	20	8 bits	0-360°	4
		Meteorological Parameters					
X	X	20-GHz sky temperature	Receiver	20	8 bits	0-350 K	
X	X	30-GHz sky temperature	Receiver	20	8 bits	0-350 K	1
X	X	Ground ambient temperature	Transducer	1	8 bits	0-316 K (0-110°F)	1
X	X	Ground wind velocity	Transducer	1	8 bits	0-44.7 m/s (0-100 m/h)	1
X	X	Ground wind direction	Transducer	1	8 bits	0-360°	1
X	X	X-band radar backscatter	Radar	1/range interval	16 bits	80 dB	100
X	X	S-band radar backscatter	Radar	1/range interval	16 bits	80 dB	100
X	X	Rainfall (gages 1-10)	Rain gage	1/gage	Tip/No Tip Single Bit	0.025 cm (0.01 in.) tip	10
		Spacecraft Parameters					
X	X	20-GHz power monitor	S/C telemetry	1.3 s	9 bits	0-3000 mW	2
X	X	30-GHz power monitor	S/C telemetry	1.3 s	9 bits	0-3000 mW	2
X	X	Multitone mode	S/C telemetry	1.3 s	Discrete	ON/OFF	1
X	X	CW mode	S/C telemetry	1.3 s	Discrete	ON/OFF	1
		Experiment Status					
X	X	Grd. antenna azimuth angle	Antenna	1	4 bit–BCD	0.00°-360.00°	1
X	X	Grd. antenna elevation angle	Antenna	1	4 bit–BCD	0.00°- 90.00°	1
X	X	Greenwich mean time	Time code translator	1	36 bits	Day:hr:min:s	1
X		20-GHz CW mode	Control panel	1	Discrete	Hi/Low/Off	1
	X	20-GHz multitone mode	Control panel	1	Discrete	Hi/Low/Off	1
X		30-GHz CW mode	Control panel	1	Discrete	Hi/Low/Off	1
	X	30-GHz multitone mode	Control panel	1	Discrete	Hi/Low/Off	1
X	X	20-GHz calibrate test mode	Control panel	1	Discrete	Cal. test	1
X	X	30-GHz calibrate test mode	Control panel	1	Discrete	Cal. test	1
X	X	S/C beam pointing earth longitude	Voice	1	4 bit–BCD	0.00°-180.00°	1
X	X	S/C beam pointing earth latitude	Voice	1	4 bit–BCD	0.00°- 90.00°	1

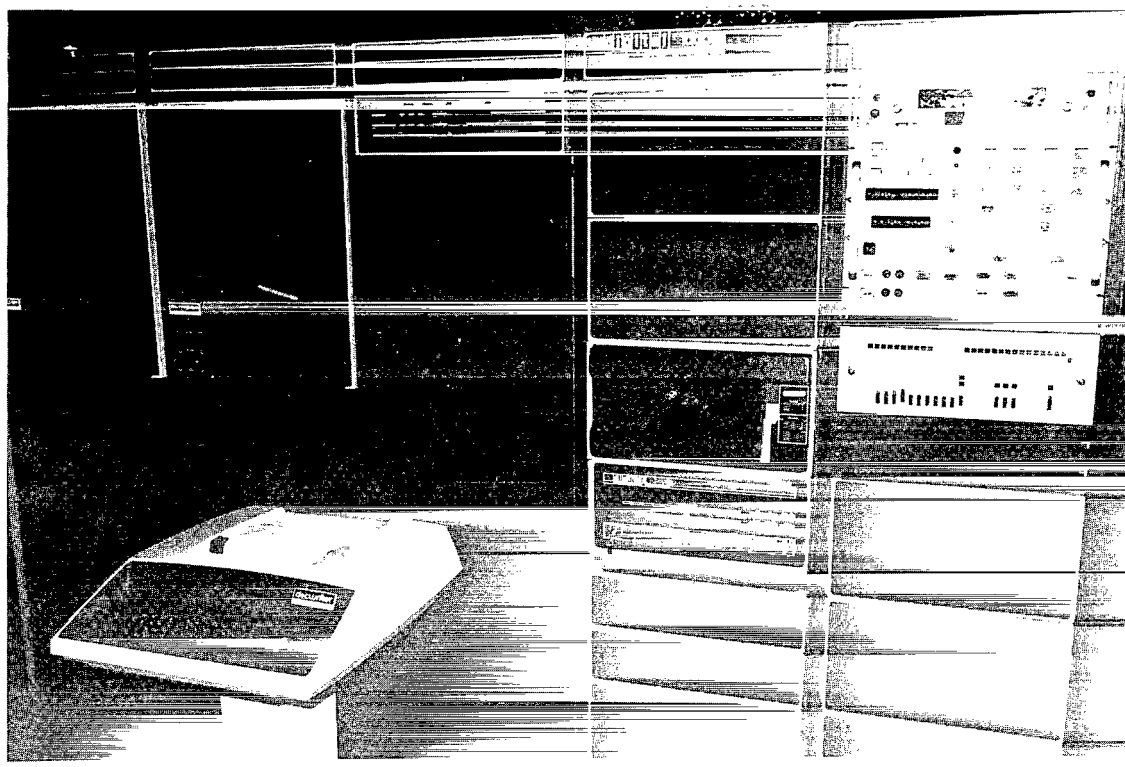

Figure 8. MWE data acquisition system, Rosman, North Carolina.

The digital tape recorded at Rosman is transferred to Goddard Space Flight Center (GSFC) via land lines, where final data reduction and analysis is accomplished. Data processing proceeds through three levels of reduction, with each succeeding step determined by the output of the step preceding it. Figure 9 presents a three-dimensional description of the many output displays that are generated from the digital processing programs at GSFC. All reduction is accomplished on IBM System 360 facilities, and the output graphics are generated on 16-mm film strips for evaluation and storage.

The ground terminal at GSFC consists of a 3-m parabolic antenna with manual tracking only. The GSFC receiver is similar to the Rosman unit, except that only the 20- and 30-GHz carriers can be received, and the front end does not utilize a parametric amplifier (paramp). Recording at GSFC is on analog tape and strip chart only, with no digital processing.

RAIN ATTENUATION

Rain attenuation is the most perplexing problem encountered in the design and operation of millimeter wavelength space communications systems. Early investigators recognized the problems of rain-induced attenuation (Ryde and Ryde, 1944), and semiempirical models were developed to describe the phenomena (Gunn and East, 1965; Medhurst, 1965).

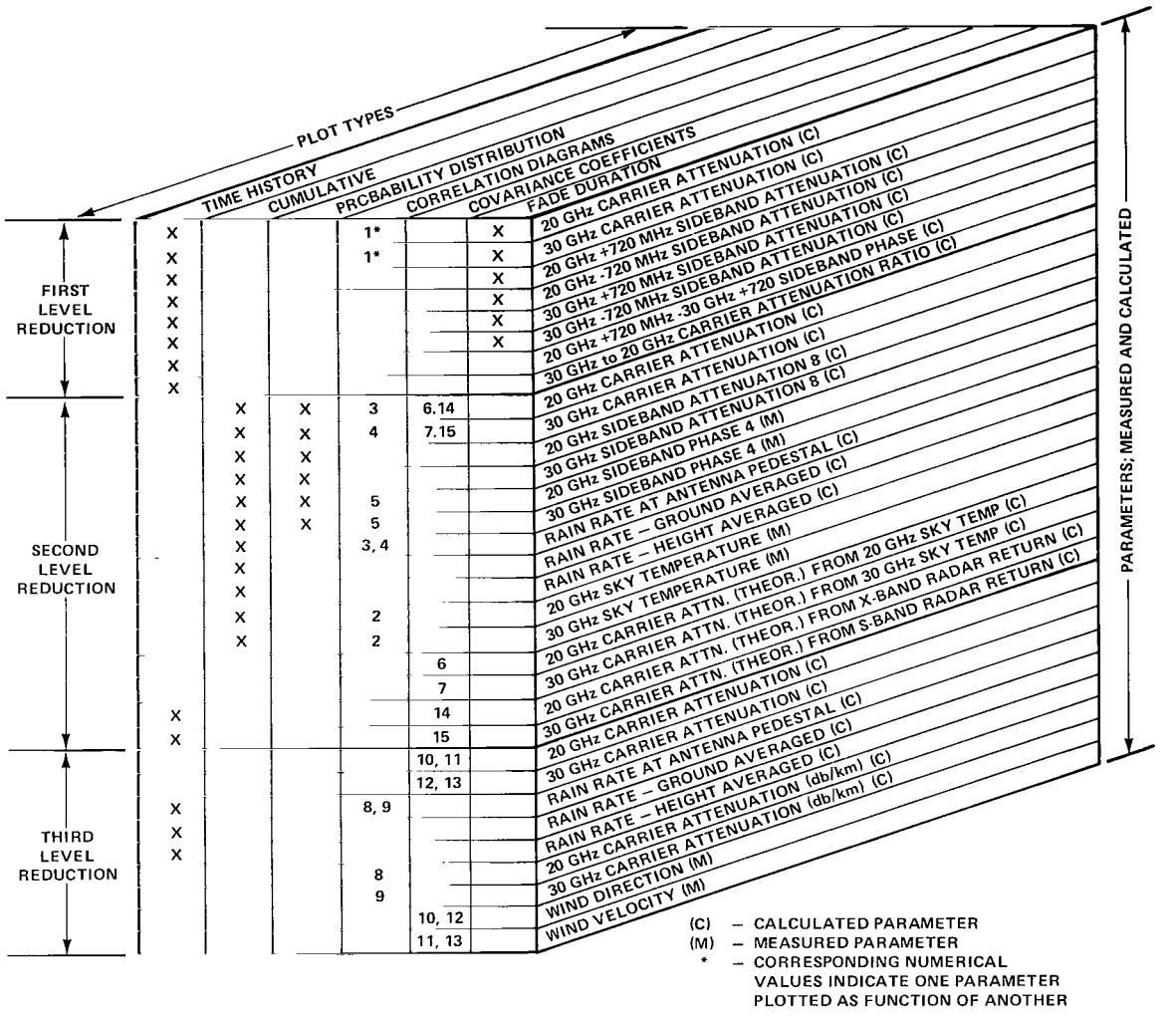

Figure 9. Central data processing output displays for the ATS-6 millimeter wave experiment.

Over the last decade or so, direct measurements of earth-space attenuation above 10 GHz have been accomplished, first with radiometers (Wulfsberg and Altshuler, 1972; Haroules and Brown, 1968) and suntrackers (Wilson, 1969), then with an earth satellite (Ippolito, 1970, 1971; Hodge, 1974). More refined models were discussed (Crane, 1971; Hogg, 1968), and the first steps in acquiring long term statistics of attenuation were begun at a number of frequencies and locations* (Craft, 1972; Straiton et al., 1972; Evans, 1971).

The attenuation due to a distribution of spherical raindrops is described by:

$$A \frac{dB}{(km)} = 4.343 \int_{0}^{\infty} N(a)\, Q(a, \lambda)\, da \qquad (1)$$

*Ippolito, L.J., "Earth-Satellite Propagation Above 10 GHz–Papers from the 1972 Spring URSI Session on Experiments with the ATS-5 Satellite," NASA Goddard Space Flight Center, TM X-65990, 1972.

where N (a) da is the number of drops per cubic meter with radii between a and a + da (cm), and Q (a, λ) is the attenuation cross section (m^2) of a single spherical drop of radius a (cm) at the wavelength λ (cm).

The relationship between raindrop size and rainfall rate was investigated empirically by Laws and Parsons (1943), and later distribution functions were developed by Marshall and Palmer (1948). They found that the drop-size distribution measurements can be represented by the relation:

$$N(a) = N(o)\, e^{-\Lambda a} \tag{2}$$

where N (o) is the value at zero radius, and

$$\Lambda = 82\, R^{-0.21} \tag{3}$$

where R is the rainfall rate, in millimeters per hour.

The attenuation cross section is calculated from the general solution of Maxwell's equations with a given refractive index of water for the wavelength of interest. Medhurst applied measured drop terminal velocities and the measured Laws and Parsons drop-size distribution to calculate the attenuation coefficient for 2 to 100 GHz (Medhurst, 1965).

A simple exponential expression relating attenuation and rainfall rate, of the form

$$A\ \frac{(dB)}{(km)} = \alpha\, R^B \tag{4}$$

first proposed by Gunn and East (1965), where α and B are frequency dependent constants, has shown reasonably good agreement with measured attenuation over short terrestrial paths. The attenuation coefficients for the ATS-6 MWE frequencies, assuming a Laws and Parsons (1943) drop-size distribution, are:

$$A\ \frac{(dB)}{km} = 0.0687\, R^{1.1} \text{ @ } 20 \text{ GHz} \tag{5}$$

$$A\ \frac{(dB)}{km} = 0.1649\, R^{1.035} \text{ @ } 30 \text{ GHz} \tag{6}$$

Figure 10 shows the attenuation as a function of rainfall rate for path lengths of 1 and 5 km. The path length is important in earth-space attenuation, and, as shown by the measured data, is a difficult parameter to define and measure.

The probability of occurrence of a given attenuation level or more precisely, the probability that the attenuation has equaled or exceeded a given level, is extremely useful in the design of systems where rain attenuation plays a significant part. A knowledge of this factor

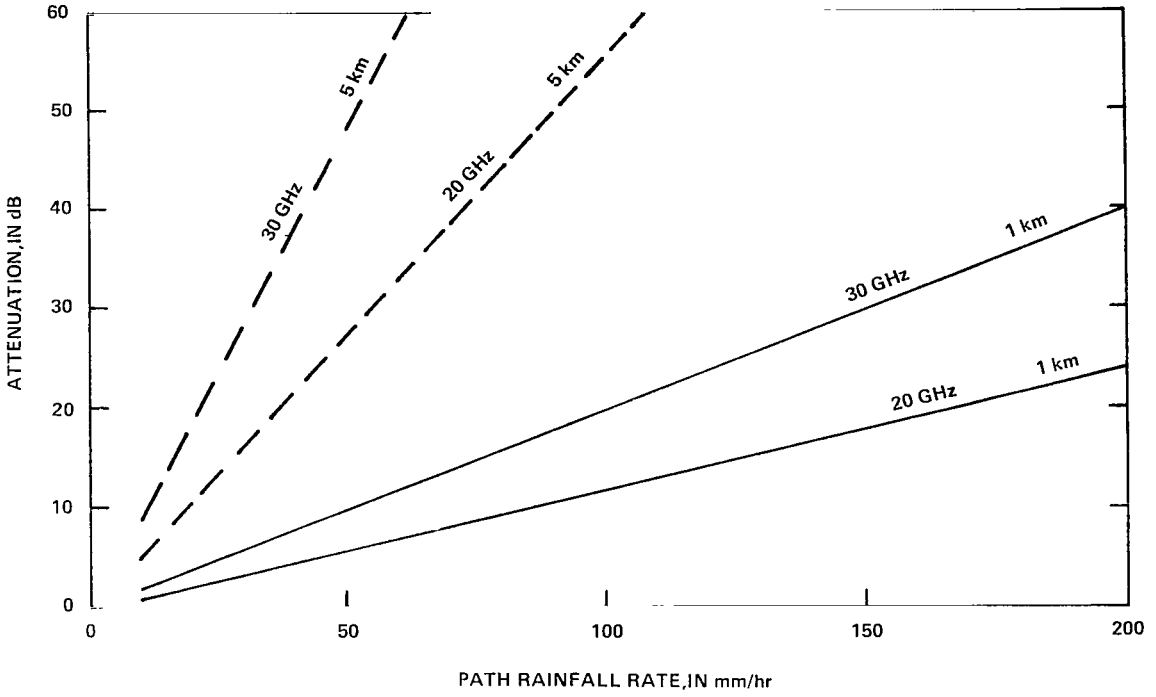

Figure 10. Attenuation at 20 and 30 GHz with Laws and Parsons drop-size distribution.

provides the basis for the power margin requirements for the link or conversely will indicate the expected outage time for a given link margin.

Attenuation distributions at 20 and 30 GHz for Rosman during July and August 1974, the two heaviest rainfall months, are shown in figure 11. For 20 GHz, the attenuation exceeded 12 dB for 0.68 percent of the 547-min test time; for 30 GHz the attenuation exceeded 28 dB 0.1 percent of the 492-min test time.

The ATS-6 MWE was operated on a callup basis during rain periods. Other experiments, primarily the health education telecommunications (HET) experiment and often the position location, aircraft communication experiment (PLACE), had priority for operations over the MWE, hence all rain periods could not be monitored.

The rainrate distribution for Rosman was continuously monitored with 10 rain gages located along the azimuth track of the satellite. Figure 12 shows the rainrate distribution for the entire 2-month, July through August period and for the period during which 20-and/or 30-GHz measurements were made. The distributions were measured at a rain gage collocated with the ground station antenna. The period of attenuation measurements, 600 minutes, represents 32 percent of the total time during July and August when rainfall greater than 1 mm/hr was measured. If the attenuation measurement period is a reasonable sample of the rainrate statistics for the total 2-month period, an estimate of the attenuation statistics for the

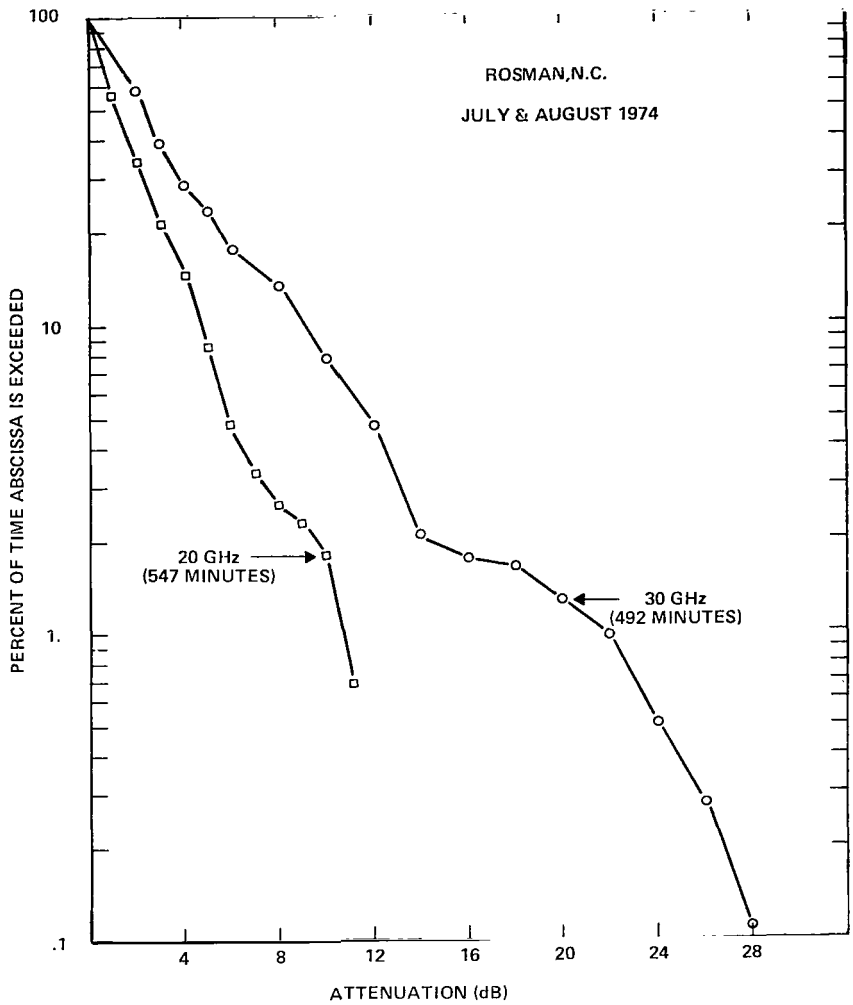

Figure 11. Attenuation distributions at 20 and 30 GHz for Rosman, North Carolina, July-August 1974.

total 2-month period can then be developed. The reasonableness of this assumption is verified by superimposing the upper curve of figure 9 on the lower curve. The similarity of the slopes of the displaced curve indicates that, up to 37 mm/hr, the attenuation measurement period was a representative sample of the rainfall statistics for the entire month.

The July through August estimate of 20- and 30-GHz attenuation can then be developed from ordered pairs of measured attenuation and rainfall rate for a given percent of time on the distribution curves given in figures 11 and 12. This technique, similar to that described for ATS-5 measurements,* is developed on figure 13 for the 20-GHz attenuation data. For

*Ippolito, L.J., "Summary and Evaluation of Results from the ATS Millimeter Wave Experiment," in "Earth-Satellite Propagation Above 10 GHz–Papers from the 1972 Spring URSI Session on Experiments with the ATS-5 Satellite," NASA Goddard Space Flight Center, TM X-65990, 1972.

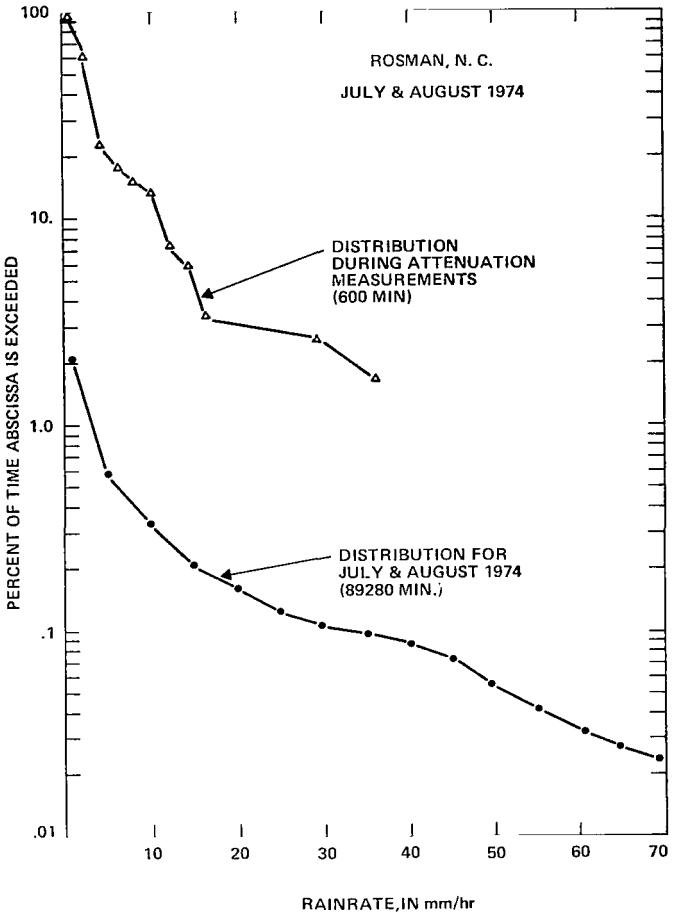

Figure 12. Rainrate distributions for July and August 1974 at Rosman, North Carolina.

example, the rainrate during the attenuation measurement period exceeded 30 mm/hr for 2.5 percent of the time (point A). The measured attenuation for the same percentage of time was about 8 dB (point B). The rainrate exceeded 30 mm/hr for 0.11 percent of the total July through August period (point C); therefore, the attenuation for the entire 2-month period would be expected to exceed 8 dB for that same percent of time, or 0.11 percent (point D). Using this approach, a prediction curve for 20 GHz was developed where rainrate and attenuation data were available, in this case up to the 10-dB level.

The 30-GHz attenuation distribution can be derived in a similar manner and is shown on figure 14. The results depicted on these curves give an indication of the kinds of margins required at Rosman for the two heaviest rainfall months. For allowable outage time of 90 minutes for July through August (0.1 percent), then link margins of 8 dB at 20 GHz and 14 dB at 30 GHz are required. Conversely, a system with a link margin of 10 dB could have expected outages totaling 82 minutes at 20 GHz and 196 minutes at 30 GHz.

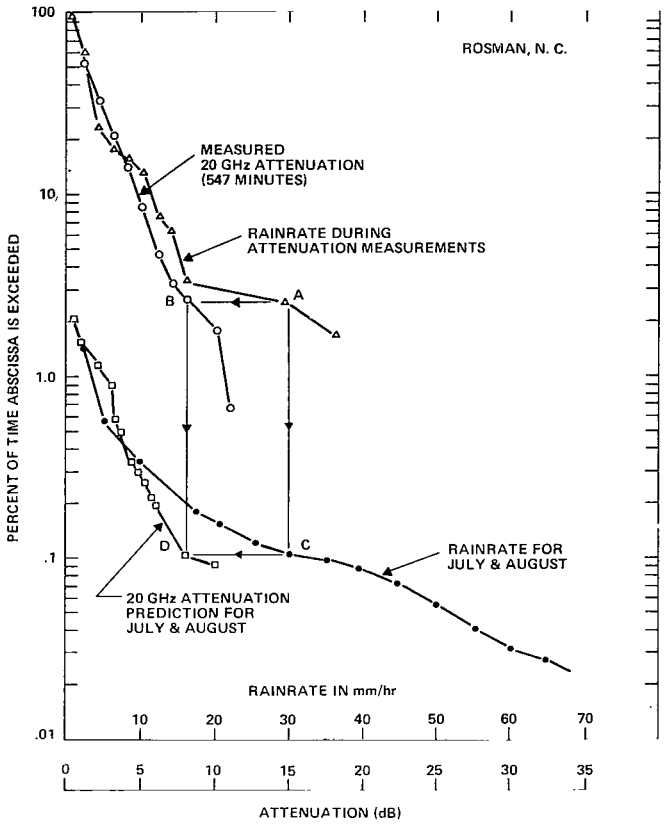

Figure 13. July through August 1974 20-GHz attenuation distributions for Rosman, North Carolina.

Data for the remaining months of ATS-6 operations at Rosman are presently under reduction, and similar statistics for the full 11-month period will be developed.

The duration, or length of the fade, is also an important parameter in the evaluation of rain attenuation. Figure 15 shows a fade duration histogram for Rosman for 931 minutes of 30-GHz measurements during July, August, and September 1974 and during January and February 1975.

Fade duration data for the 30-GHz attenuation is presented in 5-dB increment steps. A 10-s time bin size has been employed in these histograms. For convenience only, time bins up to 200 seconds have been plotted; the higher bin values and the number of fades associated with each bin (usually one fade) are listed on each figure. As shown in figure 15, a wide fade duration distribution exists for fades $\geq$5 dB. Fade durations up to 3430 seconds have been obtained. The longer duration fades are characteristic of continuous rain that exists over a long period of time. It is noticed that as the fade threshold increases, the fade duration for the number of fades decreases. These shorter duration fades are characteristic (level $\geq$15 dB) of thunderstorms or periods of high intensity rainfall. A drastic decrease in

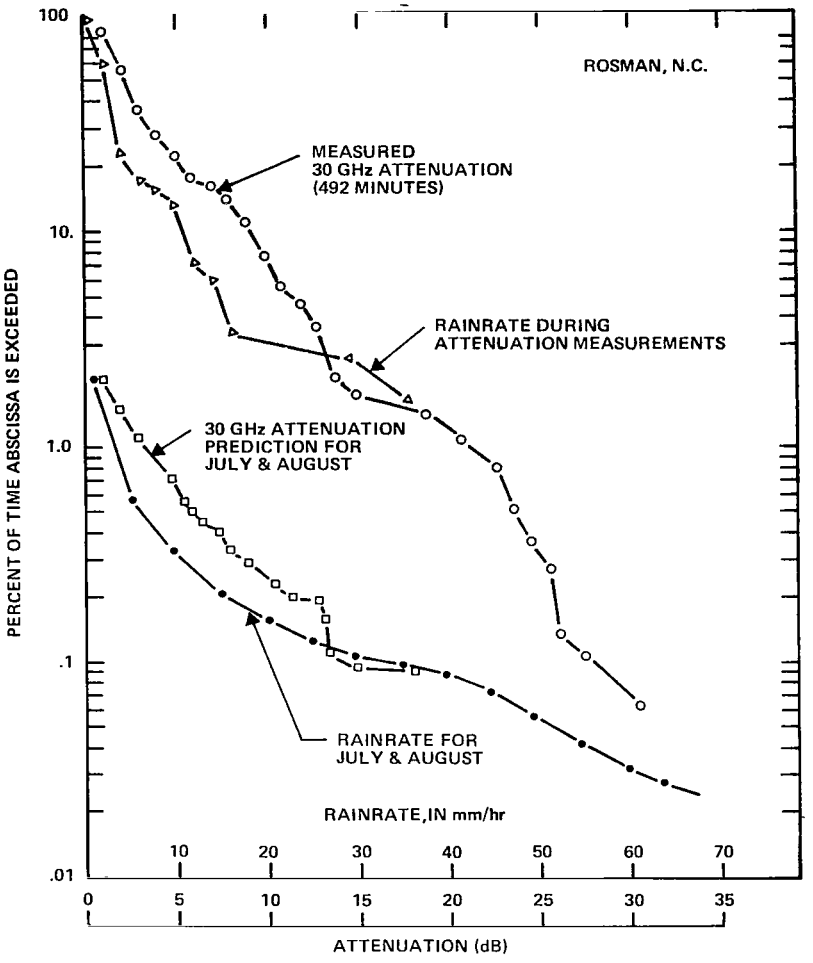

Figure 14. July through August 1974 30-GHz attenuation distribution for Rosman, North Carolina.

the fade duration characteristics occurred between the 10-dB and 15-dB threshold level. Because of the limited amount of high attenuation data (>20 dB), little information concerning fade duration trends can be obtained from the histograms to date.

The attenuation ratio, expressed as the ratio of attenuation at 30 GHz in dB, to the attenuation at 20 GHz in dB, is a useful parameter for a number of reasons. A knowledge of attenuation ratio characteristics could provide a means for predicting the attenuation at one frequency, given the attenuation at another. Also, attenuation ratio measurements are very sensitive to drop-size distribution variations; hence, an estimate of the drop-size distribution could be developed. However, both of the above applications require a consistent or at least a predictable relationship between the attenuation ratio and other measured parameters.

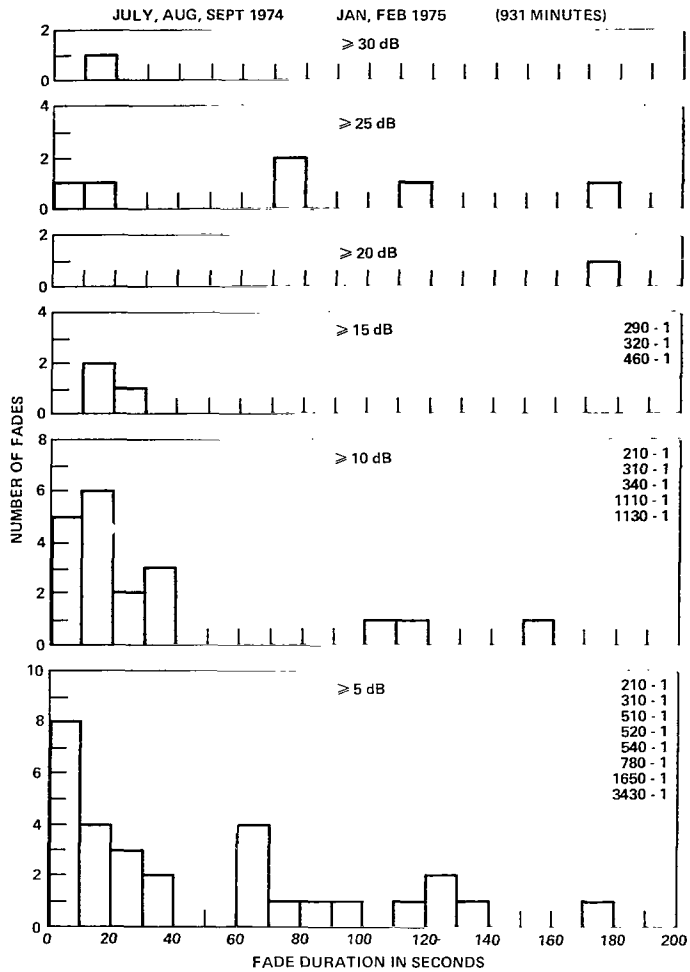

Figure 15. Fade duration histogram for 30 GHz at Rosman, North Carolina.

Assuming that the attenuation varies as a power of the rainfall rate, equations (5) and (6), then the attenuation ratio is

$$\frac{A_{30}(dB)}{A_{20}(dB)} = 2.40029\ R^{-0.06510} \tag{7}$$

A more useful expression is available by solving for R in equation (5) and substituting in equation (7). The result gives the attenuation ratio as a function of the 20-GHz attenuation

$$\frac{A_{30}(dB)}{A_{20}(dB)} = 2.04860 \left(\frac{L}{A_{20}}\right)^{0.05916} \tag{8}$$

where L is the path length in km, and A_{20} is in dB. Note that the attenuation ratio is dependent on path length, and for a given attenuation at 20 GHz, it is not in general possible to predict the attenuation at 30 GHz, unless L is known.

Measurements of attenuation ratio with the MWE have shown that the ratio varies widely with each event and during the event itself. Examples of attenuation ratio measurements for four rain periods at Rosman are shown in figures 16, 17, 18, and 19. The dashed lines on the plots are the expected values of attenuation ratio for the given path length L. Figure 20 shows an example of the variation of the ratio during a 40-min segment of the rain event on July 4. As expected, the ratio varies significantly, from 1 to 4, indicating the changing drop-size and path length conditions of each event.

A more useful evaluation of attenuation ratio is accomplished by comparing the long term statistics of 20- and 30-GHz attenuation and developing a ratio for a given percent of time.

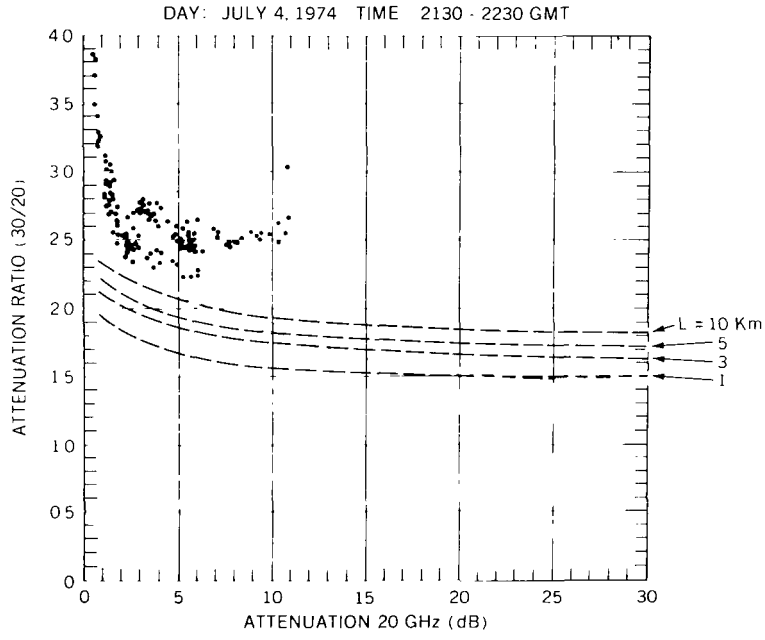

Figure 16. Attenuation ratio measurements on July 4, 1974 (2130-2230 GMT), Rosman, North Carolina.

The attenuation ratio for Rosman for the July through August period (see figure 11) is shown on figure 21 as ⊗'s. The attenuation ratio developed from the predicted curves of figures 13 and 14 is also shown on figure 21 as the solid dots. The dispersion of the ratio is reduced significantly, with ratios ranging from 1.5 to 2.1. A best fit power

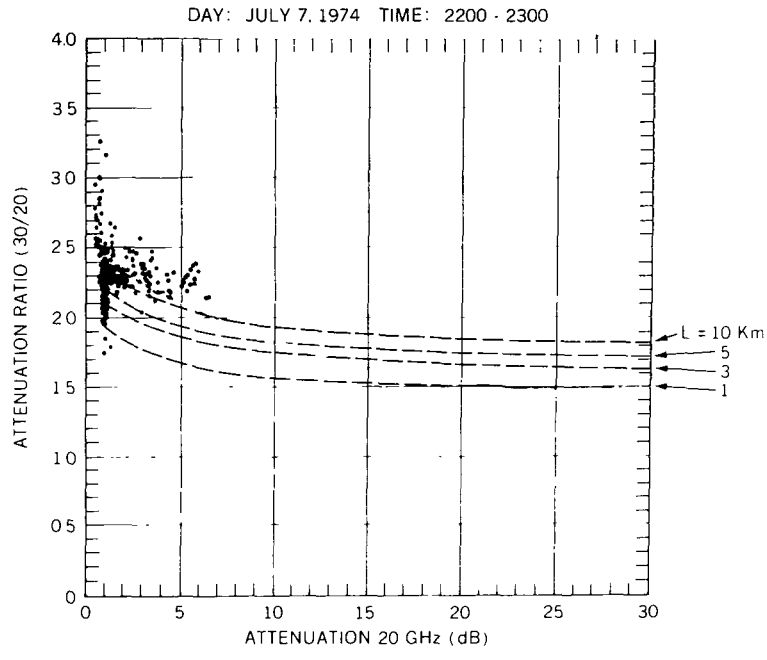

Figure 17. Attenuation ratio measurements on July 7, 1974 (2200-2300 GMT), Rosman, North Carolina.

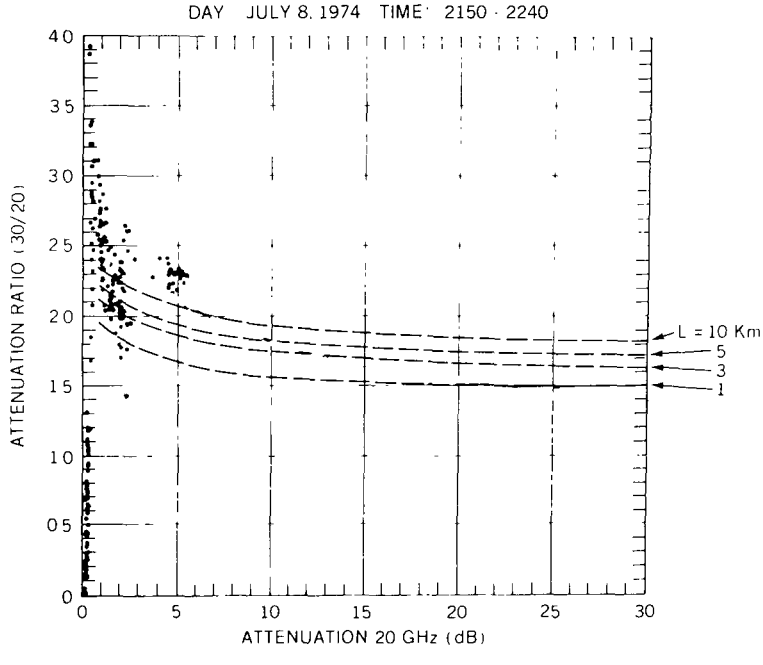

Figure 18. Attenuation ratio measurements on July 8, 1974 (2150-2240 GMT), Rosman, North Carolina.

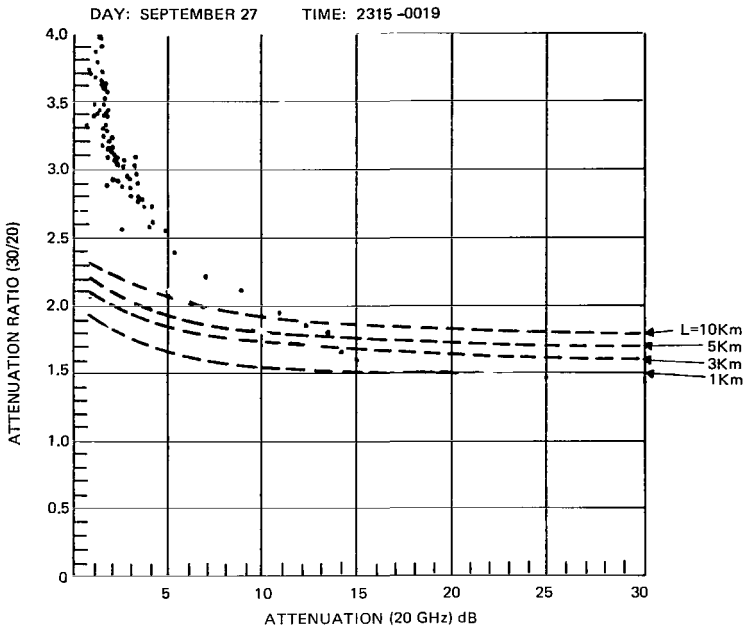

Figure 19. Attenuation ratio measurements on September 27, 1974 (2315-0019 GMT), Rosman, North Carolina.

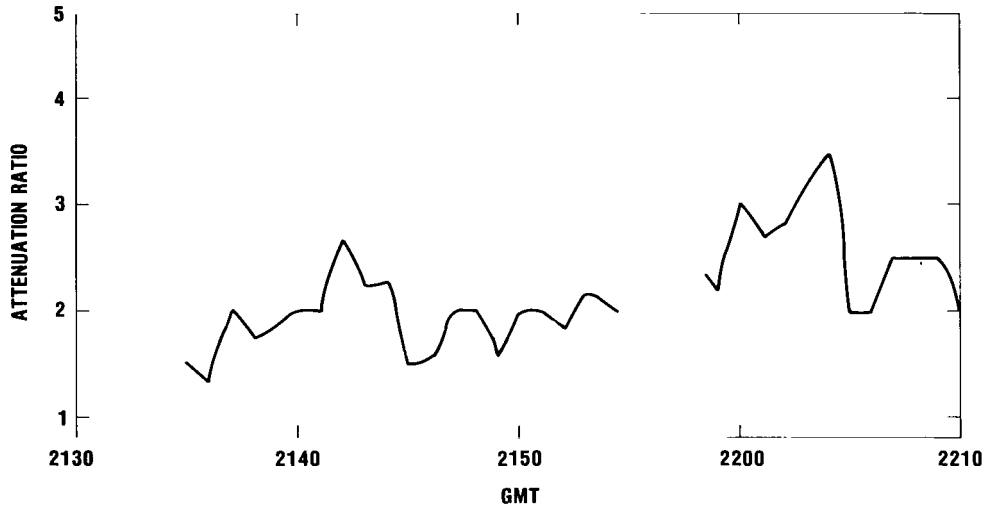

Figure 20. Attenuation ratio time plot for July 4, 1974 (2130-2210 GMT).

curve for the measurement ratios (⊗'s) is shown by the solid curve on figure 21. The resulting curve was

$$\frac{A_{30}(dB)}{A_{20}(dB)} = 1.8755\, A_{20}^{-0.0306}, \tag{9}$$

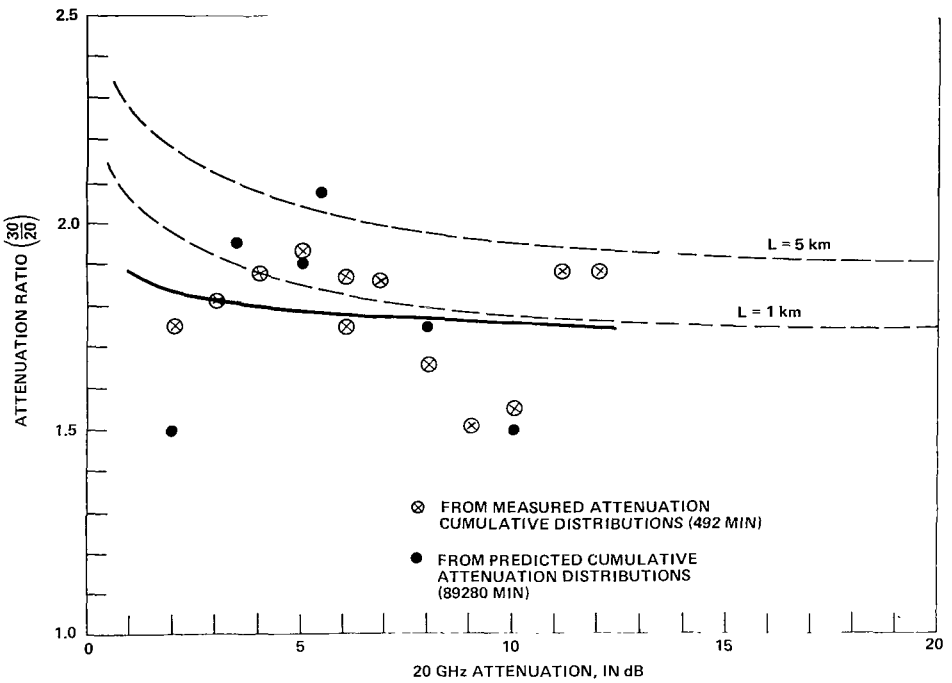

Figure 21. Attenuation ratio from attenuation statistics for July and August 1974, Rosman, North Carolina.

which is very close to the predication curve for a constant 1-km path length, and approaches a 1.7 ratio for large values of 20-GHz attenuation.

Measurements from other locations and seasons of the year will be compared to the above results, as they become available, to determine if consistent trends in the attenuation ratio variations are observed.

SCINTILLATIONS

Rapid amplitude fluctuations, or scintillations, have been observed at Rosman, GSFC, and at other participating sites.* The amplitude scintillations have been observed at both 20 and 30 GHz, and in clear and rainy weather conditions. Figure 22 shows an example of 20-GHz, atmospheric scintillations during an overcast day at GSFC. The scintillation amplitude increased from about 0.5 dB to 3 dB, peak to peak, during the passage of a cloud through the earth-satellite path. The fluctuation rate was fairly constant, at about 16 cycles per minute, or 0.27 Hz. The scintillations lasted for about 200 seconds, then settled back to the initial levels.

*"Minutes of Second ATS-6 Millimeter Wave Experimenter's Conference," Goddard Space Flight Center, December 19-20, 1974, February 28, 1975.

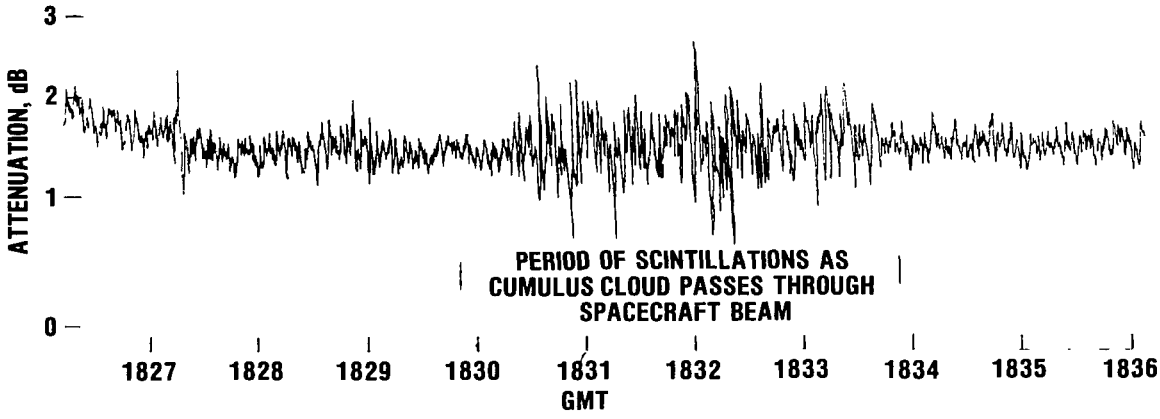

Figure 22. Amplitude scintillations during cloud movement from the GSFC Diversity Station, September 22, 1974 (20 to 80 percent cloud cover).

Examples of scintillations observed on a clear, cloudless day are shown in figure 23. The three events occurred within a 15-min period, and each consisted of a short burst of rapid amplitude scintillations which reached peak-to-peak amplitudes of 3 dB. The fluctuation rate appeared to be about 200 Hz, and each lasted from 0 to 20 seconds. The scintillations were not caused by manmade sources, such as passing aircraft or nearby radar transmissions. The spectra of the scintillations, observed with a high resolution spectrum analyzer, are shown in figure 24. The spectra of the three bursts do not appear similar; however, most of the energy appears to be below 50 Hz.

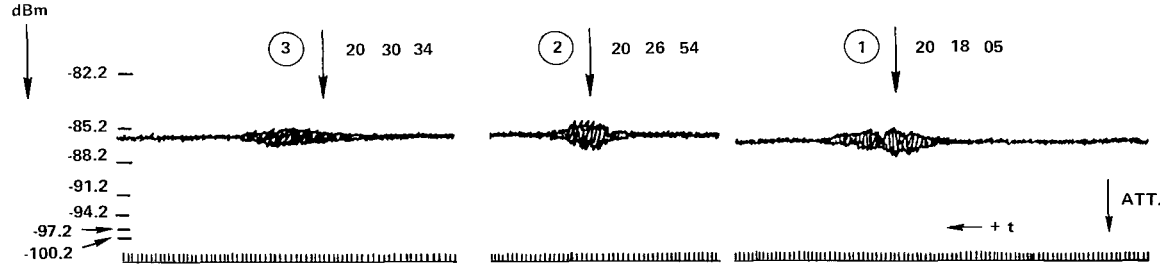

Figure 23. Clear weather scintillations, GSFC, 20-GHz carrier, November 26, 1974.

The cause or causes of scintillations of the types observed are not immediately evident. Clear air turbulence has been suggested as a possible source. Additional data from other locations are available and are under study.

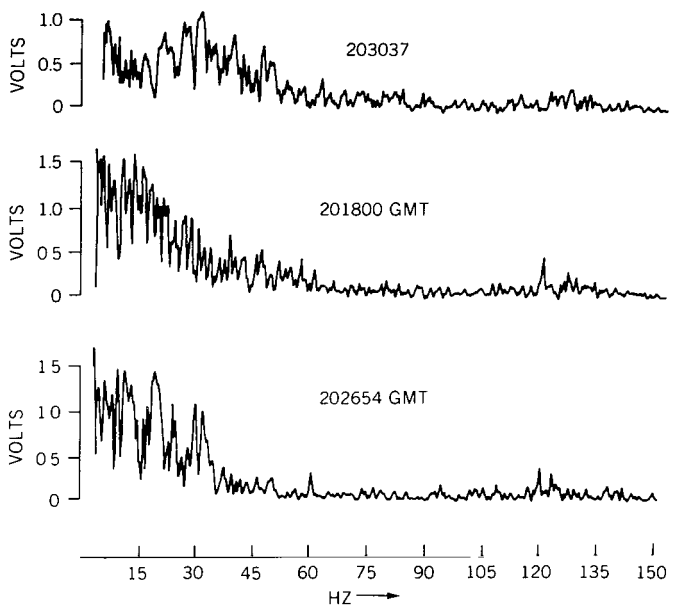

Figure 24. Spectra of clear weather scintillations, GSFC, November 26, 1974.

BANDWIDTH COHERENCE

The wideband frequency characteristics of the 20- and 30-GHz space channel were evaluated in the multitone mode of the MWE. In this mode, a carrier and eight equally spaced side tones are transmitted in the 20- and 30-GHz bands. A comb of nine tones is generated, four on either side of the carrier, spaced 180-MHz apart, and results in a total spectrum of 1440 MHz in each band. The measurements consist of the amplitude of each tone (18 total) and the relative differential phase between side-band pairs (8 total pairs).

The amplitudes of the side tones are adjusted by the modulation index to be approximately equal, and all 18 tones are calibrated by the automated receiver calibration system, described above. The relative differential phase output voltage, V_ϕ, is proportional to:

$$(\phi_u - \phi_c) + (\phi_L - \phi_c) \tag{10}$$

where ϕ_u, ϕ_L, and ϕ_c are the phases of the upper tone, lower tone, and carrier with respect to an arbitrary reference. This function provides a measure of the linearity of the channel frequency-phase characteristics. In an ideal linear system, V_ϕ would be zero; however, system noise and bandwidth limitations in a practical system cause a residual value for V_ϕ. Because of the sensitive nature of this measurement, all phase outputs were calibrated for each data run, at three input levels, and both with and without the parametric amplifier in the system. Nevertheless, the relative phase measurements were found to be extremely difficult to maintain, and only sparse data are available.

In the vast majority of measurement periods, the amplitude variations of the side tones, when compared to the carrier variations, were within the system measurement accuracy of ±1 dB. The measurements were made by comparing 1-s averages of each amplitude, with a sampling rate of 40/s. An example of a period where some selective amplitude fading was observed is shown in table 2. Each line on the table represents a 4-s average value of the 20- and 30-GHz carrier attenuations, in dB, and the side-tone differential attenuation, also expressed in dB. The time scale, starting at 20 minutes 0 seconds and progressing to 24 minutes 28 seconds, is shown on the left column of the table. Three different segments, each 36 seconds long, are shown. During the first two segments, the side tone differential attenuation values remained within the measurement accuracy. During the last segment, however, the 30-GHz carrier attenuation began to exceed 20 dB, and the outer side tones, ±720, exhibited variations of up to 6.9 dB.

At these high attenuation values, however, the measurement accuracy could be degraded above the ±1 -dB value by receiver noise and the reduction in dynamic range of the receiver output voltage. These factors are considered to be the main causes in the amplitude variations observed, rather than a selective fading effect caused by rain scattering and absorption in the channel.

An example of the 20-GHz differential phase fluctuations during a rain event is shown in figure 25. The solid lines are minute averages and the dots are the minute variance values for each plot. The +720 (20.72 GHz) and -720 (19.28 GHz) side-tone amplitudes are

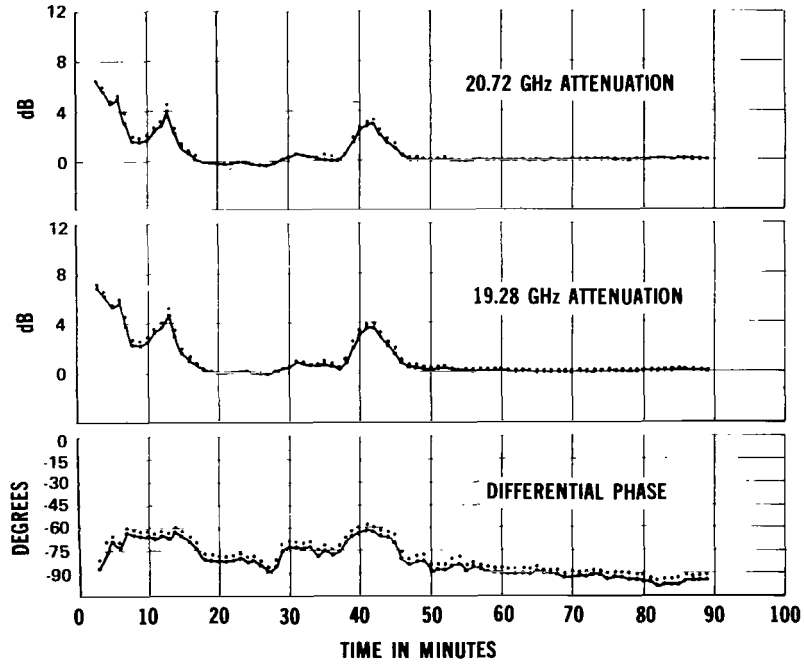

Figure 25. Differential phase measurements at 1440 MHz, Rosman, North Carolina, August 9, 1974 (2350 GMT).

Table 2

Multitone Amplitude Variations, Rosman, North Carolina, September 27, 1975

						20 GHz				
MM	SS	-720	-540	-360	-180	CARR	+180	+360	+540	+720
20	0	0.5	0.5	0.5	0.5	0.0	0.5	0.5	0.5	0.6
20	4	0.5	0.5	0.5	0.5	0.0	0.5	0.5	0.5	0.5
20	8	0.7	0.7	0.7	0.7	0.0	0.7	0.7	0.6	0.7
20	12	0.7	0.7	0.7	0.6	0.0	0.7	0.7	0.7	0.7
20	16	0.7	0.7	0.7	0.6	0.0	0.7	0.7	0.6	0.7
20	20	0.8	0.8	0.7	0.7	0.0	0.8	0.8	0.7	0.7
20	24	0.9	0.8	0.8	0.8	0.0	0.9	0.9	0.8	1.0
20	28	0.8	0.7	0.7	0.7	0.0	0.8	0.8	0.7	0.7
20	32	0.9	0.9	0.9	0.9	0.0	0.9	0.9	0.8	1.0
20	36	0.8	0.9	0.8	0.7	0.0	0.8	0.8	0.8	0.9
22	40	0.9	1.2	1.0	0.9	2.4	1.2	1.1	1.2	1.3
22	44	1.0	1.2	1.0	0.9	2.5	1.2	1.1	1.2	1.5
22	48	1.0	1.2	1.0	0.9	2.8	1.2	1.1	1.2	1.5
22	52	1.0	1.3	1.0	0.9	3.2	1.2	1.1	1.3	1.4
22	56	1.1	1.4	1.0	0.9	3.2	1.2	1.2	1.3	1.5
23	0	1.0	1.3	1.0	0.8	3.5	1.1	1.1	1.2	1.5
23	4	1.0	1.3	1.0	0.7	3.4	1.1	1.1	1.3	1.5
23	8	1.1	1.3	0.9	0.7	3.6	1.1	1.1	1.3	1.5
23	12	0.9	1.3	1.0	0.7	3.7	1.1	1.1	1.2	1.3
23	16	1.0	1.4	1.0	0.8	3.4	1.2	1.1	1.4	1.5
23	52	0.9	1.3	1.1	0.6	6.7	1.2	1.2	1.3	1.5
23	56	0.7	1.3	1.0	0.4	7.2	1.0	1.0	1.3	1.6
24	0	0.6	1.3	1.0	-0.0	8.2	0.6	0.6	1.2	1.3
24	4	0.9	1.3	1.0	-0.4	9.3	0.1	0.1	1.1	0.8
24	8	0.8	1.2	1.0	-0.7	10.0	-0.2	-0.3	0.9	0.5
24	12	0.4	0.8	0.6	-1.2	10.7	-0.7	-0.7	0.6	0.0
24	16	0.2	0.7	0.4	-1.5	11.3	-1.0	-1.0	0.3	-0.2
24	20	0.0	0.5	0.2	-1.7	11.6	-1.2	-1.3	0.1	-0.4
24	24	-0.0	0.5	0.1	-1.9	12.0	-1.4	-1.5	0.0	-0.7
24	28	-0.2	0.2	-0.0	-2.1	12.4	-1.2	-1.8	-0.3	-0.9
						30 GHz				
20	0	1.1	1.1	1.0	1.2	0.3	1.2	1.2	1.2	1.3
20	4	1.1	1.1	1.1	1.2	0.3	1.2	1.2	1.1	1.2
20	8	1.1	1.1	1.1	1.3	0.4	1.2	1.2	1.1	1.3
20	12	1.1	1.1	1.0	1.2	0.4	1.2	1.3	1.2	1.4
20	16	1.2	1.1	1.1	1.2	0.4	1.2	1.3	1.2	1.4
20	20	1.1	1.1	1.0	1.2	0.7	1.2	1.3	1.2	1.4
20	24	1.1	1.1	1.1	1.3	0.8	1.2	1.3	1.3	1.5
20	28	1.1	1.1	1.1	1.3	0.7	1.2	1.3	1.3	1.5
20	32	1.1	1.0	1.0	1.2	1.1	1.2	1.2	1.3	1.4
20	36	1.0	0.9	1.0	1.2	1.1	1.2	1.2	1.3	1.3
22	40	0.7	0.9	0.9	1.1	6.8	1.2	1.1	1.0	0.8
22	44	0.6	0.8	0.7	1.1	7.3	1.1	1.1	0.8	0.7
22	48	0.5	0.6	0.5	1.2	8.0	0.9	1.0	0.6	0.4
22	52	0.1	0.2	0.1	0.9	8.8	0.6	0.8	0.2	-0.0
22	56	0.1	0.2	0.1	0.9	9.0	0.5	0.8	0.2	-0.2
23	0	-0.3	-0.2	-0.4	0.6	9.7	0.1	0.3	-0.3	-0.5
23	4	-0.1	-0.1	-0.2	0.7	9.4	0.3	0.6	-0.1	-0.5
23	8	-0.3	-0.2	-0.3	0.6	9.7	0.1	0.4	-0.2	-0.6
23	12	-0.5	-0.4	-0.4	-0.4	10.0	-0.1	0.2	-0.4	-0.9
23	16	-0.0	0.1	0.0	0.8	9.1	0.5	0.7	0.1	-0.4

Table 2 (Continued)
Multitone Amplitude Variations, Rosman, North Carolina, September 27, 1975

		30 GHz								
MM	SS	-720	-520	-360	-180	CARR	+180	+360	+540	+720
23	52	-0.8	0.0	0.0	0.7	14.5	0.9	0.3	0.8	-0.6
23	56	-0.5	0.5	0.5	1.3	15.3	1.1	1.0	1.0	-0.8
24	0	-1.2	0.1	-0.1	0.6	17.3	0.9	0.6	0.4	-2.2
24	4	-1.5	-0.1	-0.4	0.7	19.4	0.5	0.5	0.0	-3.3
24	8	-2.0	-0.5	-1.0	-0.1	20.8	0.0	0.0	-0.4	-4.7
24	12	-2.4	-0.0	-0.6	-0.1	21.6	0.1	-0.2	-1.2	-5.1
24	16	-2.1	0.2	-0.9	0.1	21.9	0.6	-0.3	-0.7	-5.1
24	20	-2.5	-0.1	-0.9	0.1	22.6	-0.7	-0.5	-1.5	-5.8
24	24	-2.5	-0.0	-0.8	-0.3	23.1	-0.1	0.0	-1.7	-6.3
24	28	-2.4	-0.5	-1.0	-0.0	23.5	-0.6	-0.4	-1.9	-6.9

shown, along with the relative differential phase between the two side tones, referenced to an arbitrary value. The phase fluctuations show some correlation with the amplitude fluctuations for the second attenuation peak. Also, the variance of the phase measurement remained at about 4°, which is the sensitivity of the measurement. A total phase variation of about 30° occurred during the measurement period.

The examples of amplitude and phase variations given above were developed from 1-s average digital records of the data. Thus they would detect long term or slow fluctuations in the measured data, but would be insensitive to rapid fluctuations and scintillation which may be present. The short term channel characteristics of the MWE data observed at Rosman and GSFC are under analysis with analog multichannel recordings and a special purpose correlator/spectrum analyzer developed for the ATS-5 millimeter wave experiment. Estimates of the channel time-frequency transfer function, and important parameters such as coherence bandwidth, coherence time, and fading bandwidth are developed. The initial analysis of these data is proceeding and will be reported as results are available.

COMMUNICATIONS TESTS

The ATS-6 MWE provided the first operational millimeter wavelength communications link from an orbiting satellite. A 40-MHz noise bandwidth channel, 6-GHz uplink and 20, 30, and 4 GHz downlink, was used extensively for both analog and digital test transmissions.

The first successful color video transmitted through a millimeter wave space link was demonstrated at Rosman on July 12, 1974, with signal-to-noise ratios of 31.5 dB at 20 GHz, and 36.5 dB at 30 GHz. Video quality was good and compared favorably with the 4-GHz downlink. Numerous attempts were made to observe video signal degradation during heavy rain at Rosman, but all were unsuccessful. The complexity of the uplink-downlink operations required all video tests to be prescheduled, and only light rains occurred during the test periods.

Digital tests using a variable bit rate quadraphase modem were implemented in March 1975 at Rosman. Examples of 20-, 30-, and 4-GHz digital measurements are shown on figure 26. During this clear weather 4-hour test, a known code was transmitted to ATS-6 and the bit error rate (BER) for the three downlinks plotted. The BER for the closed loop (no satellite) is shown by the dashed line and solid points. When the satellite link was introduced in the system, the BER for the 20- and 30-GHz links had a negligible degradation from the closed loop calibration. No digital rain measurements were available, however, rain attenuation was simulated by rotating the ground antenna polarization during a digital transmission. The results showed that the modem performed as expected with reduced input signal to noise ratios up to 3 dB.*

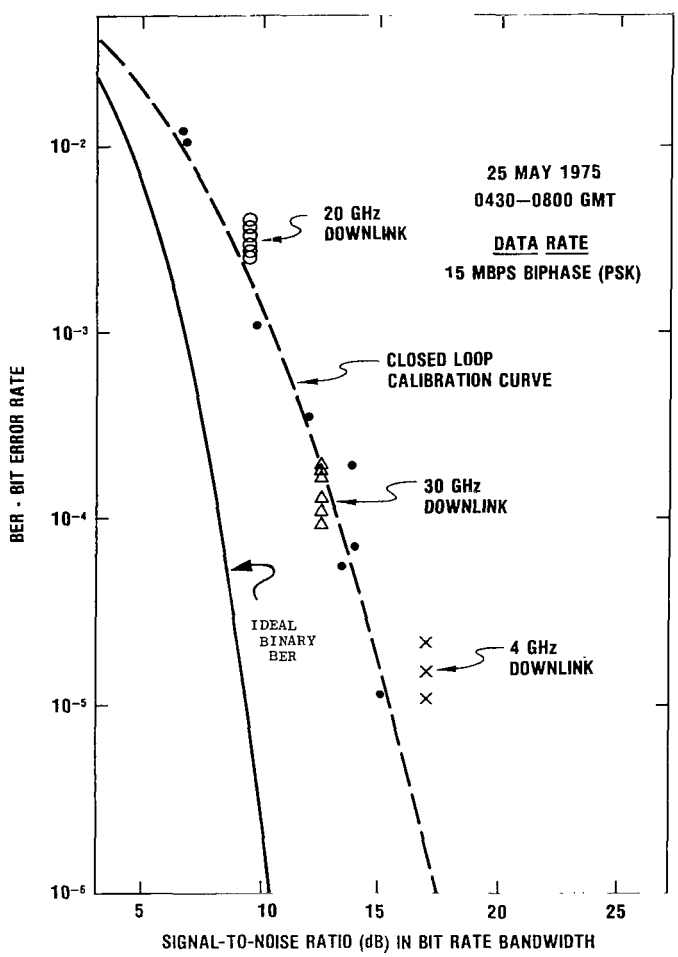

Figure 26. ATS-6 digital communications link measurements on May 25, 1975 (0430-0800 GMT).

*Tu, K., D. Kahle, and B. Batson, "ATS-6 Quadraphase Transmission Tests," Instrument Society of America Conference, Milwaukee, Wisconsin, October 1975.

ATTENUATION PREDICTION FROM RAIN GAGES AND RADARS

In addition to direct attenuation measurements, extensive correlative measurements using rain gages and meterological radars were implemented at Rosman for the investigation and validation of attenuation prediction techniques.*

A dual frequency on-beam radar, collocated with the Rosman receiver terminal, was directed along the earth-satellite path to ATS-6. A set of 10 tipping bucket rain gages was deployed along the azimuth track of the earth-satellite path, out to a distance of 2.5 km. The major characteristics of the radar and rain-gage systems are summarized on figure 27. Figure 28 shows the radar antennas, and figure 29 shows a rain gage in the field. The on-beam radars, at 8.75 GHz and 3.0 GHz, have a range-gated resolution increment of 100 meters along the path with a range of 25.6 km. The radar return power is a function of the drop-size distribution and can be related directly to the attenuation at 20 or 30 GHz through an assumed drop-size distribution. Utilizing the following empirical relationship for continuous rain between rainfall rate and reflectivity factor, Z,

$$Z = 200\,R^{1.6} \tag{11}$$

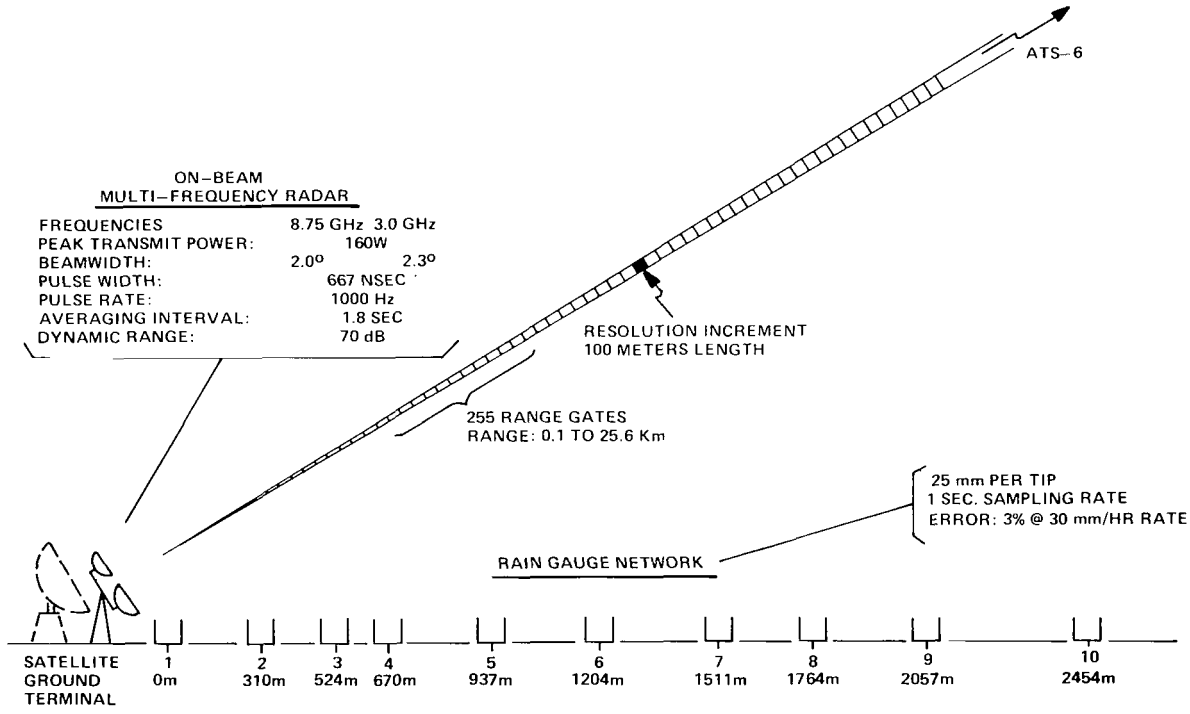

Figure 27. Radar and rain-gage measurements at Rosman, North Carolina.

*Ippolito, L.J., "The ATS-F Millimeter Wave Propagation Experiment," NASA/GSFC TMX-65752, October 1971.

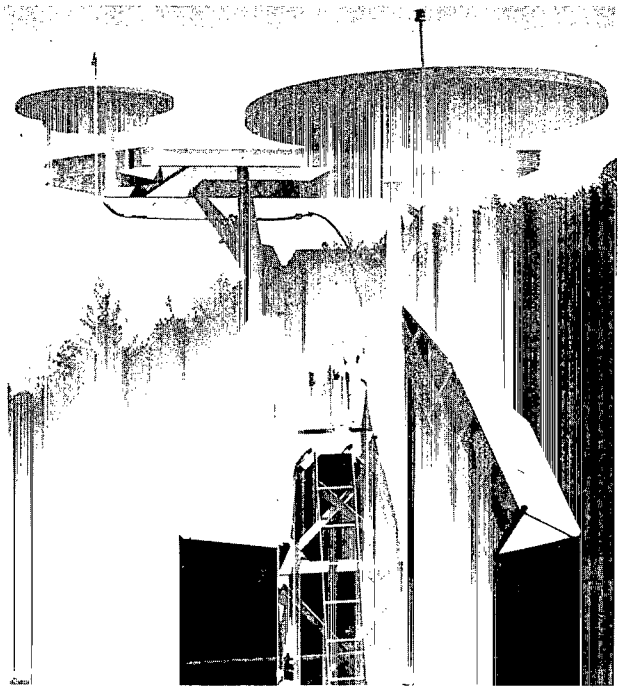

Figure 28. On-beam radar antennas at 8.75 GHz and 3 GHz, Rosman, North Carolina.

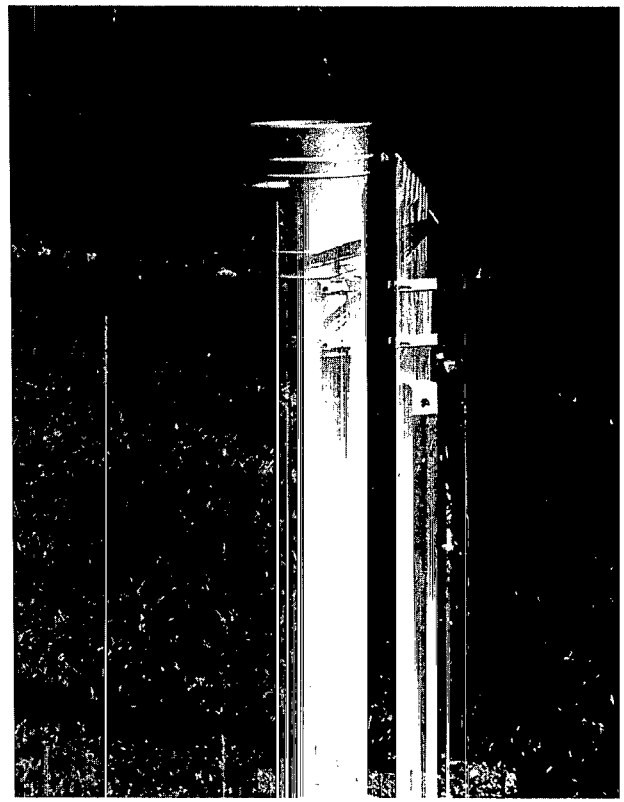

Figure 29. Rain gage, Rosman, North Carolina.

and the attenuation relationship for 20 and 30 GHz, (equations 5 and 6), the attenuation at 20 and 30 GHz can be developed (Westinghouse, 1975). The resulting expressions for the 20- and 30-GHz attenuation are:

$$A_{20}(\text{dB}) = \sum_{i=2}^{256} 0.1799 \times 10^{-3} Z_i^{0.6875} \tag{12}$$

$$A_{30}(\text{dB}) = \sum_{i=2}^{256} 0.5355 \times 10^{-3} Z_i^{0.6469} \tag{13}$$

where Z_i is the measured reflectivity factor of the *ith* range increment, in mm^6/m^3. Figures 30 and 31 are examples of results of direct attenuation measurements compared with predictions from the 8.75- and 3-GHz radars. In the 20-GHz case, the 8-GHz radar gave a slightly better prediction; however, both radars had a resulting RMS difference of less than 2 dB. The predictions at 30 GHz had larger RMS differences (see values on figure 31), but tended to give better correlation at the higher attenuation values.

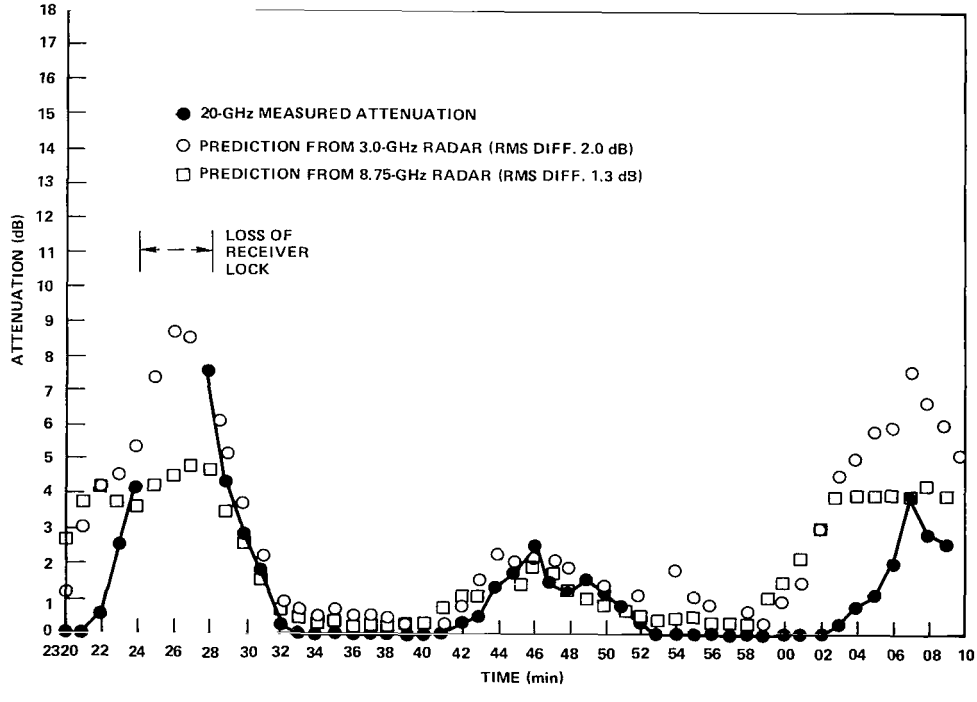

Figure 30. Prediction of 20-GHz attenuation from on-beam radar measurements for September 27, 1974.

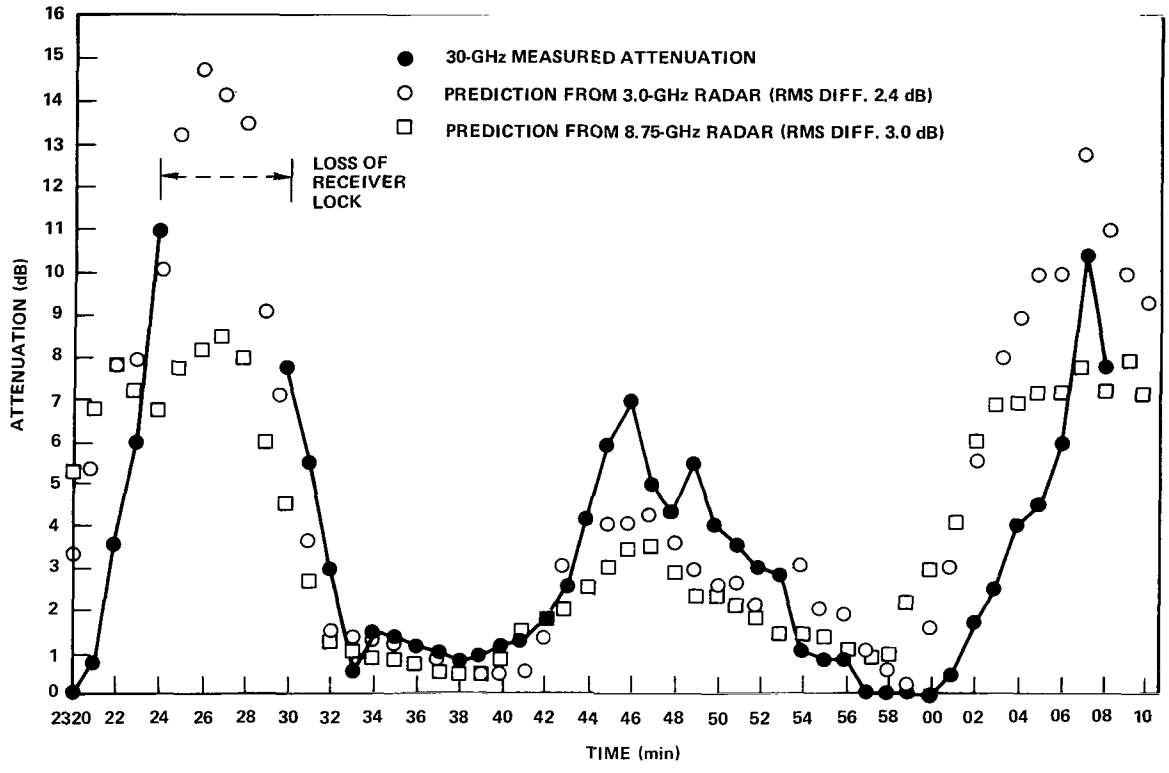

Figure 31. Prediction of 30-GHz attenuation from on-beam radar measurements for September 27, 1974.

Since the reflectivity factor, Z, is empirically related to the rainrate, R, it is possible to also use the radar to predict the rainfall rate along the path directly. This computed value can then be compared to the rainfall rate measured by the rain gage directly under that point in the path. As expected, the results show that the correlation for the nearer rain gage is good, but degrades as the distance along the path increases. Figure 32 shows the predicted (dashed) and measured (solid) rain rates for the rain gages at 310, 937, and 2454 meters. Figure 33 shows an example of how well the 8-GHz radar can predict the measured rainfall at the near rain gage for a highly variable rain event.

The radar measurements studies at Rosman are continuing, and the preliminary results summarized here provide only a sample of the versatility and utility of the meterological radar as a powerful tool for rain attenuation evaluation.

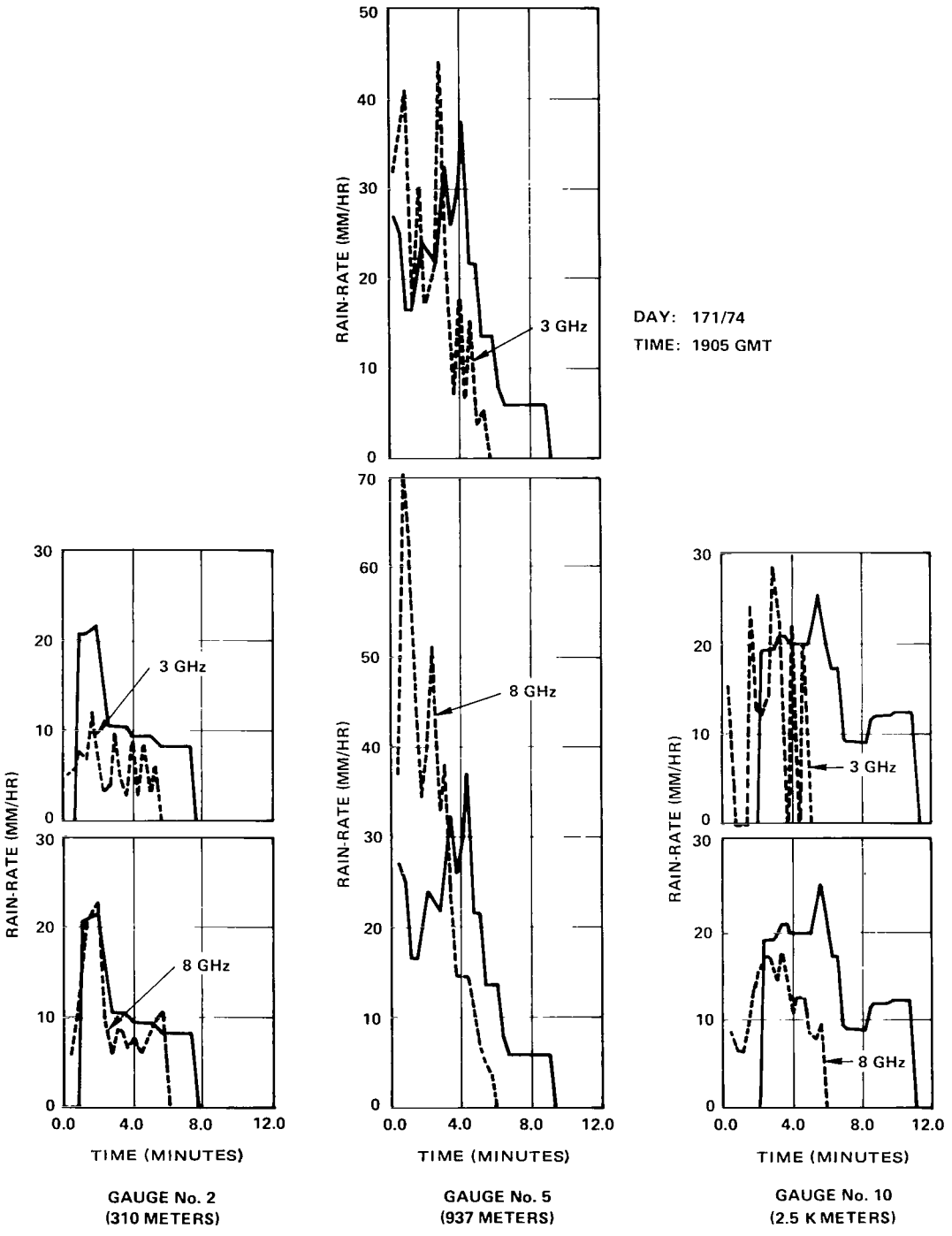

Figure 32. Rainrate prediction from radar measurements.

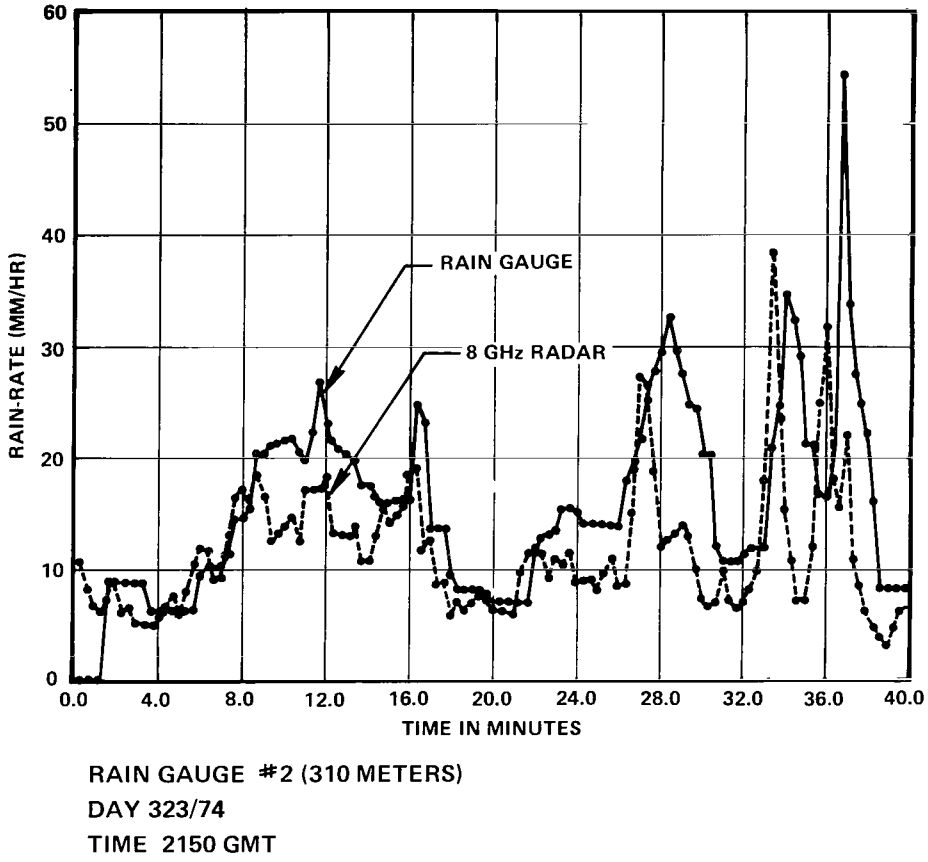

Figure 33. Rainrate computed from 8-GHz radar compared with measured rainrate.

REFERENCES

Craft, H. D., Jr., "Attenuation Statistics at 15.3 GHz for Clarksburg, MD," *COMSAT Technical Review*, **2**, (1), 1972, pp. 221-225.

Crane, R. K., "Propagation Phenomena Affecting Satellite Communication Systems Operating in the Centimeter and Millimeter Wavelength Bands," *Proc. IEEE*, **59**, (2), February 1971, pp. 173-188.

Evans, H. W., "Attenuation on Earth-Space Paths at Frequencies up to 30 GHz," *The 1971 International Conference on Communications Record*, Montreal, Canada, June 14-16, 1971, pp. 27-1,5.

Gunn, K. L. S., and T. W. R. East, "The Microwave Properties of Precipitation Particles," *Quart. J. Royal Met. Society*, **13**, July 1965, pp. 550-563.

Haroules, G. G., and W. E. Brown, "Radiometric Measurement of Attenuation and Emission by the Earth's Atmosphere at Wavelengths from 4 cm to 8 mm," *IEEE/MTT*, **16**, (9), September 1968, pp. 611-620.

Hodge, D. B., "A 15.3 GHz Satellite to Ground Path-Diversity Experiment Utilizing the ATS-5 Satellite," *Radio Science*, **9**, (1), January 1974, pp. 1-6.

Hogg, D. C., "Millimeter-Wave Communication through the Atmosphere," *Science*, **159**, January 5, 1968, pp. 39-46.

Ippolito, L. J., "Millimeter Wave Propagation Measurements from the Applications Technology Satellite (ATS-V)," *IEEE/AP*, **18**, (4), July 1970, pp. 535-552.

Ippolito, L. J., "Effects of Precipitation on 15.3 and 31.65 GHz Earth Space Transmissions with the ATS-5 Satellite," *Proc. IEEE*, **59**, (2), February 1971, pp. 189-205.

Laws, J. O., and D. A. Parsons, "The Relation of Raindrop-size to Intensity," *Trans. Am. Geophysical Union*, **24**, 1943, pp. 432-460.

Marshall, J. S., and W. Mc K.Palmer, "The Distribution of Raindrops with Size," *J. of Meteorol.*, **5**, August 1948, pp. 165-166.

Medhurst, R. G., "Rainfall Attenuation of Centimeter Waves: Comparison of Theory and Experiment," *IEEE/AP*, **13**, July 1965, pp. 550-563.

Ryde, J. W., and D. Ryde, "Attenuation of Centimetre Waves by Rain, Hail, and Clouds," Rept. 8516, General Electric Co. Research Labs., Wembly, England, August 1944.

Straiton, A. W., D. Pate, and B. M. Fannin, "Statistics on Earth-Satellite Attenuation at Two Texas Locations," Telecomm. Aspects of Freq. between 10 & 100 GHz, AGARD-CP-107, Gausdal, Norway, September 18-21, 1972, pp. 20-1,9.

Westinghouse Electric Corporation, "ATS-6 Millimeter Wave Propagation Experiment Data Analysis Report," Report No. F1S-75-005, for NASA Goddard Space Flight Center, February 1975.

Wilson, R. W., "Sun Tracker Measurements of Attenuation by Rain at 16 and 30 GHz," *Bell System Technical Journal*, May-June 1969, pp. 1383-1404.

Wulfsberg, K. L., and E. E. Altshuler, "Rain Attenuation at 15 and 35 GHz," *IEEE/AP*, **20**, (2), March 1972, pp. 181-187.

Preliminary Report On

ATMOSPHERIC ATTENUATION STUDIES ON ATS-6 SATELLITE 20/30-GHz BEACON SIGNALS

D. J. Fang and J. M. Harris
COMSAT Laboratories
Clarksburg, Maryland

ABSTRACT

This study is a part of a program of COMSAT participation in the NASA ATS-6 millimeter wave experiment. In the initial data collection phase, the measurement equipment included: (1) a 3-m-diameter antenna-receiver system for accepting 20-GHz satellite continuous wave (CW) signals and a radiometer system at 11.6 GHz for monitoring sky noise temperature; (2) a 4.6-m-diameter antenna-receiver system capable of receiving 20- and 30-GHz main CW signals plus radiometers at 20 and 30 GHz; (3) six rain gages along the boresight path toward the satellite for recording instantaneous rainfall rates; and (4) a weather radar at 5.4 GHz for detecting the motion pattern of the rain cloud in large scale.

Data analysis is done on an event-by-event basis by using received satellite signals as a basic reference for correlation with other information derived from the radiometers, the rain gages, and the radar. Important physical characteristics for prominent individual events of heavy rain storms are identified.

INTRODUCTION

There are "windows" in the frequency spectrum above 10 GHz where water vapor and oxygen absorption are relatively low. Two such windows are the frequencies below 20 GHz and a band from about 27 to 38 GHz. It follows that potential for future earth-satellite communications is greater in these bands. However, the essential propagation data base needed by system designers for predicting microwave communication system margin is not yet available.

COMSAT Laboratories' participation in the NASA ATS-6 millimeter wave experiment (MWE) was aimed at collecting propagation data at Clarksburg, Maryland, using the ATS-6 20/30-GHz beacons as the transmitting source, and obtaining data for the long base-line diversity experiment jointly with NASA/GSFC, NRL, and Westinghouse (at Baltimore-Washington International Airport). The data should be applicable to the general Washington, D.C., area and to other locations of similar climatological patterns.

The measurement equipment included three beacon signal receivers (two for 20 GHz and one for 30 GHz), three radiometers (11.6, 20, and 30 GHz), six rain gages beneath the boresight path toward the satellite, and one weather radar (5.4 GHz). The hardware aspects of these systems are discussed in the next section. Analysis of beacon signal data is oriented toward event-by-event analysis of each measured occurrence of precipitation-induced attenuation, because long term statistics of signal attenuation were not available because of the rarity of the satellite beacon transmission during precipitation events (due to the low priority accorded the MWE during most of the stay of ATS-6 at its western station). Details of the data analysis are given in the section on data analysis.

An important facet of the work which was not anticipated in the initial study program was the low-elevation-angle measurement of the satellite transmission. This measurement was made during the period when ATS-6 moved gradually from its original location at 94°W. longitude, to its present location at 35°E. longitude. It was found that strong scintillations occurred at low elevation angles, and that there was a large increase of signal level as the satellite descended towards the horizon into the diffraction region. Preliminary analysis of the data is given in the data analysis section. Conclusions are presented in the last section of the paper.

SYSTEM CONFIGURATION

Measurements were performed at COMSAT Laboratories, Clarksburg, Maryland, approximately 64 km (40 mi) northwest of Washington, D.C. Figure 1 shows the location of the Clarksburg site relative to the other diversity sites at NRL, GSFC, and Westinghouse. The measurement system can be summarized as follows:

- A 3-m-diameter transportable antenna-receiver system that included a 20-GHz receiver for receiving satellite beacon signals and a radiometric receiving system at 11.6 GHz for observing sky temperature using the same antenna.
- A 4.6-m-diameter antenna-receiver system that included 20- and 30-GHz receivers for the satellite beacon signals and two radiometric receivers at 20 and 30 GHz for observing sky temperature using the same 4.6-m antenna.
- A network of six rain gages extending for 7 km underneath the boresight path toward the satellite for examining the precipitation under the propagation path.
- A weather radar at 5.4 GHz for detecting the motion pattern of the rain cloud in large scale.

Figures 2 and 3 are the block diagrams of the 3-m and 4.6-m systems. The antennas are solid-surface aluminum paraboloids equipped with focal-point feeds and polarization rotators. Both antennas have servo-controlled elevation and azimuth positioners and decimal position readouts with a resolution of 0.1° and 0.01° for the 3-m and 4.6-m antennas, respectively. The nominal pointing direction to ATS-6 was 204° south-southwest from true north at an elevation angle of 42°.

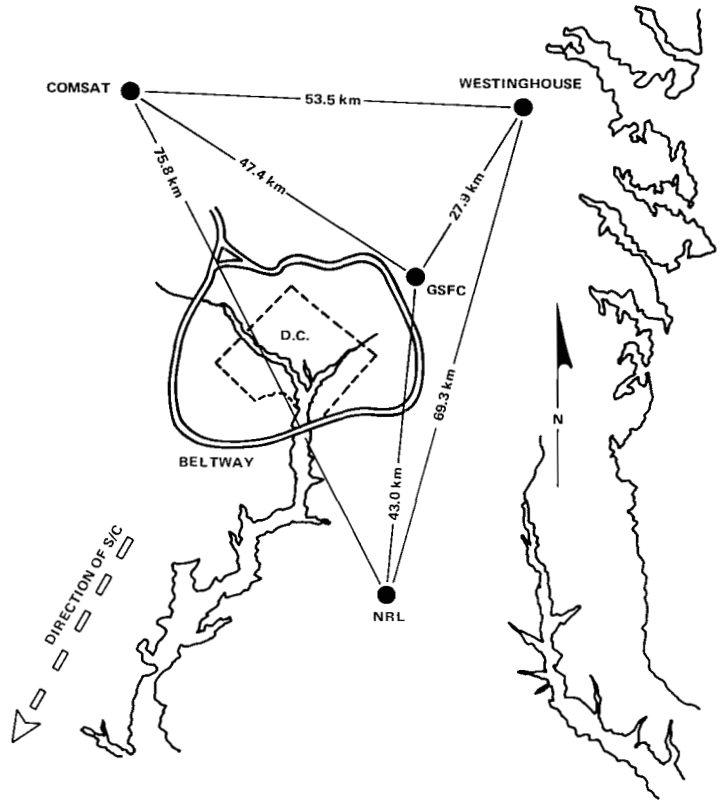

Figure 1. Location of COMSAT Laboratories, Clarksburg, Maryland, measurement and the Washington, D.C., area diversity experiment.

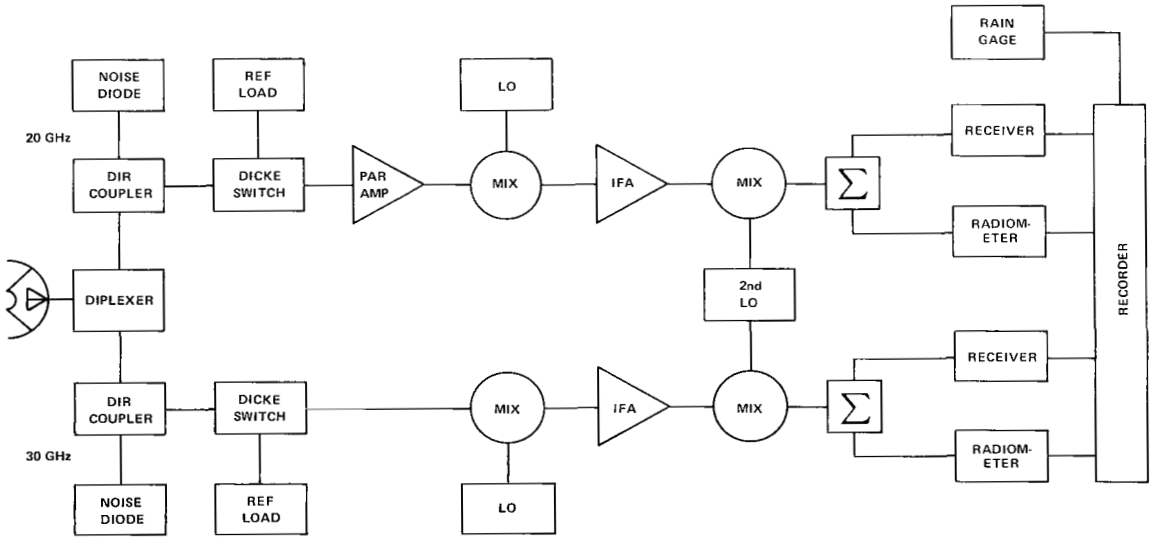

Figure 2. Block diagram: 20/30-GHz receiver/radiometer system.

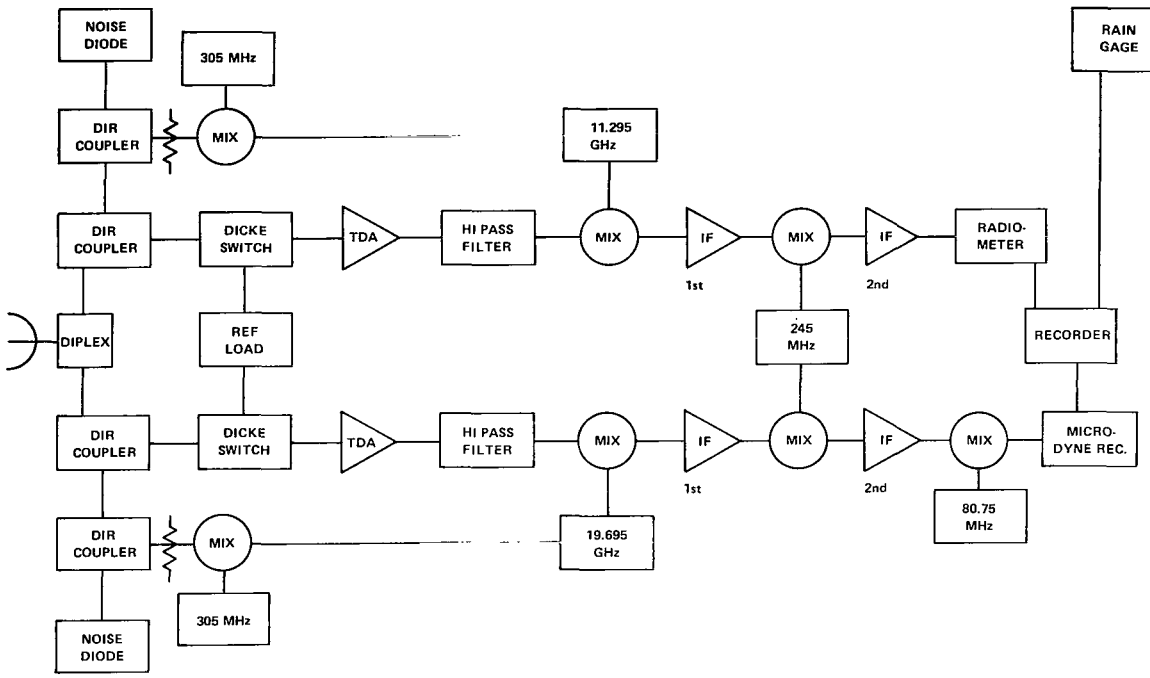

Figure 3. Block diagram: Transportable system, 11.6- and 20-GHz receiver/radiometer.

As indicated in figures 2 and 3, tunnel diode and uncooled parametric amplifiers are used in the 20-GHz front-ends of the 3-m and 4.6-m systems, respectively. The 30-GHz system has a low noise mixer front end. IF signal processors, which detect the down-converted signals by individual narrowband phase-locked receivers, give output amplitudes that are proportional to the satellite beacon signal attenuation levels. These outputs are then fed to strip-chart recorders or to data acquisition computers. Important performance parameters are shown in table 1 (3-m system) and table 2 (4.6-m system).

Table 1
Important Performance Parameters of 3-m Antenna System

	11.6 GHz	20 GHz
Antenna gain	48.7 dB	53.5 dB
Pointing accuracy	±0.1°	±0.1°
Noise figure	5 dB	8 dB
Radiometer sensitivity	1 K	–
Radiometer bandwidth	100 MHz	–
Receiver bandwidth	–	10 kHz

Table 2
Important Performance Parameters of 4.6-m Antenna System

	20 GHz	30 GHz
Antenna gain	57 dB	60.5 dB
Pointing accuracy	±0.01°	±0.01°
Noise figure	4 dB	8 dB
Radiometer sensitivity	1 K	1 K
Radiometer bandwidth	100 MHz	100 MHz
Receiver bandwidth	10 kHz	10 kHz

Both antenna systems are equipped with on-line radiometric subsystems. Operating in a Dicke-switched mode, these radiometers also include a noise source at known temperature for calibration purposes. The Airborne Instrument Laboratories (AIL) radiometric receivers (Model 2392 C) produce an output voltage proportional to the sky noise temperature. In the switched mode, the output is the net change of sky noise temperature from that of a clear sky day. Performance parameters of the AIL radiometric receivers are summarized in the list below.

Performance Parameters of AIL Radiometric Receivers

IF bandwidth	100 MHz (5 to 105 MHz)
Noise figure	7 dB
Input impedance	50 ohms
Input Standing Wave Ratio	< 2 to 1 over entire passband
Gain modulation	-3 to +3 dB, in 0.06-dB steps and continuous control of 0.1 dB
IF gain	85 dB (maximum)
IF gain control	0 to -41 dB, in 1-dB steps
Switch rate	5 to 500 Hz, stability ±0.05 percent
Switching waveform	Square wave
RF switch drive	0 to -14-V square wave into 10,000 ohms
Switched system output	±5 V maximum at 2 mA
Total power output	-5 V maximum at 2 mA
Integration time constants:	
Switched system	0.1, 1, 3, 5, 10, and 30 s
Total power system	1, 5, and 10 s
Monitor points	Second detector current; synchronous detector balance

DC reference	Up to 3.0 V (for use with total power output)
Input power	47 W nominal (capable of operation at 105 to 125 and 220 V AC, 50 to 440 Hz)

The rain gages are the tipping bucket type, where each tip represents 0.25 mm (0.01 in.) of rainfall accumulation. The gages are aligned beneath the satellite boresight path at distances of 0, 0.92, 1.08, 3.23, 5.53, and 7.4 km from the beacon receiver. Each gage is equipped with a mechanically driven strip-chart recorder with a time accuracy of better than 3 minutes per week.

The radar system is an RCA AVQ-10 weather radar operating at 5.4 GHz. Three different ranges of 37.04, 92.60, and 277.80 km (20, 50, and 150 n.m.) can be selected. Maximum elevation angle is 35°. A super 8-mm camera can be attached to the plan-position indicator (PPI) scope for filming the radar echoes. Since the radar slant path is lower than the ATS-6 slant path, no attempt has been made to incorporate the radar data for detailed analysis. However, the radar has proved useful as a device to predict the approach of a precipitating cloud.

Not all of the above systems were ready for measurement at the same time, as shown in table 3. Delays in preparation of the 4.6-m system were caused by the continuous slippage of the shipping schedule of the parametric amplifier. On the other hand, the systems have performed well once they were operational.

DATA ANALYSIS

An important constraint on the entire experiment was the lack of availability of millimeter wave 20/30-GHz beacon transmissions from the satellite during precipitation events. The priority of the millimeter wave experiment was not high. There were regular weekly transmission times assigned on an average of about one hour per day. These transmission times, although used by COMSAT for data collection and equipment calibration, were not really useful due to the fact that precipitation rarely occurred on site at these times. Requests were made consistently to NASA ATS Operations Control Center (OCC) for 20/30-GHz beacon transmission whenever precipitation was occurring or anticipated. Positive responses to the requests were infrequent. There were several occasions when beacon transmissions were abruptly terminated while valuable experimental data in a thunderstorm condition were collected.

With the above constraint in mind, data analysis was performed largely on an event-by-event basis. This includes:

(1) Correlation of the satellite 20-GHz beacon data and the radiometric sky temperature data.

Table 3
System Availability Chart

System	Equipment	Available Since	Comment
Transportable system	20-GHz CW receiver	July 1974	Varian 620 computer was equipped for automatic tracking and data collection. But it overflowed frequently. Usually only manual operation was used.
	11.6-GHz radiometer	July 1974	
	Rain gage	July 1975	
4.56 m (15-ft) system	20-GHz CW receiver	March 1975	Due to interference problem, the 20-GHz radiometer was turned off when CW receiver was taking data.
	20-GHz radiometer	March 1975	
	30-GHz CW receiver	April 1974	Paramp not available dynamic range 15-18 dB.
Others	5.4-GHz radar	September 1974	For visual observation only.
	Rain gages	February 1975	Total of six, counting the Clarksburg site.

(2) Correlation of the 20- and 30-GHz signal attenuation level.

(3) Correlation of the satellite 20-GHz beacon signals and data from the rain-gage network.

Another phase of data collection, not included with the original plan, involved observation of the satellite descending toward the horizon in late May and early June of 1975. The low elevation angle data will be presented in a separate section.

A typical data sample is shown in figure 4, (the event of March 19, 1975, lasting 150 minutes). The scattergram of the data is shown in figure 5. Empirically fit curves are shown as dashed lines. Theoretically derived attenuation curves using linear scaling for ambient sky temperature of 278 K and 300 K are also shown.

A typical data sample is shown in figure 6, the event of June 6, 1975. A scattergram of the data is shown in figure 7.

A basic problem in estimating the microwave attenuations over a satellite-earth propagation path based on rain-gage data is that for a given storm event, the attenuation and the rainfall

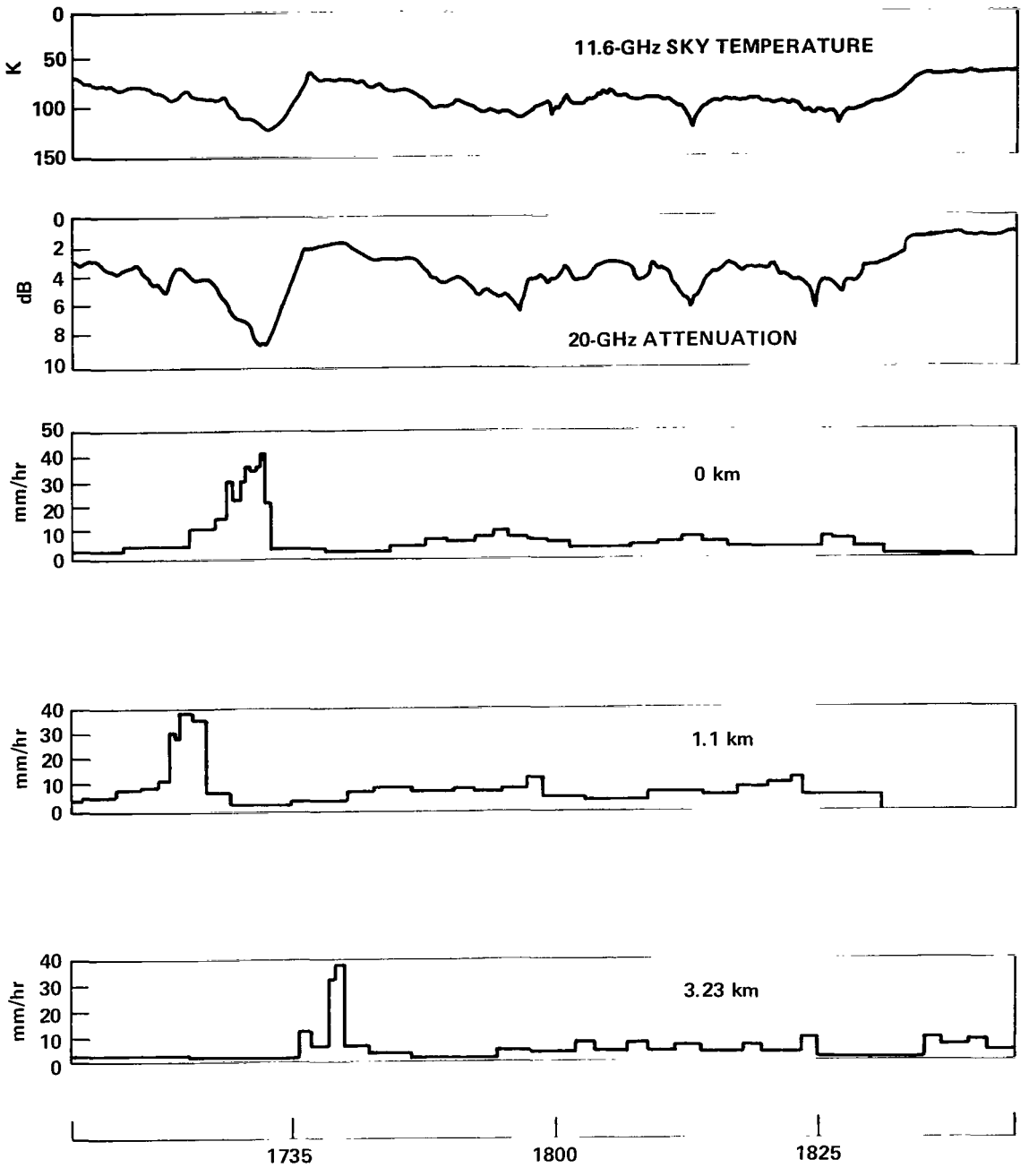

Figure 4. Typical precipitation–attenuation record measured at Clarksburg, Maryland. Ground rain gages were 0 km, 1.1 km, and 3.23 km from the 20-GHz receiver and the 11.6-GHz radiometer.

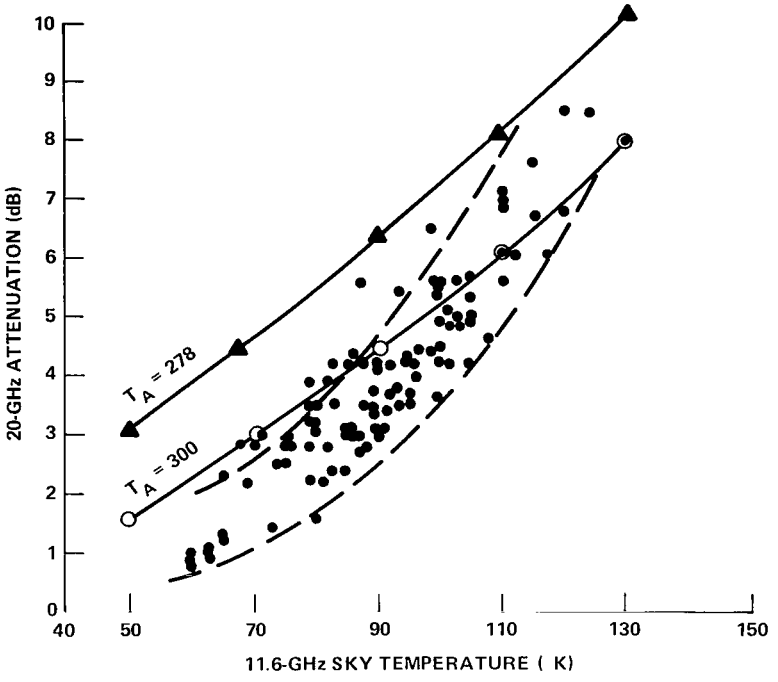

Figure 5. Scattergram of 20-GHz attenuation versus 11.6-GHz sky temperature from data given in figure 4. Solid lines theoretically derived for ambient temperature T.

records very often do not have a consistent detailed correlation. It is seen in figure 4, that while the radiometer curve correlates well with the satellite signal level, the data from rain gages do not have a consistent correlation with the 20-GHz curve. A particularly puzzling point is the peak registered on the rain gage 3.23 km away from the receiver.

We have collected and analyzed the data containing the apparent discrepancies in time and magnitude as those shown in figure 4. A model for adjusting the rain-gage data is provided below.

The rain rate, measured at an instant t by a ground rain gage consists of raindrops of sizes from 0.05 to 0.7 cm with falling velocity V ranging from 2 to 9 m/s. It follows that the rain rate at the ground rain gage, $R_g(t)$, is

$$R_G(t) = \sum_V R_v(t) \qquad (1)$$

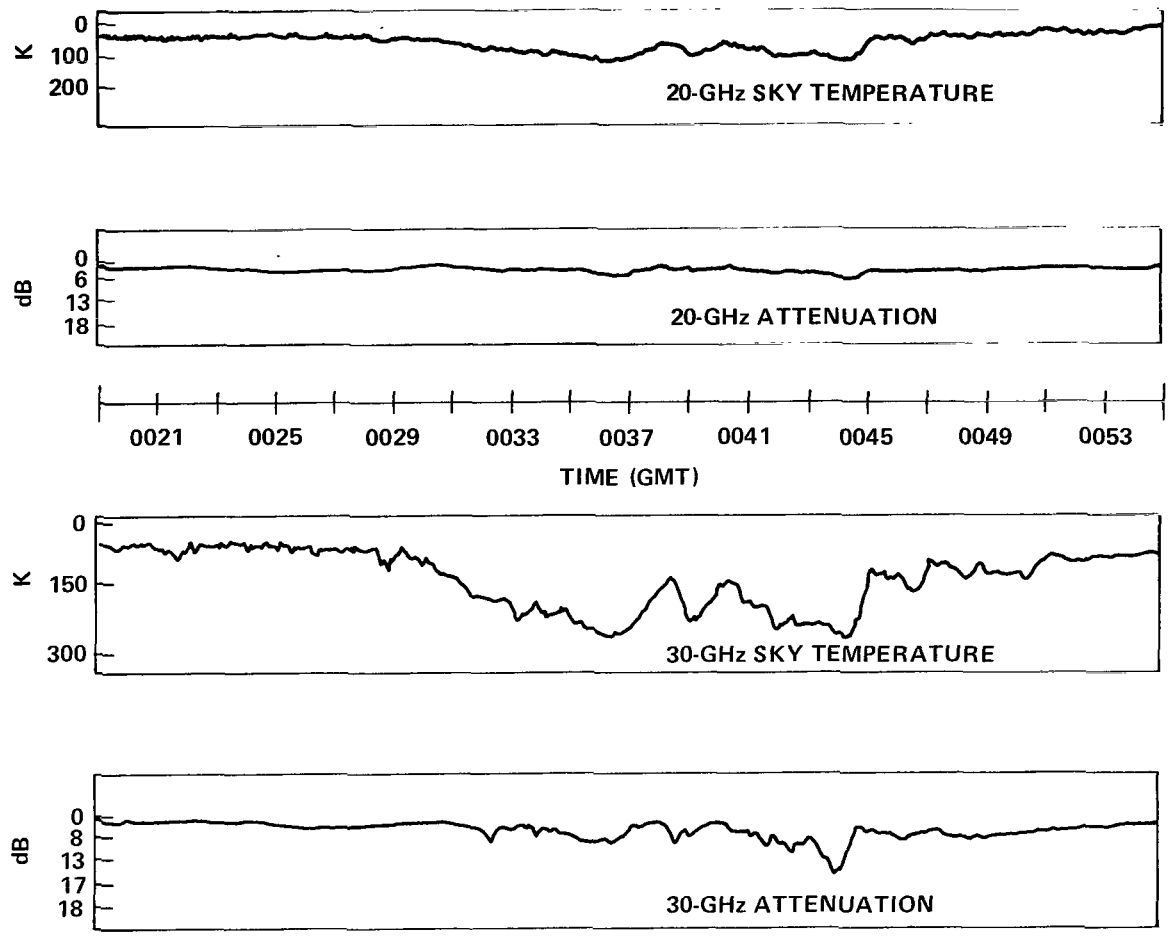

Figure 6. Typical records of simultaneously measured 20/30-GHz radiometric sky temperatures and 20/30-GHz ATS-6 signals.

where $R_v(t)$ is the portion of rain rate falling at terminal velocity v. If the rain gage is located at h meters vertically below the slant propagation path, then $R_v(t)$ penetrates across the path at an advanced time h/v when there is no wind. Therefore, the actual rain fall $R_h(t)$ at height h and instant t′ is

$$R_h(t') = \sum_{t,v} R_v(t) \left[t - \frac{h}{v} = t' \right] \qquad (2)$$

The summation is over all the components of $R_v(t)$ in $R_G(t)$ for an all t and v such that $t - h/v \approx t'$. The decomposition of R_G into R_v for a different advanced time with h = 1000 m is shown in table 4.

Table 4
Actual Rain Rate at 1000-meter Height Estimated from a Ground Rain-Gage Rainfall Reading*

Advanced Time (minutes)										Ground Measured Rain Rate (mm/hr)
8.09	4.14	3.09	2.57	2.25	2.07	1.95	1.89	1.85	1.83	
0.07	0.13	0.05	0	0	0	0	0	0	0	0.25
0.14	0.46	0.39	0.17	0.16	0.02	0.01	0	0	0	1.25
0.18	0.07	0.82	0.48	0.20	0.08	0.04	0	0	0	2.5
0.24	1.02	1.55	1.11	0.59	0.29	0.13	0.05	0.02	0	5
0.33	1.44	3.06	3.18	2.16	1.26	0.54	0.29	0.15	0.09	12.5
0.43	1.9	4.6	5.98	4.98	3.20	2.05	0.88	0.53	0.48	25
0.6	2.7	6.25	9.95	10.45	7.8	5.45	3.35	1.65	1.8	50
1.0	4.6	8.8	13.9	17.1	18.4	15.0	9.0	5.8	6.4	100
1.5	6.15	11.4	17.55	20.85	26.55	24.15	17.85	11.55	12.45	150

*The estimate is based on J.O. Laws and D.A. Parsons ("The Relation of Raindrop Size to Intensity," *Trans. Am. Geophys. Union*, **24**, 1943, pp. 432-460) drop size distribution and Davies' terminal velocity profile (R.G. Medhurst, "Rainfall Attenuation of Centimeter Waves: Comparison of Theory and Experiment," *IEEE/AP*, **13**, July 1965, pp. 550-563).

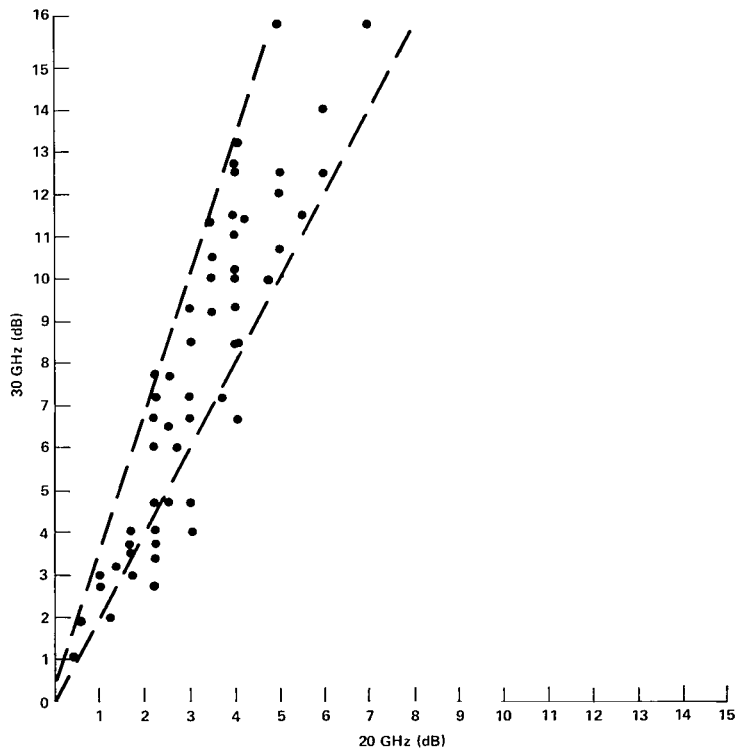

Figure 7. Scattergram plot of 30-GHz attenuation versus 20-GHz attenuation measured June 6, 1975.

The model has been applied to the rain-rate records collected from the six rain-gage networks in correlating rain data with the ATS-6 20-GHz beacon signals. In most cases, the method has the merit of relocating and dispersing the peaks of precipitation curves of field rain gages in the direction of better alignment with the pattern of attenuation curves. Figure 8 is the outcome of the adjusted rain-rate distribution of the same event shown in figure 4. Assuming that the same rain rate of a rain gage applies over the distance between the middle points of the two adjacent rain gages, attenuation can then be estimated from theoretical considerations. The estimated value and the actual 20-GHz attenuation value are compared in figure 9. The scattergram of figure 9 (b) was derived from the adjusted rain data of figure 8 and exhibits a significant improvement in comparison with the scattergram of figure 9 (a), which was derived directly from figure 4.

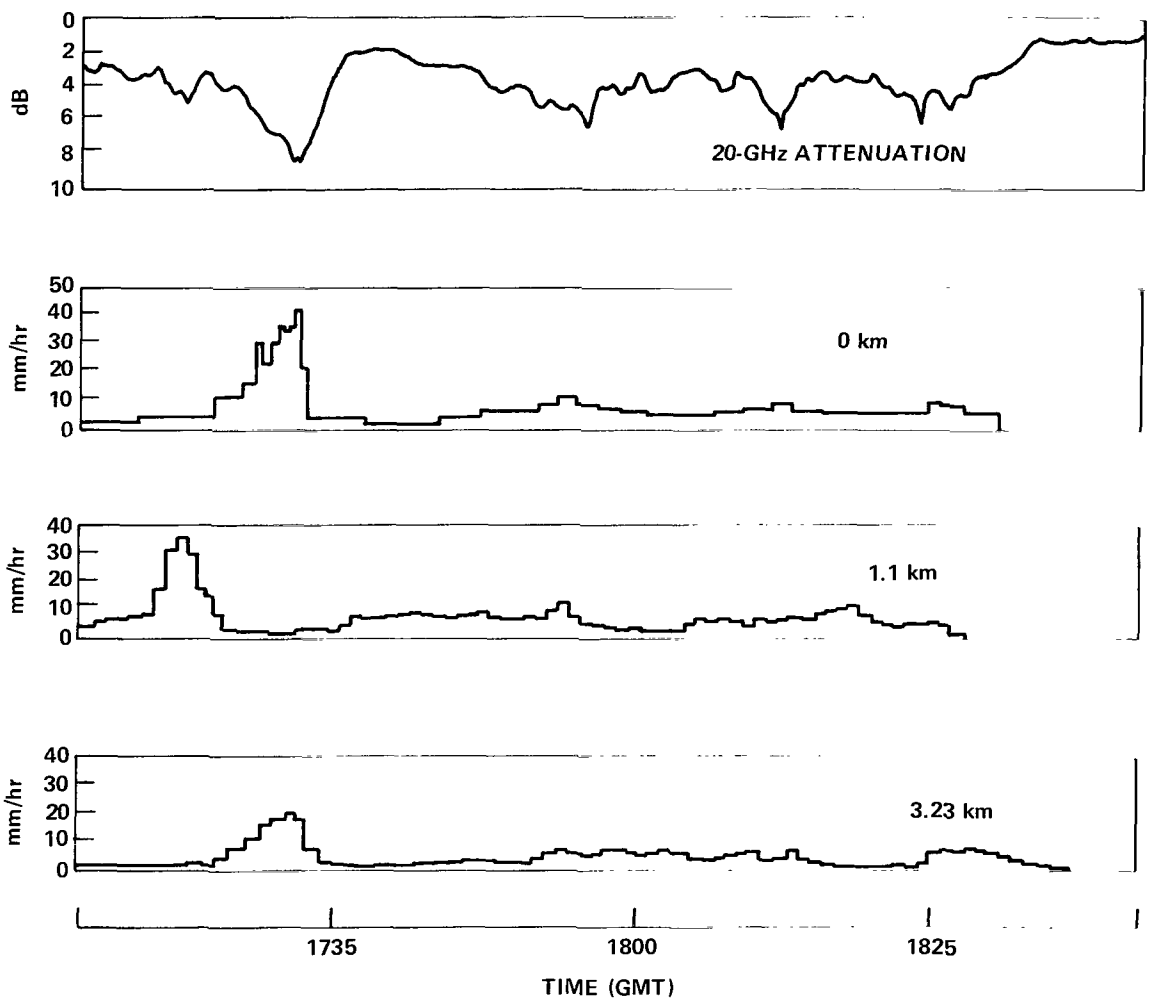

Figure 8. Model adjusted rain rate from original data given in figure 4.

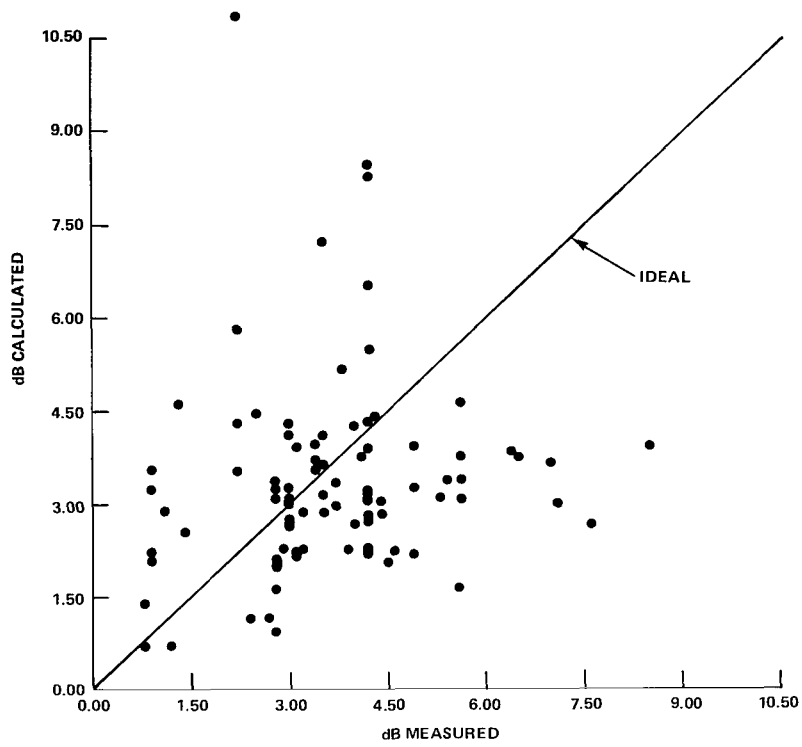

Figure 9(a). Scattergram of 20-GHz attenuation calculated versus measured for a 2-hour period on March 19, 1975, using original rain data from figure 4.

LOW ELEVATION ANGLE MEASUREMENT

In late May 1975, ATS-6 began to move slowly from its original location toward its new position over the Indian Ocean. The path vector elevation angle at the COMSAT receivers station decreased steadily to zero over a three week period. While the 20- and 30-GHz beacon signals were not continuously available, several hours of data were collected at varying elevation angles. As ATS-6 approached the horizon (local horizon was at an elevation angle of 1.2°), strong scintillations occurred as well as an increase in the average level of the received signals.

The scintillations appear to be caused by irregular refraction and scattering in the earth's lower atmosphere. Although antenna tracking difficulties and calibration errors, among other things, may also have contributed to the signal variations, a continuous effort was made to minimize this effect. The magnitude of the scintillations showed a strong dependence on path elevation angle and local climatological conditions. Peak-to-peak magnitude of the variations grew to greater than 10 dB during the final hours of data acquisition near 3° elevation angle. In addition, sharp nulls in the signal level were frequently observed and believed to be caused by angle of arrival or low elevation angle multipath. These

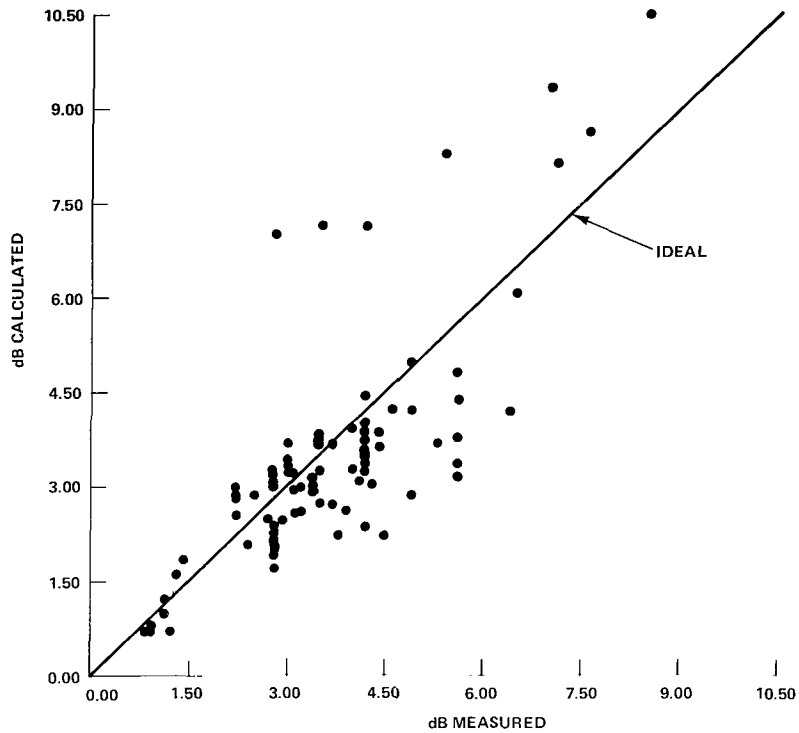

Figure 9(b). Scattergram of 20-GHz attenuation calculated versus measured for a 2-hour period on March 19, 1975, using model adjusted rain data from figure 8.

scintillations have a periodicity in the range from 15 s to greater than 1 min that showed a large dependence on the local weather. A typical record of simultaneous 20- and 30-GHz scintillations is given in figure 10(a) and (b).

While several different physical mechanisms are probably responsible for the scintillations recorded, the occurrence of low elevation angle scintillation was expected. As noted earlier, the observed effect was no doubt a result of the combined influence of such phenomena as scattering by tropospheric irregularities, angle of arrival variations, and rain. However, most notable and identifiable was the effect of water-laden rain clouds and rain. The weather radar operated at the receiving site proved particularly useful in identifying the presence and movement of cloud systems. An interesting example is the 30-GHz recordings shown in figures 10(c) and (d). Steady variations in the signal level of 5-dB peak-to-peak had been continuously recorded for well over an hour when the scintillation magnitude increased, significant absorption was also occurring as indicated by the average decrease in the signal strength and the radiometers. Figure 11 shows the extreme contrast in the nature of scintillation recorded during rain and during early morning clear skies.

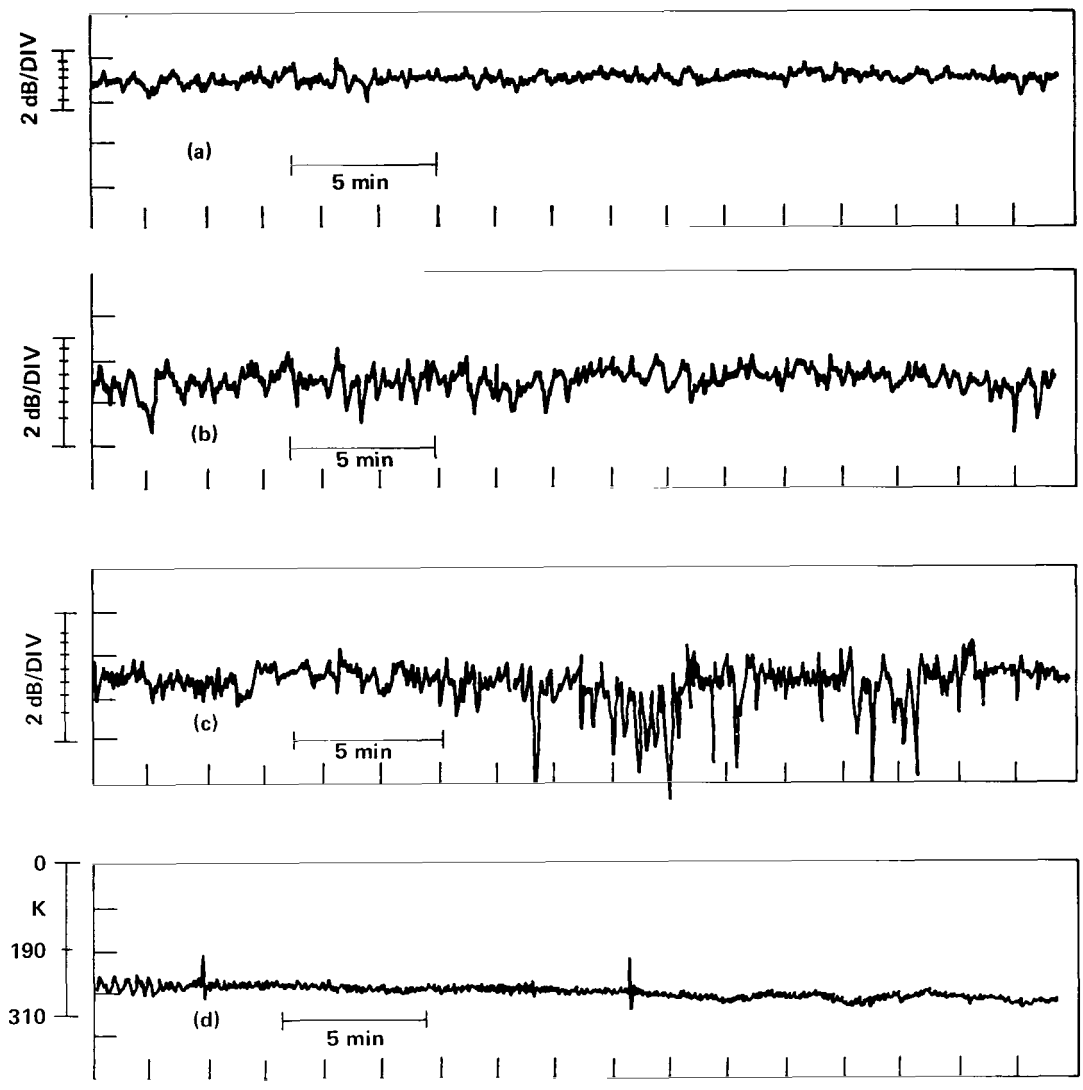

Figure 10. Recordings of 20/30-GHz low elevation angle signals. Strip charts (a) and (b) show steady variations at 20 GHz and 30 GHz, respectively. Strip charts (c) and (d) show simultaneous recordings of the 30-GHz ATS-6 signal and 30-GHz radiometer as light rain began. Antenna elevation angle is 6.5°.

Because the scintillation magnitude is expected to be proportional to the path length through the lower atmosphere, the magnitude would be expected to be proportional to the cosecant of the antenna elevation angle. Because of the extreme variability of the local weather throughout the time when scintillations were recorded, the relationship between elevation angle and scintillation magnitude cannot be easily obtained. In spite of the strong effect of the weather however, some elevation angle dependence is evident from the data. The peak-to-peak magnitude of the 30-GHz scintillations were generally greater than that simultaneously recorded at 20 GHz. This fact was particularly evident during cloud and rain scintillations.

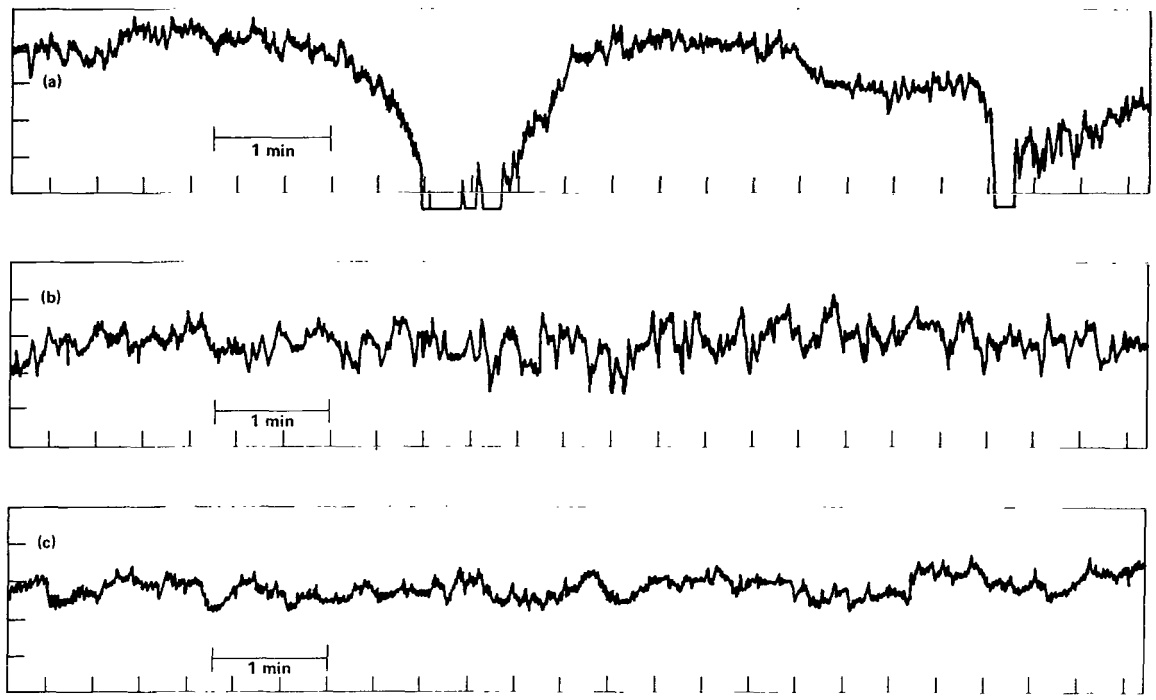

Figure 11. Recordings at 20 GHz: (a) rapid scintillations during moderate rainfall at ~6° elevation angle; (b) strong scintillations during heavy local cloud cover at ~6° elevation angle; and (c) slow scintillations during overcast skies at ~3.5° elevation angle.

CONCLUSION

As we have mentioned, due to the rigid assignment of priorities, there was a considerable difficulty in securing the 20/30-GHz beacon transmission from the satellite during heavy precipitation at the Clarksburg site. This severely curtailed the data base of the whole experiment.

However, the program did yield many important results. For example, a new and more efficient method of estimating the slant-path microwave attenuation using a network of rain gages was established. From event-by-event analysis, one can determine the accuracy of using a radiometric measurement of sky temperature as a substitute of direct satellite-signal attenuation measurement. The validity of using a radiometer to derive the yearly attenuation statistics will be shown in the final report of this program when a 1-year radiometric observation has been completed. Other meaningful analyses which will be generated later from the existing data base include an estimate of the scattering effect in radiometric measurement obtained by comparing the data at 11.6-, 20-, and 30-GHz frequencies and the low-elevation propagation characteristics obtained by studying the records of the descending satellite. The additional data, to be presented in the final report, will be useful in identifying the precipitation phenomena that degrade microwaves communications at 20 and 30 GHz.

RESULTS FROM THE ATS-6 20-GHz DEPOLARIZATION EXPERIMENT AT VIRGINIA POLYTECHNIC INSTITUTE AND STATE UNIVERSITY

C. W. Bostian, W. L. Stutzman, E. A. Manus, P. H. Wiley, and R. E. Marshall
Virginia Polytechnic Institute and State University
Blacksburg, Virginia

INTRODUCTION

The Virginia Polytechnic Institute and State University (VPI&SU) ATS-6 experiment was primarily concerned with the depolarizing effects of precipitation at millimeter wavelengths. Since raindrops, snowflakes, and ice crystals are not spheres, they scatter electromagnetic waves anisotropically and change their polarization. This depolarization will produce cross talk in communication systems which employ orthogonal polarizations for frequency reuse, and an understanding of atmospheric depolarization phenomena is necessary for the design of future earth-satellite systems.

Depolarization is described quantitatively by two related variables; these are illustrated in figure 1. The cross polarization ratio (CPR) is the decibel ratio of the cross-polarized component of the received electric field to the copolarized component.

$$\mathrm{CPR} = 20 \log_{10} \left| \frac{E_{\mathrm{cross}}}{E_{\mathrm{co}}} \right| \tag{1}$$

Because it is directly related to the electric field, the CPR is more frequently used by investigators studying the scattering process itself. Communicators are more concerned with cross talk and the relevant parameter here is the cross-polarization isolation (CPI). In a two-channel communications system, the CPI is the decibel ratio of the power received from the copolarization transmitter to the power received from the cross-polarized transmitter to the power received from the cross-polarized transmitter. Thus

$$\mathrm{CPI} = 10 \log_{10} \frac{\text{power received from copolarized transmitter}}{\text{power received from cross-polarized transmitter}} \tag{2}$$

The relationship between CPR and CPI is discussed in the literature (Watson, 1973; Bostian et al., 1974). In practice, the CPI value is essentially the negative of the CPR value, and the terms and numerical magnitudes are often interchanged.

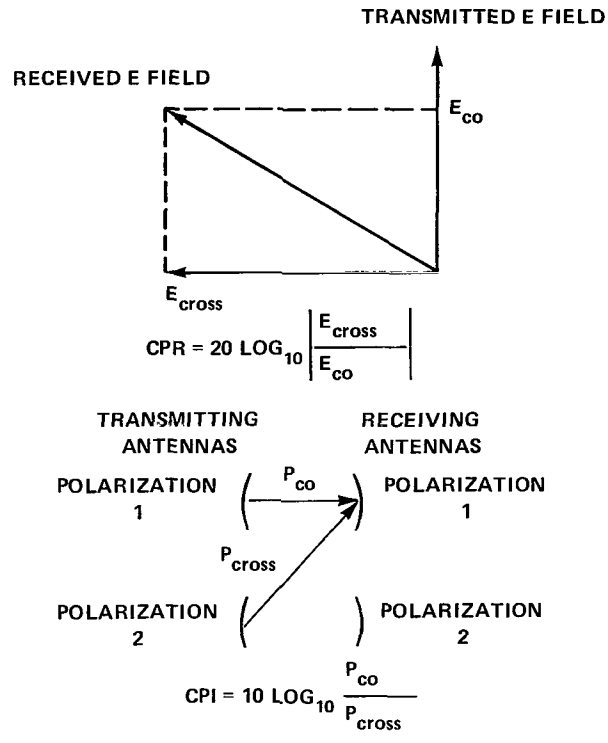

Figure 1. Definition of depolarization parameters.

Several groups are studying or have studied depolarization in terrestrial millimeter wave radio systems and at least two mutually consistent theoretical models have been developed (Watson and Arbabi, 1973; Wiley et al., 1974). The theoretical problem is complicated, but if one assumes that all of the drops are aligned and that their size and shape distributions are known, it is possible to calculate CPR and CPI as a function of path averaged rainfall rate, path length, and canting angle (the angle between the minor axes of the drops and vertical). The predictions of the theoretical models agree well with experimental data taken on linearly polarized ground paths, but the extent to which the existing models must be modified to describe satellite path depolarization is at present unknown. Additional statistical data are needed and will be collected when the Communications Technology Satellite becomes operational.

Depolarization on a ground-to-satellite path may be different from depolarization along a ground path for three reasons: (1) differences in size and shape distributions of the raindrops, (2) the presence of snow and ice in the freezing layer, and (3) the possible influence of cirrus cloud ice crystals. To investigate these factors and to study depolarization effects in satellite communications systems, several experiments are planned or in progress. The first measurements were made at 4 GHz by Roger Taur (1974) of COMSAT; our group and our colleagues at Bell Laboratories (Gray, 1975) worked at 20 GHz with ATS-6, and later efforts are planned by Bell Laboratories (Cox, 1974), COMSAT, and NASA.

EXPERIMENT DESCRIPTION

The ATS-6 satellite transmits a linearly polarized signal at 20 GHz; in our experiment we measured the incoming power in the copolarized and cross-polarized components of the incident signal. From these we can compute the CPR. Under clear weather conditions, the CPR is small (-28 to -50 dB, depending upon antenna alignment); precipitation depolarization causes it to rise.

Figure 2 shows the 1.22-m (4-ft) antenna and terminal building for the experiment. A Ku-band radar, shown on the roof of the building, is used to probe weather conditions along the satellite path.

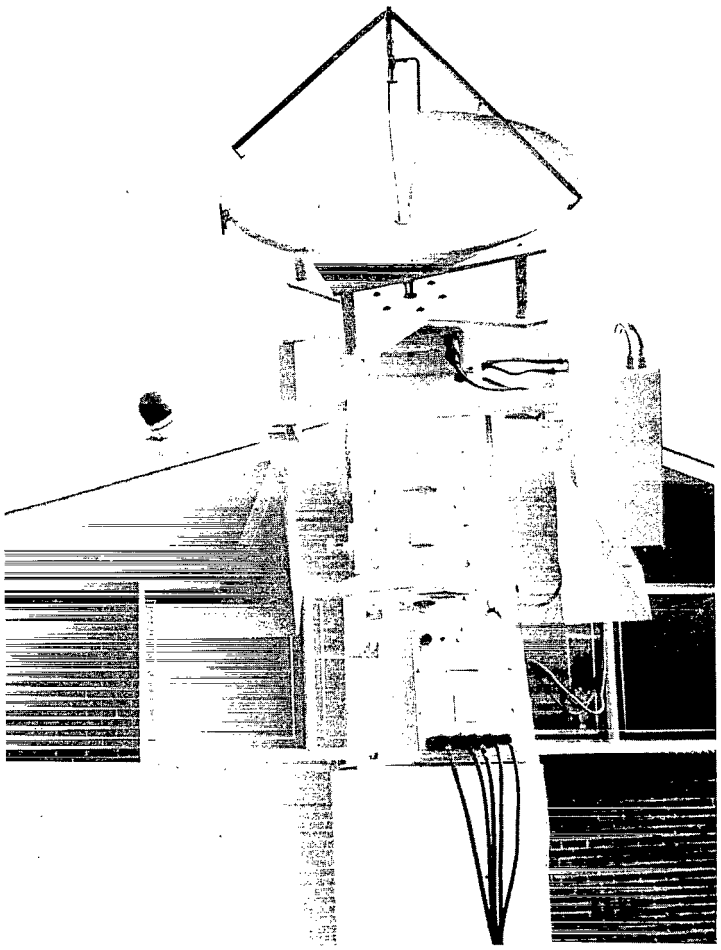

Figure 2. VPI&SU antenna system.

A block diagram of our experimental system appears in figure 3. In addition to the CPR of the incoming signal, it records attenuation and ground-level rain and wind data. All of the equipment is under the real-time control of a dedicated Raytheon PB-440 digital computer (see figure 4) which updates the antenna pointing at 10-min intervals and performs initial data processing. The receiver switches between the cross-polarized and copolarized antenna feeds once every 2 seconds. The receiver, antenna controls, and radar display are shown in figure 5.

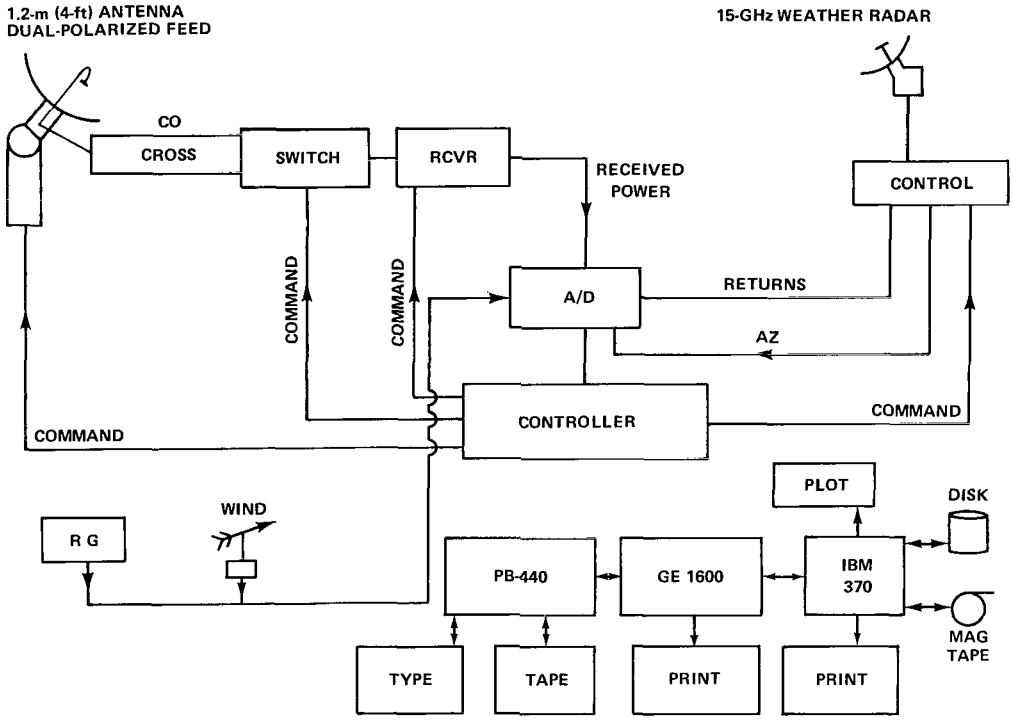

Figure 3. Experimental system block diagram.

The results from the experiment were in the areas of rain effects, snow effects, low elevation angle effects, and clear weather effects. These results are discussed in the remainder of this paper. More details on the experiment and results are available in the literature.*

RAIN DEPOLARIZATION

In order to successfully collect data, it is necessary that (1) the satellite be available with correct pointing and be operating nominally, (2) the ground station equipment be operating properly, and (3) a relatively intense rain event occur. During the ATS-6 project, these three

*Bostian, C. W., W. L. Stutzman, E. A. Manus, P. H. Wiley, and R. E. Marshall, "A 20 GHz Depolarization Experiment Using the ATS-F Satellite," Final Report, NASA Contract NAS5-21984, to be published.

Figure 4. Raytheon PB-440 computer.

requirements were seldom satisfied simultaneously. Thus, a large data base for satellite-to-ground propagation at 20 GHz does not yet exist. There are essentially only three storms which have data worthy of reporting: those on March 30, May 27, and June 12, 1975. In this section, the data obtained from the first two of these storms is discussed, and the June 12 storm is discussed in a later section because it occurred during low elevation angle pointing.

Almost all of the rain data was collected during the last few months of the project. Typically, data reduction procedures are developed by processing a few storms by hand and then writing computer programs to replace the hand computations. With the short time frame for data reduction, the computer programs were not developed until very late in the project. Thus, for the sake of expediency, all data presented in this section was obtained from chart recordings and processed by hand.

On March 30, 1975, the first significant rain depolarization data were collected. In figure 6 the rain rate, CPR, and the attenuation were plotted for the storm. The CPR and attenuation data points represent samples taken at 1-min intervals, and the blank spaces are times when the receiver lost phaselock. The rain-gage data in figure 6 are from three tipping bucket gages. Gage 1 (solid line) is directly beside the receiving antenna. Gage 2 (dashed line)

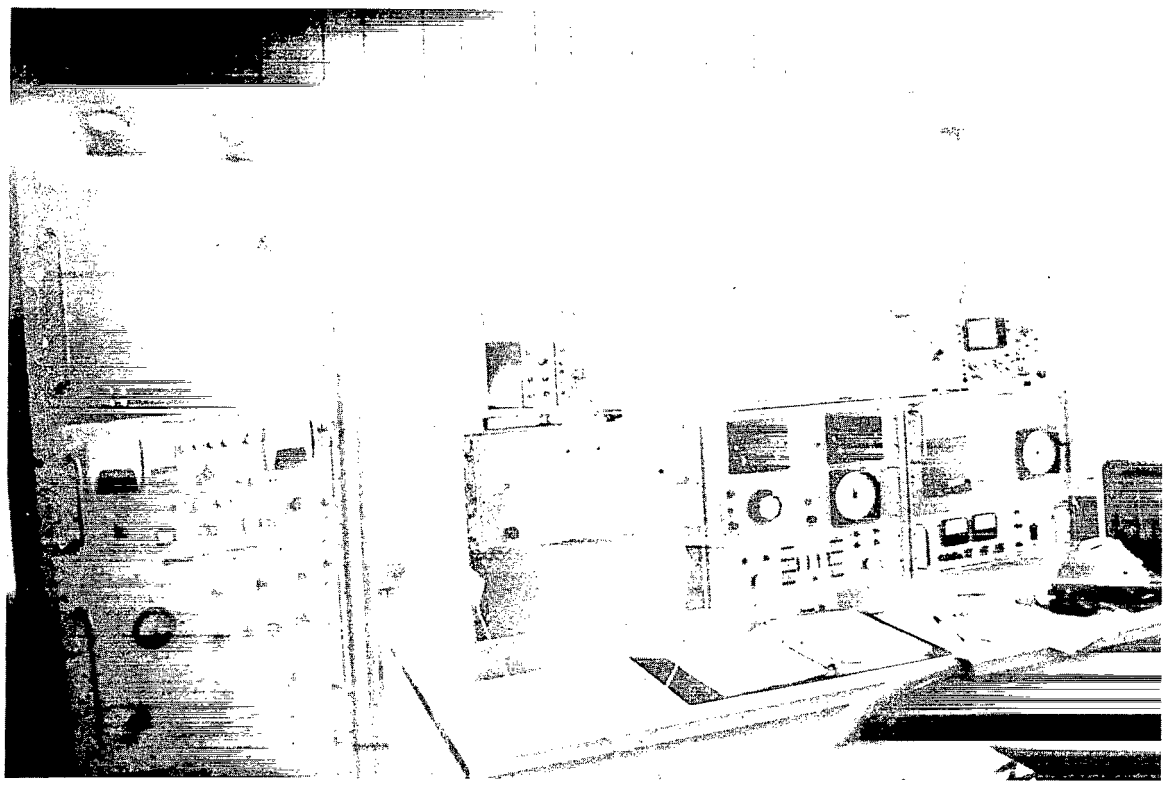

Figure 5. Receiver, antenna controls, and radar display.

is 198.1 m (650 ft) away and approximately 198.1 m (650 ft) directly below the radio path. Gage 3 (dotted line) is approximately 762.0 m (2500 ft) away in the general direction of the satellite and about 762.0 m (2500 ft) below the path. Since our 15-GHz radar indicated the rain was about 14.5 km (9 mi) deep (in the direction of the satellite) and 4.8 km (3 mi) high, we suspect that gage 3 may have malfunctioned and reported only during the most intense rain.

A striking feature of these data is the strong correlation between the rain-rate peaks and the CPR peaks. The CPR peaks occurred slightly earlier than the rain-rate peaks because of the time required for the raindrops to fall from the path to the gages.

Unlike what we have observed on terrestrial radio systems, the attenuation and CPR are not well correlated with each other. The plot of attenuation versus CPR from terrestrial path data follows a well-defined curve. Peaks of attenuation and peaks of CPR occur simultaneously (Bostian et al., 1972). Figure 7 shows average attenuation for each integer value of observed CPR. The attenuation does not continually increase with CPR. No explanation is offered for the lack of correlation between attenuation and CPR from satellite path data. More experimental observations are needed.

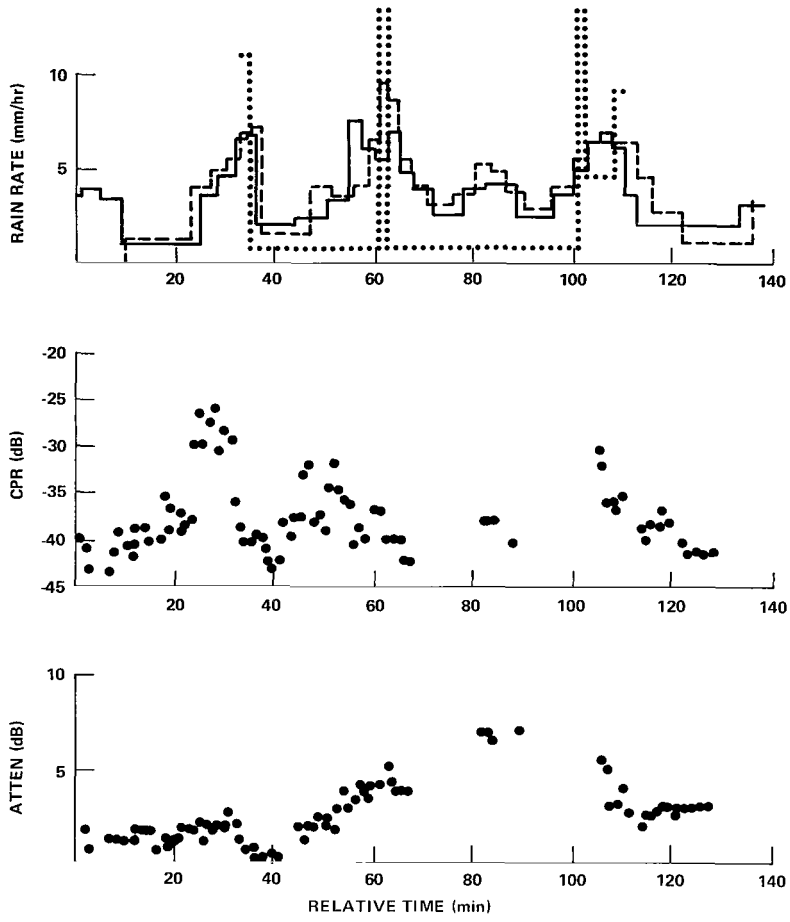

Figure 6. Rain depolarization data from the storm of March 30, 1975.

The storm of March 30, 1975, was the only hard rain for which we were able to get data prior to the movement of the satellite toward 35°E. As the satellite moved east, the clear weather polarization angle that we observed at our station began to increase toward 0° from its nominal -21° value. It passed through 0° when the spacecraft was directly south of us and increased to about +50° when we lost signal on June 13, 1975.

On May 27, 1975, the polarization angle was +6°, and on that day we experienced a severe thunderstorm with fading in excess of 14 dB. The data for this storm are presented in figure 8. The blank portions in the attenuation data are when the receiver lost phase lock due to power failures. The interesting feature is that there was essentially no change in the CPR during this rain. One possible explanation for this is that the polarization angle was so close to vertical that the incident electric field was aligned with the raindrop minor axes and thus there was no depolarization.

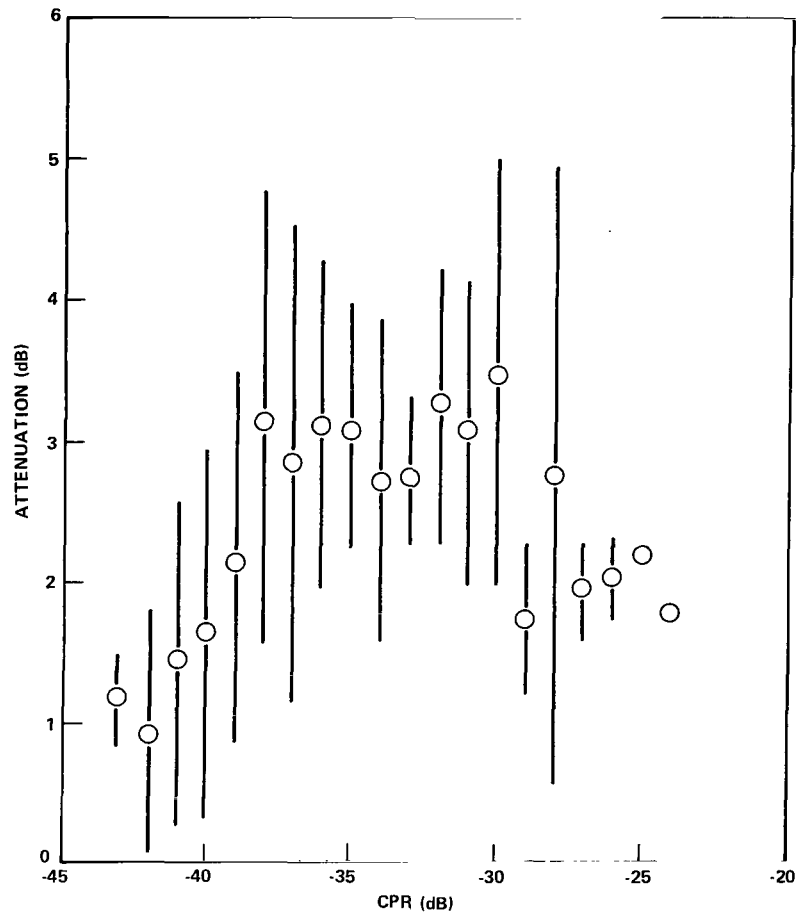

Figure 7. Attenuation versus CPR for the storm of March 30, 1975. Each point represents the average attenuation at each 1-dB interval of CPR. The vertical bars extend ± one standard deviation from the average.

SNOW DEPOLARIZATION

A severe snow storm lasting from November 30 through December 2, 1974, yielded what we think are the first snow depolarization data for a satellite path. Snow and occasional freezing rain fell during most of this time interval, but from time to time there was considerable variation in the ground precipitation rate. The net snow accumulation was measured at 0.25 m (10 in.) by our local U.S. Weather Service observer.

Because the spacecraft operational restrictions prevented us from obtaining a continuous look at the signal from beginning to the end of the storm, we made a series of separate observations, each several hours in length. After the storm was over, we made clear sky calibration runs on December 3 and 6 to aid in data analysis.

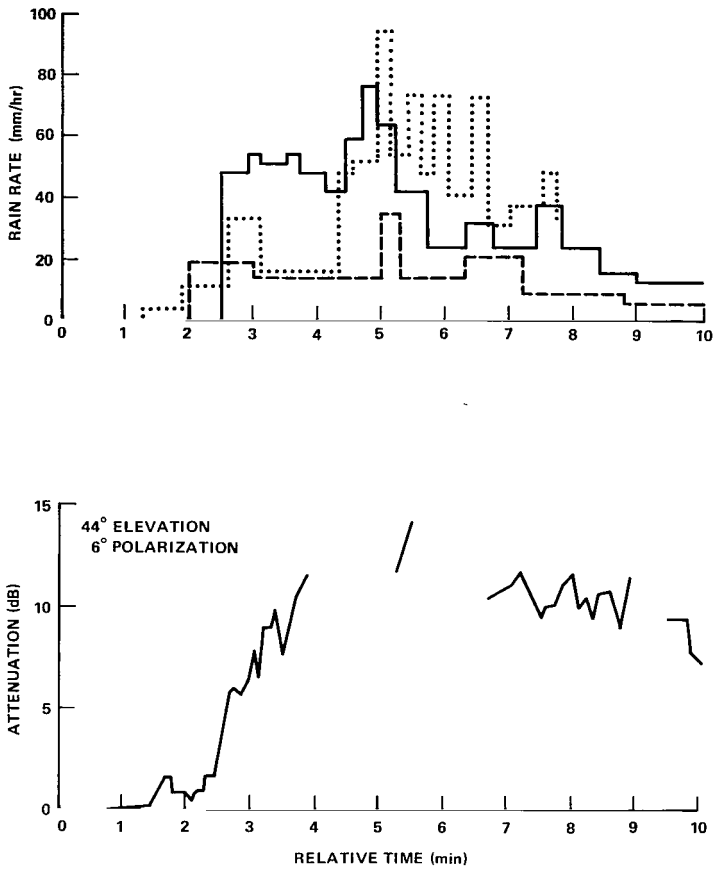

Figure 8. Data from storm of May 27, 1975. No CPR was observed.

Figure 9 displays average measured values of attenuation and cross-polarization ratio versus time for the data runs between November 30 and December 6, 1974. Breaks in the time axis emphasize that this figure is a collection of data from five different runs spread over six calendar days.

The θ variable in figure 9 is the antenna polarization angle. Under clear weather conditions at the time of measurement, the incoming signal was polarized at or near $\theta = -19.5°$, but with this antenna polarization the cross-polarized component was below the receiver phase-lock threshold. Since then, we have improved the receiver sensitivity to the point that it maintains lock on the cross-polarized components. But at that time we normally operated the antenna at $\theta = -16.5°$; this provided a clear weather isolation of -28 dB and enabled the receiver to work properly. However, on December 2, the snow depolarization was such that we were able to make measurements at $\theta = -19.5°$.

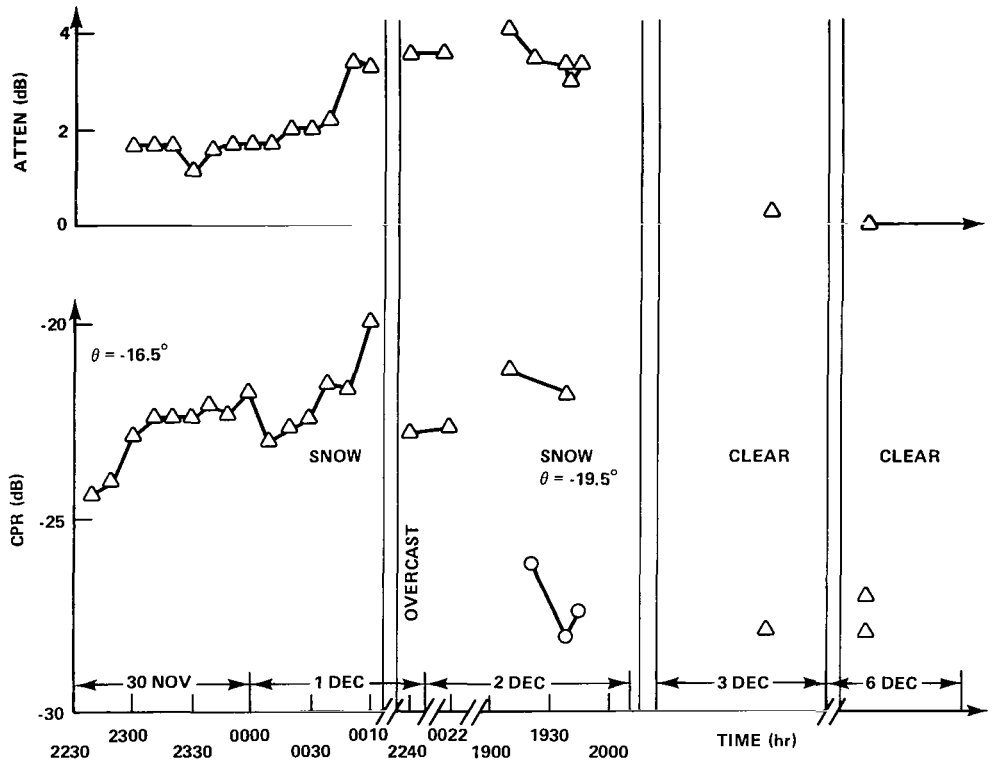

Figure 9. Attenuation and CPR data for the snowstorm of November 30 to December 2, 1974, and subsequent clear weather calibration periods.

On November 30 and the early part of December 1, heavy snow was falling. During the second run on December 1, the ground snowfall rate was negligible, but heavy cloud cover remained and surprising attenuation and CPR values were measured. On December 2, the satellite was available during an intense snow shower. As the hour progressed, the snow rate decreased, and we saw corresponding changes in the attenuation and CPR. Unfortunately, we had to relinquish use of the satellite before the snow ended.

Snow depolarization is somewhat more difficult to analyze than rain depolarization because at present a theoretical model is nonexistent even for a terrestrial path. In addition, we have no handy "snow rate" parameter analogous to rain rate. One approach is to plot attenuation versus CPR and examine the result. This is done in figure 10 for the data presented in figure 9.

The data in figure 10 bear some resemblance to the attenuation versus cross-polarization isolation plots calculated for rain depolarization in terrestrial radio systems using nonideal antennas (Bostian, 1974). Figure 11 is a typical plot for a 19.3-GHz, 1-km, rain-filled path with 45° linear polarization and a variety of residual (clear weather) CPR values (Bostian, 1974). This is not a theoretical model for our 20-GHz snow data for the satellite path; it is introduced to show the trend of these curves and the effect on them of the residual isolation.

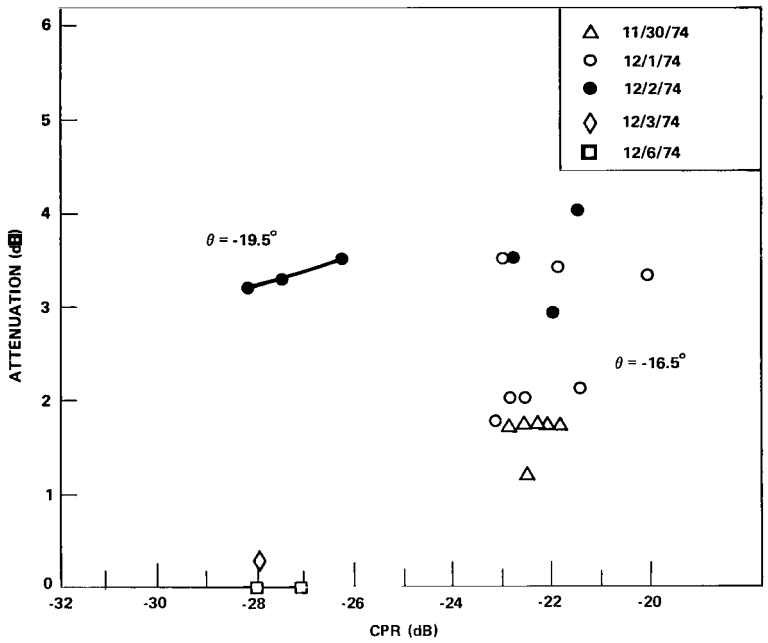

Figure 10. Attenuation versus CPR for the November 30 to December 2, 1974, snowstorm and subsequent clear weather calibration periods.

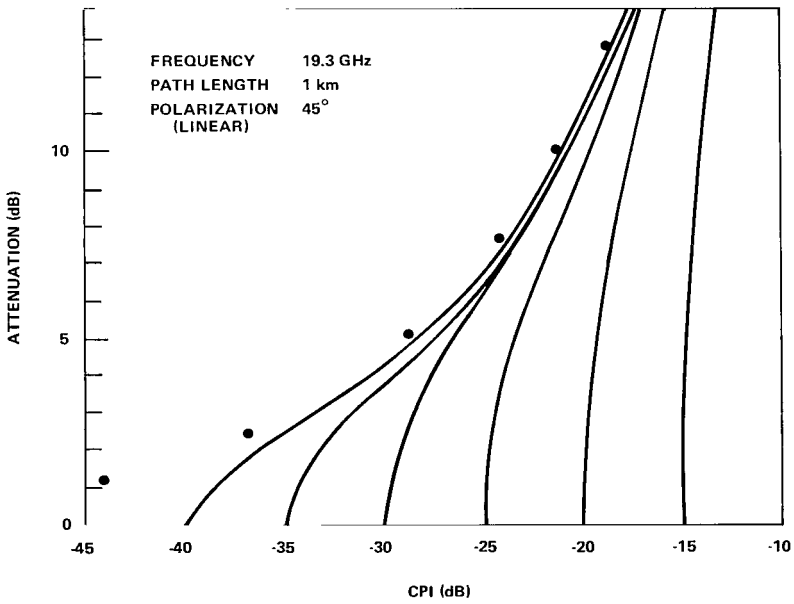

Figure 11. Rain-induced fade versus cross-polarization level (including antenna effects). Points indicate scattering model theory for no antenna effects.

The effect of varying our antenna polarization angle is to change the residual CPR. At $\theta = -16.5°$, the clear weather CPR is -28 dB; the measured data at $\theta = -16.5°$ bear some resemblance to the -30 dB theoretical curve for rain.

A question to be resolved is the location of the occurrence of the depolarization and attenuation. The snowflakes near the ground, the clouds overhead, or both should be considered. Certainly our data of 2240 UT on December 1 through December 2, 1974, implicate the clouds, because little or no ground precipitation occurred during this time. On the other hand, the attenuation and CPR levels noted from 1900 to 1950 UT on December 2, 1974, were correlated with the snow intensity at ground level by visual observation of the snow and the radar A-scope. When both clouds and snow were gone, the clear weather signal levels returned to their normal values. The obvious conclusion is that ground precipitation and higher altitude phenomena both play a role; the only sure way to separate the two is to compare snow depolarization data measured simultaneously on terrestrial and satellite paths.

Another potential source of error related to the antennas is apparent depolarization resulting from off-axis reception.* Ghobrial and Watson (1973) first reported this as being caused by refractive effects on long paths; on a satellite path it could conceivably come from refraction or from antenna pointing errors. To eliminate both possibilities we made plots of CPR versus azimuth and elevation offset during the clear weather tests on December 6. These showed the CPR levels associated with off-axis reception to be well below the values measured during the storm (at least for the high residual CPR associated with $\theta = -16.5°$) and would seem to eliminate off-axis reception as a source of error in our data.

A striking feature of the snow data displayed in figure 10 compared to rain data from a terrestrial link (Bostian et al., 1974) is the large depolarization observed for a given attenuation. To get a CPR of -28 dB (the leftmost $\theta = -19.5°$ point in figure 10) with rain on a ground path would require at least 7-dB attenuation and possibly as much as 20 or 30 dB, depending on path length and raindrop canting angle.

A theoretical case can be made for associating small attenuation and severe depolarization with scattering by bodies which are relatively lossless but lack rotational symmetry. Certainly snowflakes and high altitude ice crystals fit this description, but the very fragmentary data available for snow do not necessarily support this conclusion. Watson (1973), working at 11 GHz with a 13.7-km path, reported a huge fade (24 dB) in wet snow accompanied by a CPR of -22 dB. On the other hand, a rain fade of only 8 dB on the same path was associated with a -20-dB CPR. Because our frequency is almost twice that of Watson's and his snow was wet while ours was dry, it is very possible that he could have been dealing with scatterers that were relatively more isotropic than ours were. Some U.S.S.R. work (Babdin et al., 1970), at a much higher frequency, also indicates that, for the same water content, snow attenuates more highly than rain, but this tells us nothing about depolarization.

*So far as could be determined, snow and ice accumulation on our antenna reflector and feed were negligible throughout the storm.

Clearly more research is needed. We should operate a terrestrial path link and a satellite downlink simultaneously, and also study the high altitude conditions with a polarization diversity radar.

MEASUREMENTS AT LOW ELEVATION ANGLES

At the conclusion of this experiment, we were able to monitor the satellite more or less continuously for elevation angles ranging from about 9° down to 1°. This gave our group and many of the other East Coast ATS-6 millimeter wave experiment participants a unique opportunity to study 20-GHz propagation at extremely low angles.

During the observing periods, the weather changed rapidly, alternating between sunshine, rain, and fog; at times all three seemed to be occurring simultaneously on different segments of the path. For this reason, it was frequently difficult to associate changes in the received signal with any particular weather condition.

Narrative Discussion of the Data

When the satellite was at 22° elevation, our antenna pedestal went out of control and broke a number of cables. We were able to repair the equipment and then acquire the signal at 9.12° elevation, but our data have an unfortunate gap between these two angles.

At the time we acquired the satellite, after repair, the clear weather signal was 12 dB below what it had been at 45° elevation. This measurement provided the first set of points in figure 12 which shows the overall behavior of the copolarized signal. The maximum and minimum signals occurred no more than 4 minutes apart. These represent two sets of observations taken before and after a light rain.

The data measured at 7.61° elevation was taken after a storm that reached 30 mm/hr and before a 6-mm/hr sprinkle. Although the weather radar indicated no rain along the downlink, the sky was partly cloudy and there was light rain in the area. The time between the maximum and minimum signal strengths was no more than 2 minutes. The clearest sky observed during tests below 10° elevation (excluding 1.1°) occurred at the elevation angle of 5.6°. The sky was hazy; however, the weather radar gave no indication of rain within 24 km (15 mi) of the station. The scintillation frequency was approximately 1/6 Hz. As the elevation angle moved to 5.46°, rain began moving into the area. The 1-dB scintillation was observed before the rain entered the path. At one time, rain extended 14.5 km (9 mi) up the path. As the rain began to dissipate, the signal, as expected, began to increase. Before the signal returned to the clear weather reference, it started down again even though the radar indicated that the rain had completely dissipated along the path. The receiver then lost and regained phase lock 3 times in 10 minutes, although there was no radar indication of rain along the path. When the receiver did regain phase lock on a strong signal, the copolarized signal would fall about 0.5 dB/s until the receiver again lost phase lock. After the receiver acquired the 20-GHz continuous wave (CW) signal for the third time, the signal strength returned to the clear weather level with the same scintillations observed initially

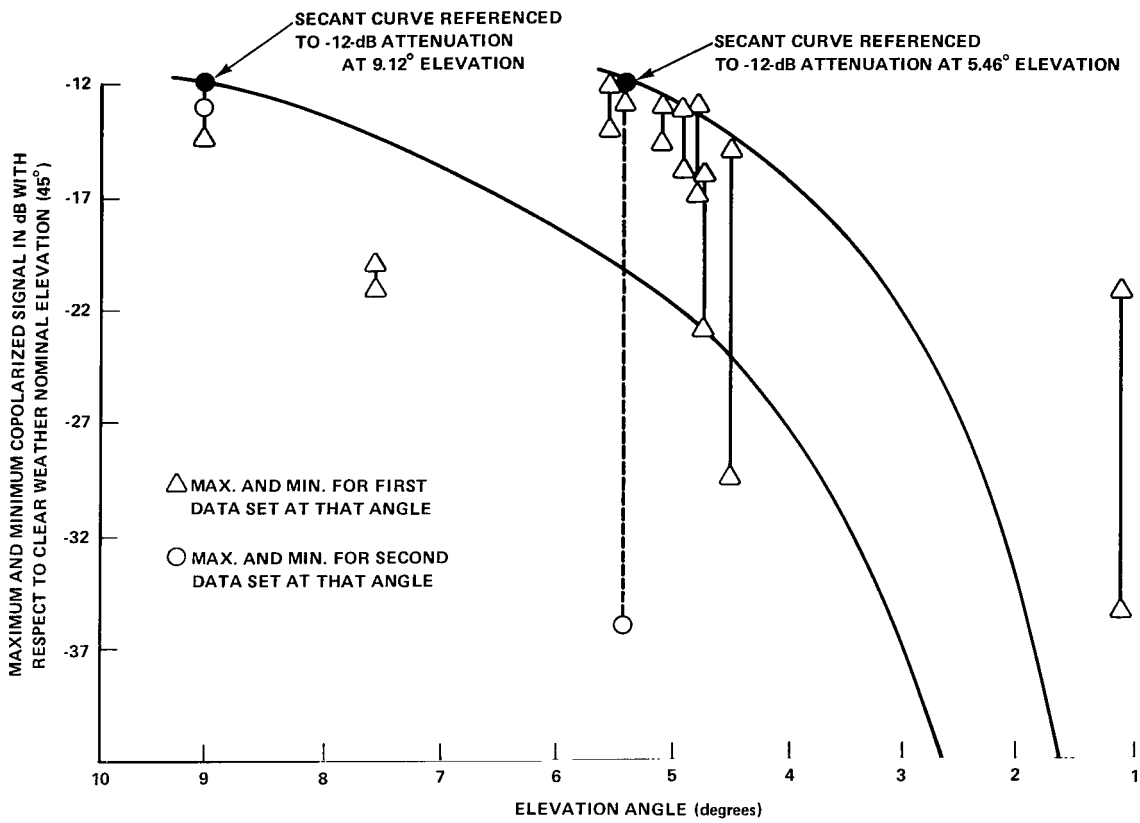

Figure 12. Attenuation data at low angles.

at 5.46° elevation. The data measured at 5.11° elevation were taken after a storm that reached 25 mm/hr. The data taken from 4.95° elevation were not interrupted by rain; however, the sky was hazy along the path. The scintillations tended to become larger and more frequent as the angle decreased. A 15-mm/hr drizzle preceded the measurements at 4.8° elevation; and although there was no radar indication of rain along the path, the signal level never came up to the clear weather reference. The scintillation patterns were composed of the higher frequency variations noted at 5.46° elevation but superimposed on 60-s scintillations of the magnitude indicated in figure 12. The large variation indicated at 4.54° elevation only occurred once. The remaining 12 minutes of data taken at 4.54° elevation produced scintillations up to 8 dB of the type described at 5.46° elevation. The sky was partly cloudy at this time.

Antenna Pattern Broadening

After the satellite was acquired at 9.12°, we noticed a pronounced broadening of the antenna radiation pattern in the elevation plane. The signal remained quite sharp in azimuth, but in elevation the 3-dB points were frequently separated by several degrees. The same effect was noted by our colleagues at COMSAT Laboratories.

On the last day that we were able to receive the signal, the broadening disappeared, and the elevation pattern returned to its former sharpness. At this time the peak copolarized signal occurred at an elevation angle of 1.1°, and the boresight telescope indicated that at this elevation the antenna was pointed below the crest of a nearby mountain. Presumably the propagation mechanism was knife-edge diffraction, but in that case the signal should have originated from the crest of the mountain.

We think that multipath propagation was responsible for the pattern broadening. Given the low elevation angle, and assuming horizontal stratification in the atmosphere, it is easy to hypothesize rays entering the receiving antenna from a statistical distribution of elevation angles. Certainly the scintillations, and the focusing and cross-polarization effects (both described below), indicate the presence of multipath.

Clear Weather Attenuation at Low Angles

As the satellite elevation angle decreased, the tropospheric part of the propagation path lengthened. In a horizontally stratified atmosphere, this would cause a decrease in signal strength proportional (in dB) to the secant of the elevation angle. Our intent was to measure the copolarized signal clear weather level at 45° elevation and look for this secant behavior. This effort was complicated by the lack of any data between 22° and 9.12°. Taking the signal levels at 9.12° and 5.46° elevation as references, we have plotted two secant curves in figure 12. These show fair agreement with the data in the 9° to 4° range. Of course, at extremely low angles the horizontal stratification model breaks down.

Rain Attenuation at Low Angles

We were able to observe significant rain attenuation at 7.59°, 5.35°, and 4.70°. The results are displayed in figures 13, 14, 15. In each case, these display attenuation (calculated from the clear weather signal level immediately before or after the storm) and the rain rate at the rain gage located beside the receiving antenna. The correlation between the rain rate and attenuation in figures 13 and 15 is outstanding. The high attenuation for a given rain rate is a result of the extremely long rain path.

Polarization Effects at Low Angles

The polarization response of our antenna was a sharp "V" at 45° elevation; below 9.12°, however, the polarization null became very wide, and measuring the polarization angle with precision was more difficult. Nevertheless, finding the null location and finding the average of the two polarization angles for which the copolarized and cross-polarized signal levels were equal gave similar results. Presumably the broadening was due to multipath.

At first the measured polarization angles tracked the theoretical predictions. Thus, for measurements made at 9.12° elevation and 7.61° elevation the polarization angle was +49.0°. Data taken from 5.60° to 5.11° were recorded at a polarization angle of +52.0°. As expected, the polarization angle moved to 52.5° for the data sets at 4.95° and 4.85° elevation;

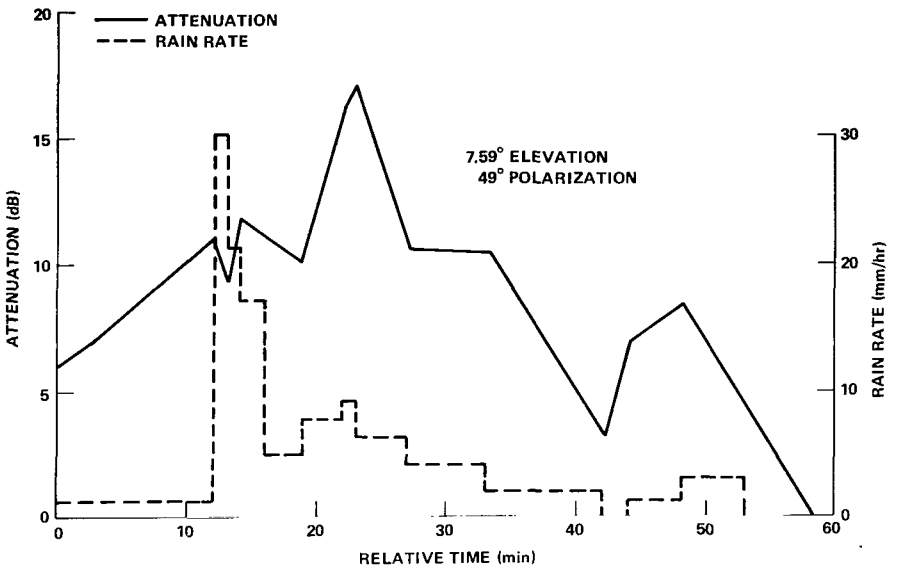

Figure 13. Data from rain storm of June 12, 1975 (0359-0502).

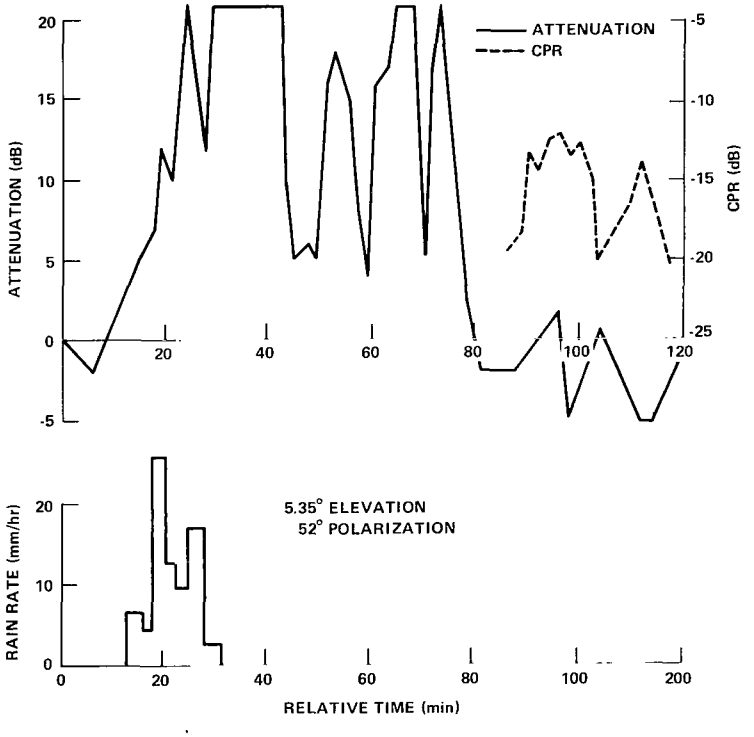

Figure 14. Data from rain storm of June 12, 1975 (1615-1810).

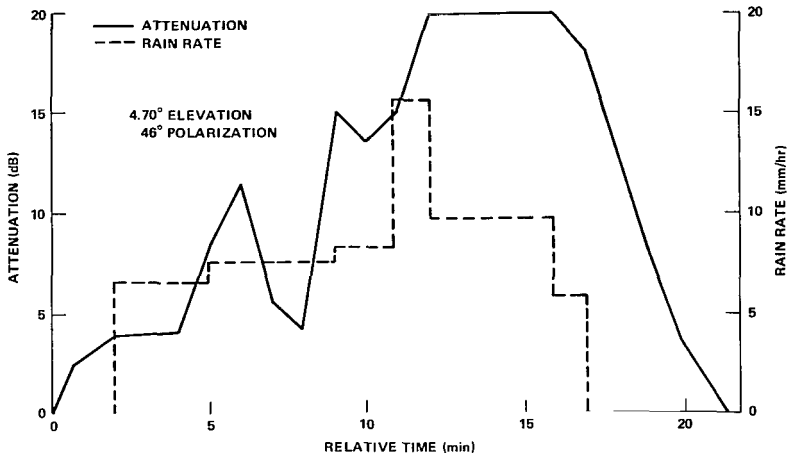

Figure 15. Data from rain storm of June 12, 1975 (2053-2113).

however, at 4.80° the polarization angle was measured to be +47.0°, and it moved to +46.0° at 4.54° elevation.

We have no explanation for this reversal at 4.8°. Perhaps it is related to the clear weather polarization angle effects noted at higher elevation.

The 12-dB loss in signal level between 45° and 9.12° that was discussed earlier forced us to remove the last 12 dB of front-end attenuation from the copolarized channel. Given the limited dynamic range of the ATS receiver, this means that we would only measure CPR values greater than -20 dB. Rain depolarization of this magnitude requires considerably harder rain than we experienced; hence,we observed no rain depolarization at extremely low angles. However, we did record one case of severe CPR increase due to multipath; this appears in figure 14.

The event began at about 1735 on June 12 when the copolarized signal level abruptly jumped from 20 dB below clear reference to as much as 5 dB above (an attenuation of -5 dB). Simultaneously, the CPR rose sharply and peaked at about -12 dB. Negative attenuation and high CPR continued for about 40 minutes. When we saw this happening, the operator carefully rechecked the antenna polarization angle and found it to be correct.

What was observed here appears to be a case of severe multipath. The 6-dB increase in copolarized signal level over clear weather corresponds exactly to the arrival of equal-amplitude in-phase signals at the copolarized channel. The situation for the cross-polarized signal is more complicated, but we feel that it can be explained as follows. The cross-polarized pattern of the antenna has a sharp null on axis. For the same incident polarization, a signal arriving off-axis will be out of the null, and the antenna will receive a larger cross-polarized component than it would if the signal came in on-axis. This is the central point of Watson's work on clear weather depolarization on ground paths. Because the phase response of the antenna also varies with angle of arrival, the CPR measured by

an antenna for two signals with the same polarization but different arrival angles will be very similar to the CPR measured for two signals with slightly different polarizations and (perhaps greatly) different phases.

An analytical treatment of the second situation is relatively straightforward. Consider the electric field vectors drawn in figure 16, where $\bar{E}_{NI}$ represents the normal incident signal and $\bar{E}_{MP}$ is a multipath signal which differs in orientation from $\bar{E}_{NI}$ by θ spatial degrees and is out of phase with $\bar{E}_{NI}$ by ϕ phase degrees. The total received electric field $\bar{E}_T$ is given by

$$\bar{E}_T = \bar{E}_{NI} + \bar{E}_{MP} \tag{3}$$

Its complex polarization factor (Beckmann, 1968), ρ, is

$$\rho = \csc\theta\, e^{-j\phi} + \cot\theta \tag{4}$$

From ρ we may calculate the Stokes parameters of $\bar{E}_T$, and from there we may calculate the average power received by the copolarized and cross-polarized antenna fields. The ratio of these quantities is the CPR. This was done and the results are presented in figures 17, 18, and 19.

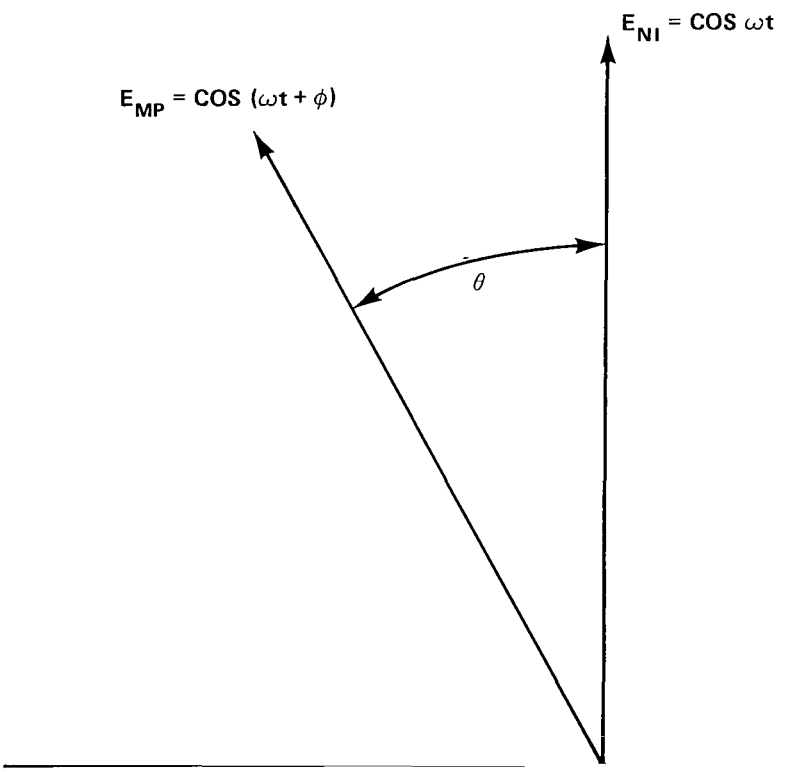

Figure 16. Relative spatial and temporal orientation of direct $\bar{E}_{NI}$ and multipath $\bar{E}_{MP}$ electric fields arriving at the receiver.

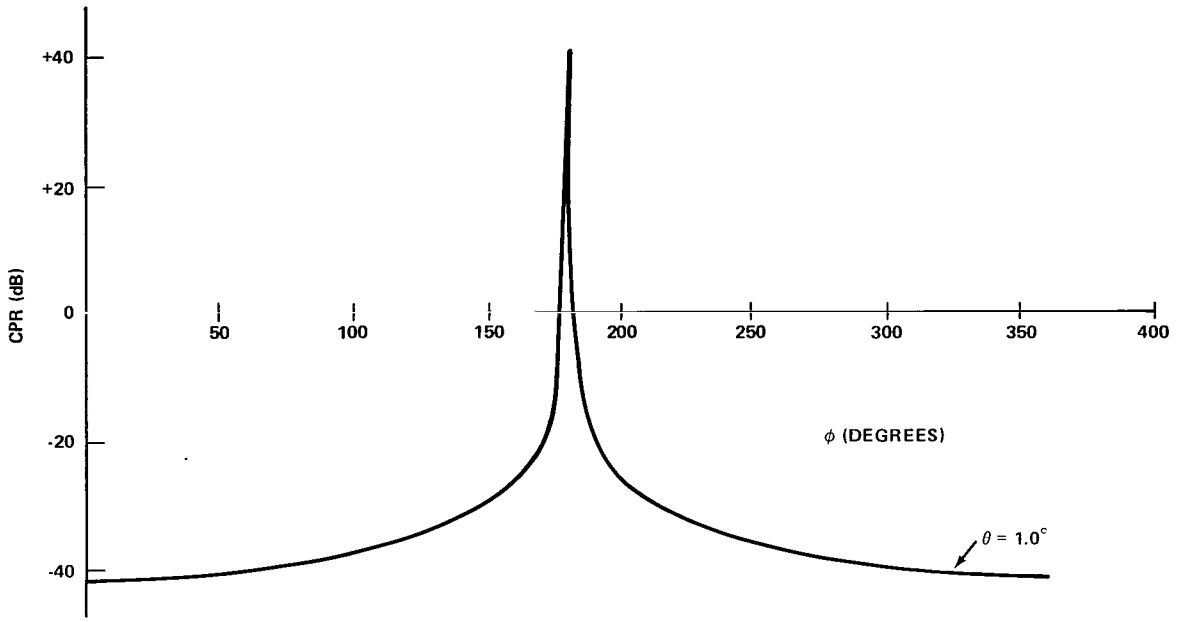

Figure 17. Cross-polarization ratio due to a boresight signal and an equal amplitude multitude signal displaced 1° from the boresight linear polarization and separated ϕ degrees in phase.

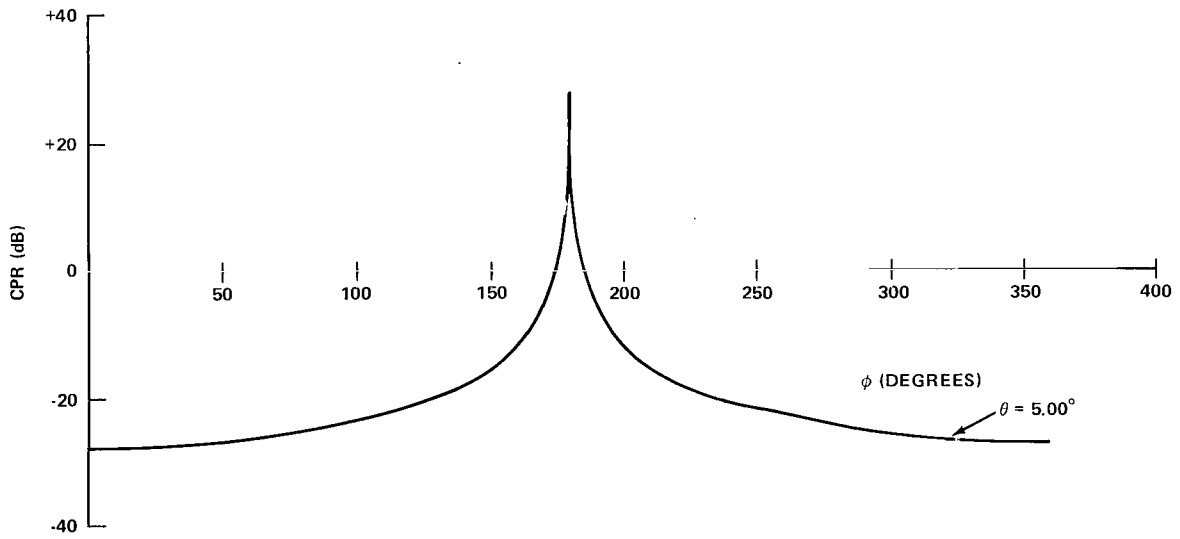

Figure 18. Cross-polarization ratio due to a boresight signal and an equal amplitude multipath signal displaced 5° from the boresight linear polarization and separated ϕ degrees in phase.

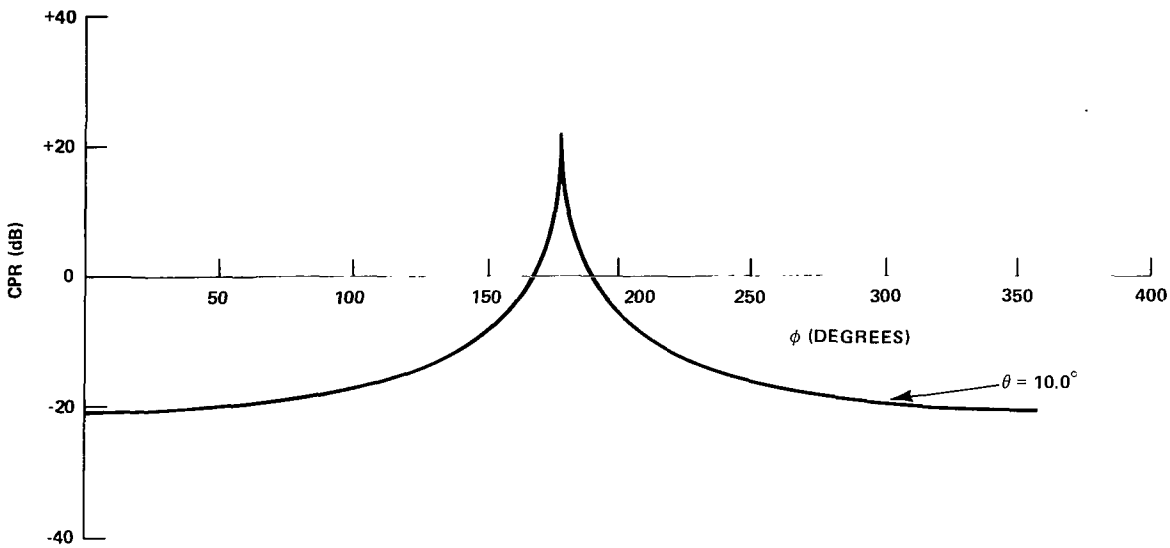

Figure 19. Cross-polarization ratio due to a boresight signal and an equal amplitude multipath signal displaced 10° from the boresight linear polarization and separated ϕ degrees in phase.

At first glance, these results are somewhat surprising because, for example, two signals differing in polarization by only 1° can produce a CPR of +40 dB if their relative phase difference is near 180°. This happens because for this particular combination of parameters, the cross-polarized components add and the copolarized components subtract. Hence, multipath depolarization is potentially a more serious problem at low elevation angles than is rain depolarization.

CLEAR WEATHER EFFECTS

In the simplest kind of a dual-polarized satellite communication system, the ground antenna polarization would be aligned with the nominal clear weather polarization of the satellite signal and left for long periods without adjustment. With linear polarization, the proper antenna alignment may be found by rotating the receiving antenna until the cross-polarized signal components pass through a null. But even with perfect polarization alignment and clear weather, cross-polarization coupling in the transmitting and receiving antenna will cause the system to retain a finite level of cross-polarization isolation; this is called the residual isolation of the system (better than -50 dB for our station). The clear weather isolation observed in a dual polarized satellite communications system depends upon the residual isolation and the accuracy of the antenna polarization alignment. Slightly misaligned good (high-isolation) antennas may be used to simulate aligned poor (lower-isolation) antennas. If the satellite or ground antenna alignments change, the clear weather cross-polarization isolation will change with them. This will raise the cross-talk level, and the designer must

allow a cross-talk margin large enough to absorb the clear weather variations and rain effects or else develop some means for periodic polarization matching.

When the ATS-6 experiment began, the consensus of NASA engineers was that the spacecraft attitude control system was so precise that no ground antenna polarization adjustments would be necessary to maintain a residual isolation close to optimum. The theoretical clear weather polarization of the ATS-6 signal at VPI (when the spacecraft antenna is pointed at VPI) is -17°, where the minus sign indicates a westward or right-hand tilt as seen by an observer standing at our station and facing the spacecraft. Our initial measurements indicated an actual value of -19.5°; given the uncertainties involved in making an absolute measurement of the polarization angle, this was acceptably close to the theoretical prediction and for about seven months we kept our antenna polarized at -19.5°.

In December 1974 and January 1975 our station was off the air for receiver repairs and modifications and after resuming operations, we rechecked the clear weather polarization angle. To our surprise, it had changed to -21.4°. We could find no reason for the change and began a program of measuring the clear weather polarization whenever the spacecraft was available. Table 1 presents the results of measurements made in February and March 1975. The values indicated have a mean of -20.97° and a standard deviation of 1°. A much larger sample is needed to more accurately establish the 3σ value.

The spacecraft yaw is supposed to be held to within 0.05°. A careful review of the spacecraft telemetry data by the satellite controllers and repeated checks of our antenna positioning system have shown no mechanical misorientations that could cause the observed polarization angle changes. Before each measurement, our antenna pointing is carefully adjusted to maximize the received signal (to an accuracy of ±0.1°); hence, off-axis reception (Ghobrial and Watson, 1973) would not seem to be at fault.

Table 1
Measured Clear Weather Polarization Angles
with Spacecraft Antenna Directed at VPI&SU

Date (UT)	Time (UT)	Polarization Angle
February 6, 1975	2100	-21.4°
February 7, 1975	1900	-21.1°
February 20, 1975	2200	-20.5°
February 28, 1975	2230	-21.6°
March 4, 1975	1917	-21.6°
March 10, 1975	1800	-21.7°
March 20, 1975	2005	-18.9°

At present, the cause of these clear weather variations is unknown. In all possibility they lie in some undetected error in the spacecraft control system or in the ephemeris data rather than any propagation phenomenon, but whatever the cause, variations like these would degrade any dual polarized satellite communications system. With our equipment a 1° rotation in either direction reduces the clear weather CPR from about -40 dB to about -35 dB. This in itself would not be unacceptable for a commercial system, but the effect should be watched by other investigators.

CONCLUSIONS

The ATS-6 satellite signal on 20 GHz was used to measure depolarization along a satellite-to-ground path. Possible sources of depolarization are rain along the path, snow along the path, multipath effects at low elevation angles, and clear air effects. The data base was not sufficiently large in any of these areas to form statistically meaningful conclusions from the experiment. Also, not enough is known to develop an accurate theoretical model. However, the experiment revealed several trends which in many cases are supported by simple theoretical explanations.

It was found that there is more depolarization on a satellite path (at -21.5° polarization angle) due to rain for a given rain rate than has been observed for a terrestrial link. From our measurements of one rain storm at a polarization angle near vertical, we tentatively conclude that depolarization may be significantly less for a dual polarized system whose polarizations are vertical and horizontal. From several measurements made during snow, we conclude that snow can introduce significant depolarization (and without high attenuation). Higher altitude phenomena may contribute to this depolarization.

Observations at very low elevation angles showed that attenuation can be introduced during clear weather by multipath effects. When rain is present, further significant attenuation is also present; furthermore, depolarization occurs.

REFERENCES

Babdin, Yu. S., I. A. Iskhakov, A. V. Sokolov, L. I. Stroganov, and Y. V. Sukhonin, "Attenuation of Radiation at Wavelength of 0.96 mm in Snow," *Radio Engineering and Electronic Physics*, **15**, (12), 1970, pp. 2171-2174.

Beckmann, P., *The Depolarization of Electromagnetic Waves*, Boulder, Colorado: The Golem Press, 1968.

Bostian, C. W., "Antenna and Path Interaction in Rain Depolarization," *1974 International IEEE AP-S Symposium Digest*, June 1974, pp. 392-394.

Bostian, C. W., W. L. Stutzman, P. H. Wiley, R. E. Marshall, "Initial Results of an Experimental Study of 17.65 GHz Rain Attenuation and Depolarization," *1972 International IEEE G-AP Symposium Digest*, December 1972, pp. 250-253.

Bostian, C.W., W.L. Stutzman, P.H. Wiley, and R.E. Marshall, "The Influence of Polarization on Millimeter Wave Propagation Through Rain," Final Report, VPI&SU, Blacksburg, Virginia, NASA CR-143686, January 1974.

Cox, D. C., "Design of the Bell Laboratories 19- and 38-GHz Satellite Beacon Propagation Experiment," *IEEE 1974 ICC Digest*, June 1974.

Ghobrial S. I., and P. A. Watson, "Cross Polarization During Clear Weather Conditions," *IEE Conf. on Propagation of Radio Waves at Frequencies Above 10 GHz,* (IEE Conference Publication 98), 1973.

Gray, D.A., "Depolarization of ATS-6 Satellite 20-GHz Beacon Transmitted Through Rain," *USNC/URSI June 1975 Meeting Abstracts*, Urbana, Illinois, 1975, p. 30.

Taur, R. R., "Rain Depolarization: Theory and Experiment," *COMSAT Technical Review*, **4**, Spring 1974, pp. 187-190.

Watson, P. A., "Crosspolarization Isolation and Discrimination," *Electronics Letters*, **9**, November 1973, pp. 516-517.

Watson, P.A., and M. Arbabi, "Rainfall Cross Polarization at Microwave Frequencies," *Proc. IEEE* (London), **120**, April 1973, pp. 413-418.

Watson, P.A., N.J. McEan, S.I. Ghobrial, M. Arbabi, "Cross Polarization Studies at 11 GHz," Final Report, European Space Research Organization Contract 1247/SL, University of Bradford, England, June 1973.

Wiley, P.H., W. L. Stutzman, and C. W. Bostian, "A New Model for Rain Depolarization," *J. Recherches Atmospheriques* (France), **8**, January-June 1974, pp. 147-153.

SUMMARY OF BATTELLE-NORTHWEST PARTICIPATION IN THE ATS-6 MILLIMETER WAVE PROPAGATION EXPERIMENT

Karl C. Davis
Battelle-Northwest Laboratories
Richland, Washington

ABSTRACT

Attenuation on a space-to-earth path was measured at 20 GHz for a ground terminal at approximately 1-km elevation in an arid (16-cm annual precipitation) region of eastern Washington State. Precipitation intensity and radiometric sky temperature at 20 GHz were also measured. Attenuation greater than 1 dB was observed only in the presence of wet snow on antenna surfaces. The most intense rain observed, 22 mm/hr, was accompanied by a measured sky temperature of 180 K, implying a ground-to-space attenuation of 4.6 dB.

INTRODUCTION

Battelle-Northwest participation in the ATS-6 millimeter wave propagation experiment was designed to determine the effect of Pacific Northwest weather on satellite-to-earth propagation at 20 GHz. Battelle Observatory has a 9.1-m (30-ft) diameter Cassegrain antenna system (figure 1) located in the southeastern part of Washington State on the Hanford ERDA Reservation. The site was chosen for minimum meteorological interference with millimeter wavelength radio astronomical observation, in particular for low precipitable water. The region is arid, receiving an average of about 160 mm total precipitation per year. The antenna is located near the top of a 1060-m high ridge close to the Observatory's optical astronomy and geophysical observing equipment.

INSTRUMENTATION

The major instrument used was a 20-GHz receiver-radiometer system installed on the 9.1-m antenna to measure received 20-GHz carrier level and simultaneously radiometric sky temperature in the same antenna pattern at similar frequencies. A single balanced diode mixer was used for both purposes. The mixer input port was switched between the antenna and an ambient temperature wave-guide termination at a 1-kHz rate. Figure 2 is a block diagram of the parts of the receiver radiometer mounted in the antenna. A photograph of the antenna-mounted unit showing most of the RF components appears as figure 3. A single IF

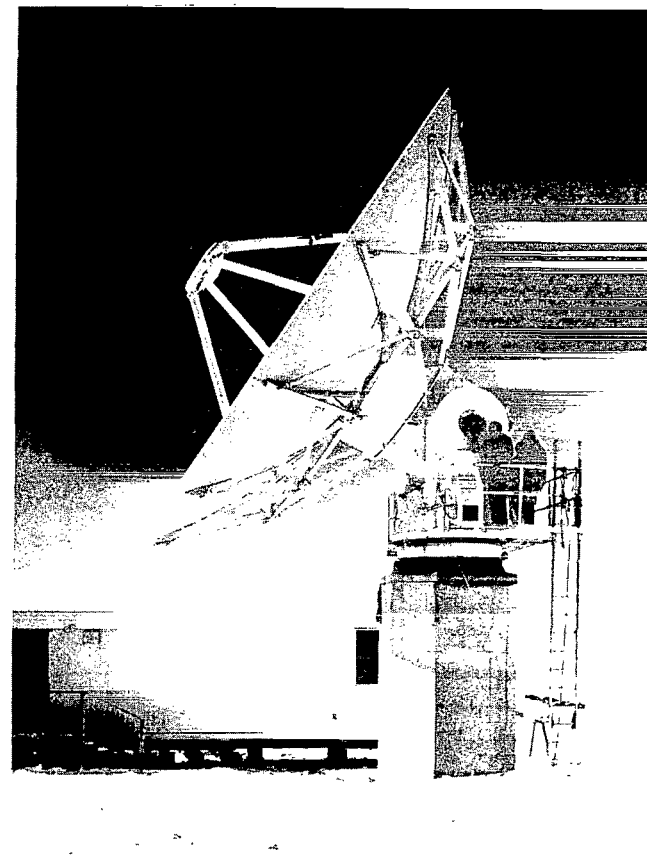

Figure 1. Battelle-Northwest 9.1-m (30-ft) radio telescope.

preamplifier fed a power splitter and filters to define separate carrier and radiometer IF channels. The carrier IF system had remotely switchable filters defining passbands of 60 MHz ± 13, ± 2.5, and ± 0.5. The radiometric IF passband was fixed from 340 to 380 MHz. No RF preselector was used, therefore both channels were double sideband. The local oscillator was set to 19.940 GHz to put the 20-GHz signal in the center of the carrier IF passband. Figure 4 shows the frequencies used.

The carrier level was measured by a wide dynamic range (30-dB) video detector and a 1-kHz tuned amplifier-rectifier feeding a logarithmic amplifier and recorder. The carrier amplifier channel bandwidth used was 1 MHz and the post detection-tuned amplifier bandwidth was 20 Hz. Computed fade margin for the ATS-6 20-GHz transmitter using the parabolic antenna was approximately 50 db for this configuration for unity signal-to-noise. The RF switching, AC measurement technique actually determined the difference between total power from the ambient temperature wave-guide load in a 2-MHz passband and the 20-GHz signal. The computed signal-to-comparison-noise ratio was 30 dB. We would like to point out that this level of performance was achieved without a high-stability local oscillator or a phase-locked receiver by making use of signal modulation produced by the ferrite switch.

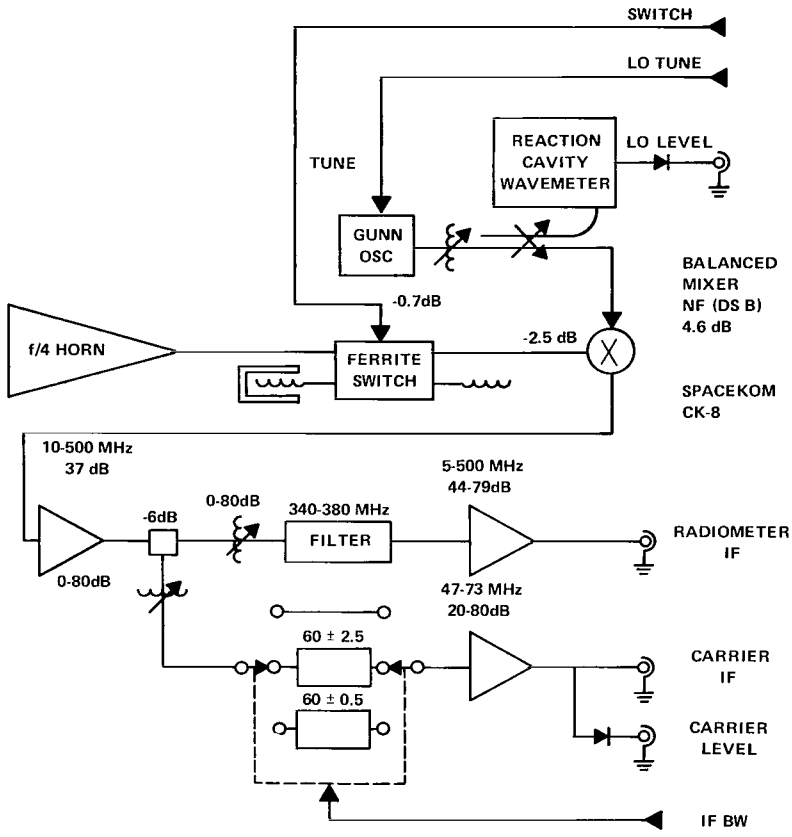

Figure 2. Receiver package.

The radiometer IF channel output was detected and synchronously rectified to measure the difference between radiometric sky temperature and ambient wave-guide load temperature. The difference was recorded on a second channel of the data recorder.

A tipping bucket rain gage with a heated collecting funnel was used to determine precipitation intensity. Each bucket tip, representing 0.24 mm (0.01 in.) of water, was recorded with the 20-GHz signal level and sky temperature. The rain gage was located about 100 m from the antenna in an open area. Additional instruments were provided to measure wind speed and direction, relative humidity, temperature, and barometric pressure. A block diagram of the control room equipment appears in figure 5.

OPERATING PROCEDURE

The receiver-radiometer system was operated almost continuously with the antenna pointed at the zenith. For 20-GHz path attenuation measurements, the look angles for the appropriate time interval supplied by NASA were entered in the tracking computer and the antenna slewed to the designated initial position. The computer interpolated linearly

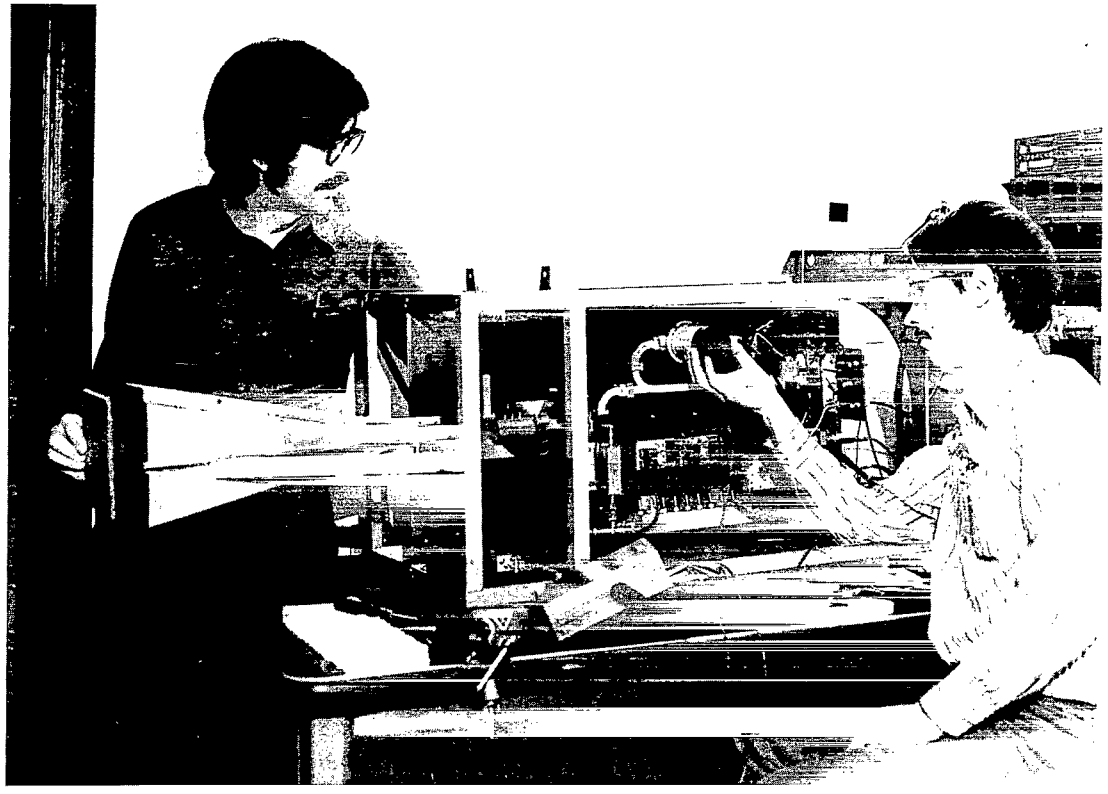

Figure 3. Antenna-mounted RF package.

between provided values to update the antenna position every 60 seconds. Manual fine adjustment of position was performed to peak received signal strength at the start of measurements. The local oscillator was tuned manually, if necessary, to center the received signal in the 60-MHz carrier signal IF channel. This manual tuning procedure, using a spectrum analyzer to locate the received signal, was the weakest link in the acquisition procedure. It was found that the signal margin for acquisition was approximately 30 dB at most favorable satellite pointing.

RESULTS

All components were installed by March 19 and the first attempt at satellite acquisition was successful on March 20. Routine operation began with a clear weather calibration on March 21 and continued until loss of satellite on June 3. Weather at our site was slightly drier and cooler than normal for this time period. Average total precipitation for the period is 28 mm, and 25 mm was measured this year (1975) (see figures 6 and 7).

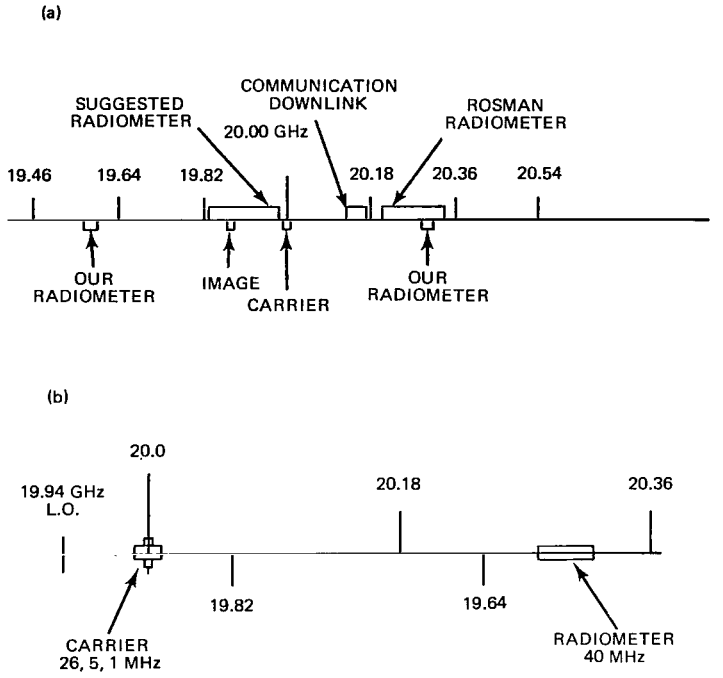

Figure 4. (a) Multitone spectrum. (b) Spectrum folded by mixer.

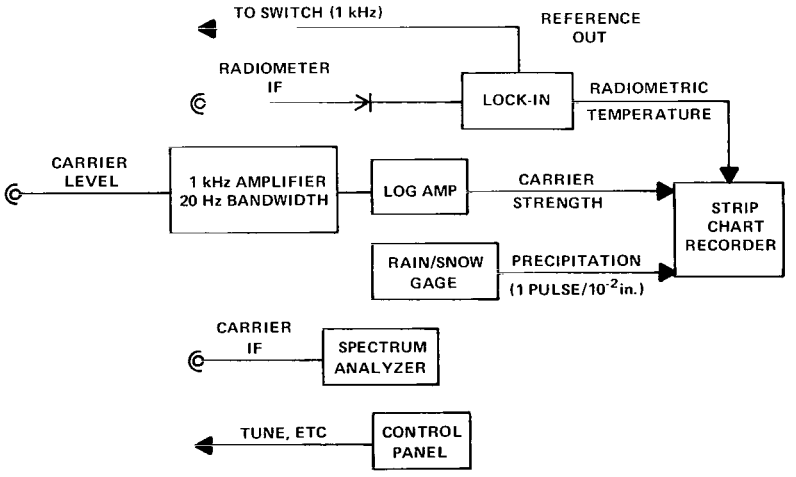

Figure 5. Control room equipment.

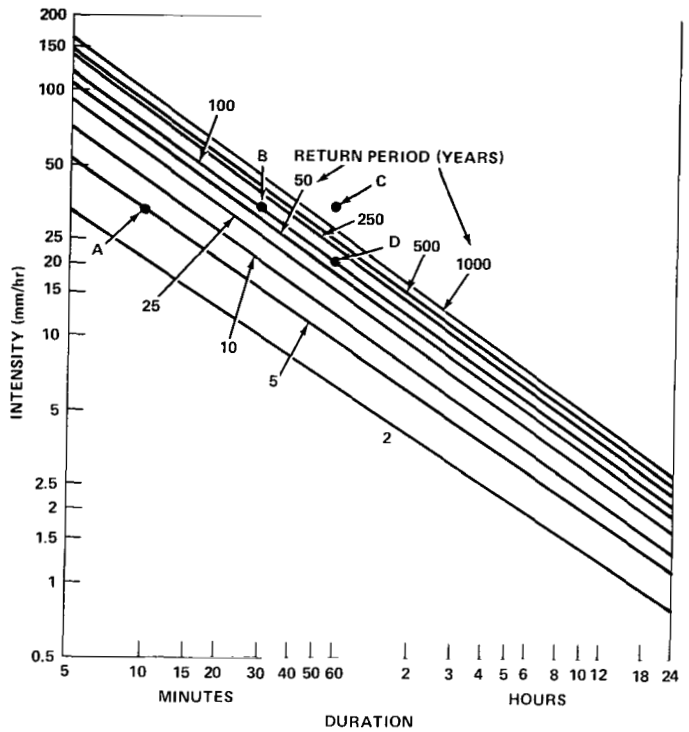

Figure 6. Average total precipitation, Richland, Washington, area.

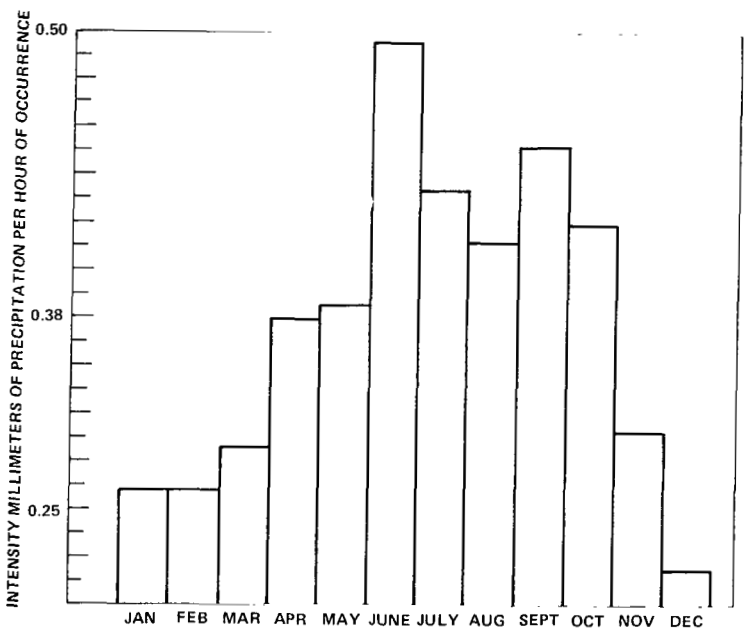

Figure 7. Average monthly precipitation intensity factors based on the period from 1946-1970.

20-GHz ATTENUATIONS

The 20-GHz transmitter was observed for a total of 14 hours. There was measurable precipitation, that is, intensity greater than 0.3 mm/hr during approximately four of these hours. The highest intensity precipitation through which 20-GHz signal attenuation was measured was wet snow equivalent to 1.5 mm of water per hour. No significant attenuation (i.e., greater than 1 dB) was observed which could be attributed to atmospheric absorption or scattering. Attenuation exceeding 10 dB and radiometric sky temperatures approaching ambient, above 250 K, were observed on this occasion but occurred half an hour to an hour after passage of the precipitation and coincided with the melting of snow on most of the reflector surface. Similar attenuation and sky temperature were observed on another occasion following snow and coincided with the melting of snow on the antenna. There was substantially identical behavior of measured zenith sky temperature on a third occasion about an hour after a light fall of wet snow. Our conclusion is that the observed high attenuations were due to wet or melting snow on the antenna primary reflector and/or feed cover rather than atmospheric path attenuation.

SKY TEMPERATURE

Observations of zenith sky temperature have been made almost continuously since operation began. In addition to the incidents described above, we observed significantly elevated sky temperatures in the following cases:

Precipitation Rate mm/hr	Radiometric Sky Temperature	Implied Attenuation
1.2	160 K	3.5 dB
2.3	127 K	2.5 dB
22*	180 K*	4.6 dB*

*Occurred while the site was manned; more information is available.

The first two cases occurred in May and may have been snow, sleet, hail, or rain. Our heated rain gage does not distinguish between the various forms. Relative timing of the precipitation and the rise in sky temperature imply that these were not due to melting snow and are probably genuine path attenuations. Since both events occurred at night during unattended operation, we do not know the weather class at our mountain site (which often differs markedly from that observed in the valley).

On July 30, there was a short period of intense rain, at least intense for this area. The antenna was pointed to 30°elevation and 120° azimuth, representative of ATS-6 look angles and, in this case, the direction in which the storm appeared most intense by visual observation. Peak rain intensity, recorded at the antenna site, was approximately 22 mm/hr (0.06 in. in four minutes) and coincided with an observed radiometric sky temperature of 180 K, suggesting an atmospheric attenuation of 4.6 dB.

SUMMARY

The ATS-6 millimeter wave propagation experiment has as its goal the characterization of the satellite-earth propagation path at 20 and 30 GHz and the correlation of its properties with observable radiometric and meteorological phenomena.

Our part of this experiment was to assemble and operate a 20-GHz ground station using our 9.1-m radio telescope antenna. In operation, we observed and recorded, particularly during storms, the carrier strength of the 20-GHz beacon aboard the satellite, radiometric sky temperature, precipitation rate, and other meteorological parameters. Data analysis was performed to identify interrelationships among recorded data to aid in the prediction of path attenuation for communication links.

CONCLUSIONS

Weather conditions producing attenuation greater than 5 dB on a space-to-earth path at 20 GHz will probably occur less than one hour per year at our arid, eastern Washington State site.

RECOMMENDATIONS

Further atmospheric path attenuation studies for regions of low precipitation intensity are probably needed only for (1) much higher operating frequencies or (2) where extremely low probability of outage is required.

NASA-Langley, 1976

"The aeronautical and space activities of the United States shall be conducted so as to contribute . . . to the expansion of human knowledge of phenomena in the atmosphere and space. The Administration shall provide for the widest practicable and appropriate dissemination of information concerning its activities and the results thereof."

—NATIONAL AERONAUTICS AND SPACE ACT OF 1958

NASA SCIENTIFIC AND TECHNICAL PUBLICATIONS

TECHNICAL REPORTS: Scientific and technical information considered important, complete, and a lasting contribution to existing knowledge.

TECHNICAL NOTES: Information less broad in scope but nevertheless of importance as a contribution to existing knowledge.

TECHNICAL MEMORANDUMS: Information receiving limited distribution because of preliminary data, security classification, or other reasons. Also includes conference proceedings with either limited or unlimited distribution.

CONTRACTOR REPORTS: Scientific and technical information generated under a NASA contract or grant and considered an important contribution to existing knowledge.

TECHNICAL TRANSLATIONS: Information published in a foreign language considered to merit NASA distribution in English.

SPECIAL PUBLICATIONS: Information derived from or of value to NASA activities. Publications include final reports of major projects, monographs, data compilations, handbooks, sourcebooks, and special bibliographies.

TECHNOLOGY UTILIZATION PUBLICATIONS: Information on technology used by NASA that may be of particular interest in commercial and other non-aerospace applications. Publications include Tech Briefs, Technology Utilization Reports and Technology Surveys.

Details on the availability of these publications may be obtained from:

SCIENTIFIC AND TECHNICAL INFORMATION OFFICE

NATIONAL AERONAUTICS AND SPACE ADMINISTRATION

Washington, D.C. 20546